EFFECTS OF SOURCE DISTRIBUTIONS AND CORRELATION ON FRACTIONALLY SPACED BLIND CONSTANT MODULUS ALGORITHM EQUALIZERS

A Dissertation

Presented to the Faculty of the Graduate School

of Cornell University

in Partial Fulfillment of the Requirements for the Degree of

Doctor of Philosophy

by

James Paul LeBlanc

August 1995

EFFECTS OF SOURCE DISTRIBUTIONS AND CORRELATION ON FRACTIONALLY SPACED BLIND CONSTANT MODULUS ALGORITHM EQUALIZERS

James Paul LeBlanc, Ph.D.

Cornell University 1995

A common assumption in blind equalization schemes using the Constant Modulus Algorithm (CMA) is that the source sequence is drawn from an independent, uniform distribution. Much of the analysis demonstrating the global convergence of CMA to an open-eye setting uses such an assumption. Also, much of this analysis has been performed in the baud-spaced equalizer setting, in which an infinite order equalizer is necessarily assumed to avoid the existence of local minima. However, recent results in the literature show that a *finite* fractionally-spaced equalizer allows for perfect equalization of moving average channels (under certain channel conditions known as *equalizability*). Furthermore, CMA has been shown to converge to a perfect equalizing setting under independent, uniformly distributed source.

This thesis work investigates the effect of source statistics on the location of CMA stationary points in the fractionally-sampled equalizer case under the conditions of equalizability. The work identifies the stationary points as the solution set

of a system of multivariate polynomial equations with monomial coefficients given by the source moments. The work is divided into three main areas.

First, an investigation of the properties of the CMA error surface is performed assuming source independence. This section revisits some previously known results and then extends them by quantifying aspects of the error surface based on the source kurtosis. The relevancy of the results here point to the tradeoffs between coding gain (a function of the source distribution) and the error surface curvature (with its effects on convergence).

Next, features of a topological nature of the CMA error surface are discussed. Such properties, which hold independent of source statistics assumptions, form a bridge to the third section describing stationary point locations under temporal source correlation.

The mathematical tools used here (e.g. Groebner bases and Homotopy Methods) are just starting to appear in applications in signal processing. The results include a Monte-Carlo study of the effects of source correlation due to periodic inputs as well as an example of source sequences resulting from Markov models.

Biographical Sketch

James P. LeBlanc was born in Kenmore, New York on July 4, 1961. After receiving his BSEE from Rensselaer Polytechnic Institute in 1983, he worked in industry as an electrical engineer with the Raytheon Company and later Motorola Inc. He attended Cornell University under Raytheon's Miccioli scholarship, obtaining the MEng degree in 1987. In 1991, Mr. LeBlanc returned to Cornell University seeking the PhD. He was married to MeeYoung Yim in April, 1991. They have a son Pascal YongSu LeBlanc, born February 18, 1994.

To MeeYoung

Acknowledgements

I wish to express my sincere gratitude to MeeYoung for the endless support she has given me over the years. Her dedication, cheerfulness, and patience has made all this possible. Her sidekick for the past 18 months, Pascal, deserves high praise for being such a joyful baby and giving me the drive to finish.

Thanks are also due to my mother and father, not just for their support and encouragement over the last few years here at Cornell, but for all the "too-many-things-to-mention" starting since my first on day here on this planet.

A warm "thanks" is extended to my advisor, Prof. C. Richard Johnson, Jr. (a. k. a "Rick"). His advisement spanned many facets of my experience here. The extra time and effort he spent with me on many issues (academic, professional, and personal) is greatly appreciated.

I also need to acknowledge the efforts of Prof. T. L. Fine from the stimulating technical conversations in my early years here, to the careful reading of my thesis and thoughtful suggestions for its improvement. Prof. Mike Stillman is also thanked for his participation as a thesis committee member. His discussions and suggestions have been beneficial to my work.

Prof. Bernd Sturmfels exposed me to an area of mathematics that has been most stimulating and fruitful. His contributions to my education are deeply appreciated.

Through Prof. Sturmfels, I was introduced to Birk Huber. Working with Birk has been a pleasant and rewarding experience for me, and I wish to thank him for his time, company, and PELICAN.

Additional thanks are due to my good friends and fellow students Dr. Michael Turmon and Knox Carey. Our technical/philosophical conversations and friendships made the Cornell experience more rewarding and will be fondly remembered.

Financial support of the National Science Foundation (NSF grants ECS–9022785 and MIP–950911) and Applied Signal Technology, Inc. (Sunnyvale, CA) is acknowledged and greatly appreciated.

Table of Contents

List of Tables

List of Figures

Chapter 1

Introduction

In a digital communication setting, the transmitted signal is often distorted through a dispersive channel with multipath effects which introduce intersymbol interference (ISI) in the received signal. Removal of this ISI from the received signal must be performed to effectively estimate the transmitted sequence. In a high SNR situation, where ISI is the limiting factor more so than channel noise or interference, a linear equalizer may be used to remove ISI. Such a method is presently utilized in a variety of high speed transmission systems such as microwave and satellite communications.

Figure 1.1 illustrates the problem in a simple case. An independent, uniformly distributed discrete source sequence with elements $s(k)$ is formed from elements of a discrete alphabet $\mathcal{A}$. Here $\mathcal{A} = \{-3, -1, 1, 3\}$ represents a 4 level pulse amplitude modulated alphabet (4-PAM). The source sequence $s(k)$ is passed through a noiseless, discrete time, dynamic causal channel C resulting in the received sequence $r(k)$. The existence of ISI in the received signal is seen by the many different values

$r(k)$ attains. That is, $r(k) \notin \mathcal{A}$ due to the convolution of the $s(k)$ with C. Each received sequence element $r(k)$ consists of sums of previous source sequence elements determined by channel C's impulse response. The received signal $r(k)$ is then passed through a discrete-time linear equalizer D which reduces ISI of the equalizer output $y(k)$ (seen by the improved clustering around the alphabet points). Figures 1.2, 1.3, and 1.4 plot the parametrizations of C, D, and their cascade response H (i.e. the combined channel-equalizer impulse response) respectively. Notice that H consists of one large valued tap weight (corresponding to a delay of 4) with the rest of the tap weights being relatively small. This means that each equalizer output value $y(k)$ is due mainly to $s(k-4)$ with some residual component due to the small tap weight components of the convolution sum (e. g. $y(k) = \sum_{i=0}^{n} h(i)s(k-i)$). In this case, the source sequence may be successfully estimated from the equalizer output by use of a decision device choosing nearest neighbor (e.g. a quantizer) if enough of the ISI is removed, so that, $y(k) \approx s(k-4)$. Such a condition on the combined channel-equalizer (H) resulting in perfect source sequence recovery is known as an "open-eye" condition.

Due to the fact that the (unknown) channel impulse response often varies over time (due to environmental conditions, or physical motion between the transmitter and receiver) an adaptive equalization scheme, with its ability to track time-varying system is considered as an attractive solution.

A standard adaptive filtering scheme (e.g. LMS) adjusts the tap weights based on an error signal which is the difference between filter (equalizer) output and the desired output (e.g. the transmitted sequence). The twist here in the equalization problem is that the transmitted signal is unknown (if it were known a priori for

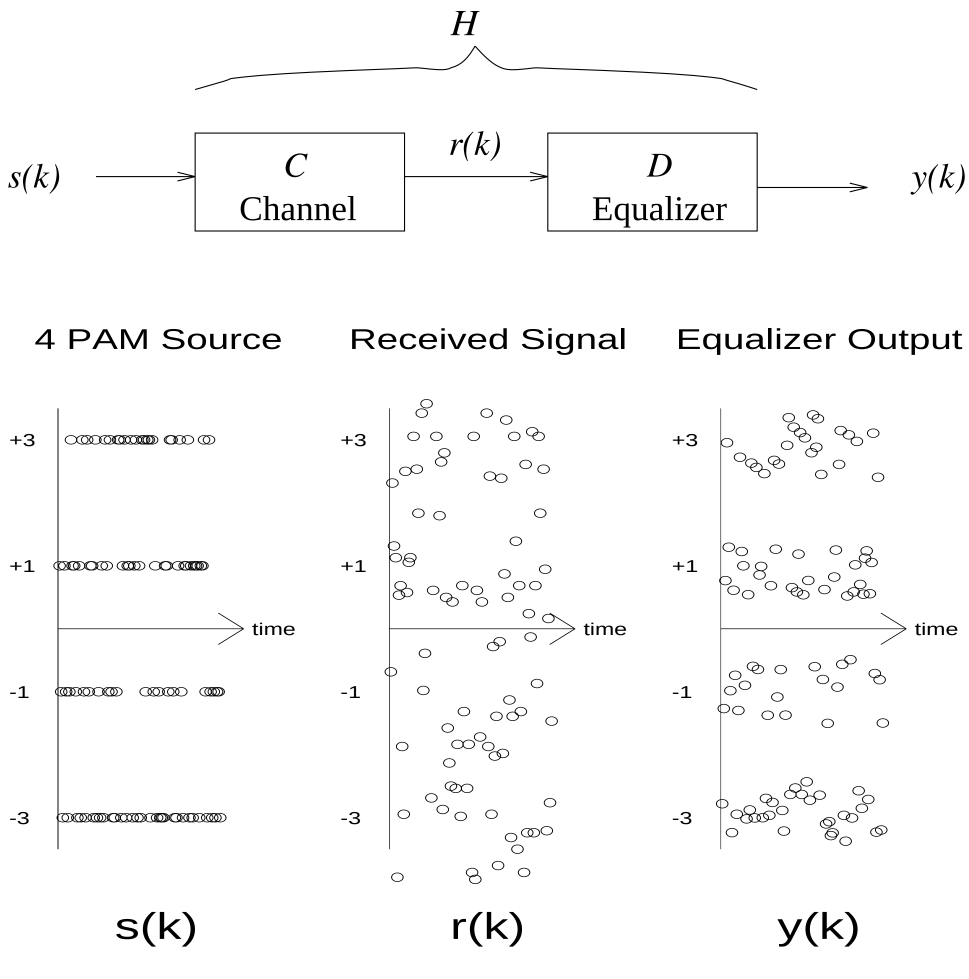

Figure 1.1: Equalization Diagram Block and Example Signals

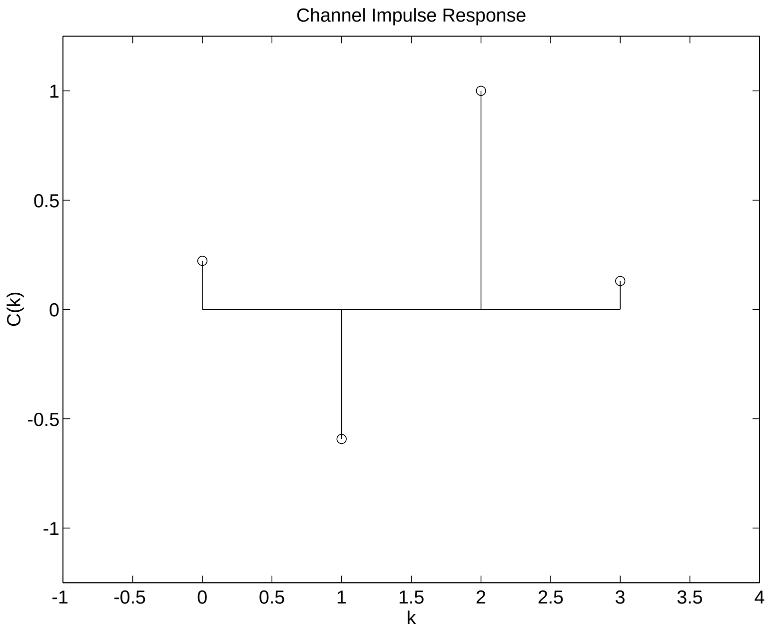

Figure 1.2: Channel Impulse Response

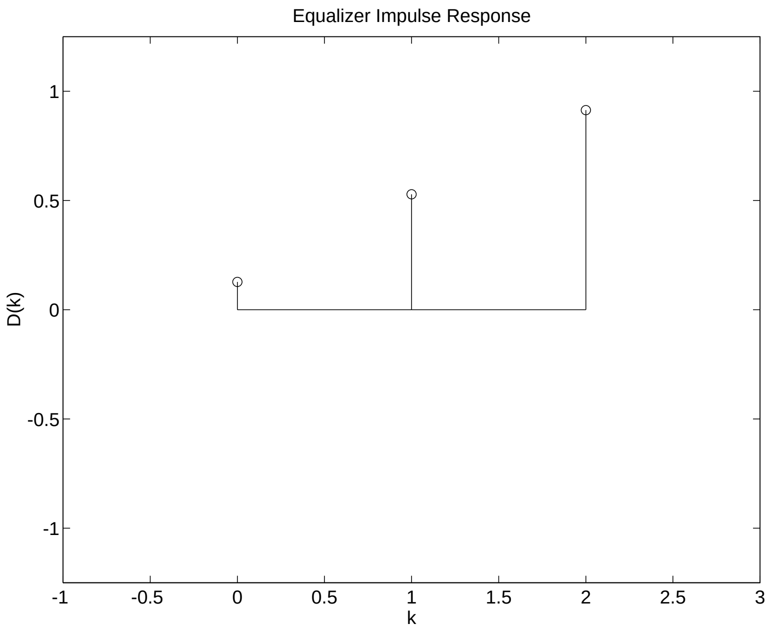

Figure 1.3: Equalizer Impulse Response

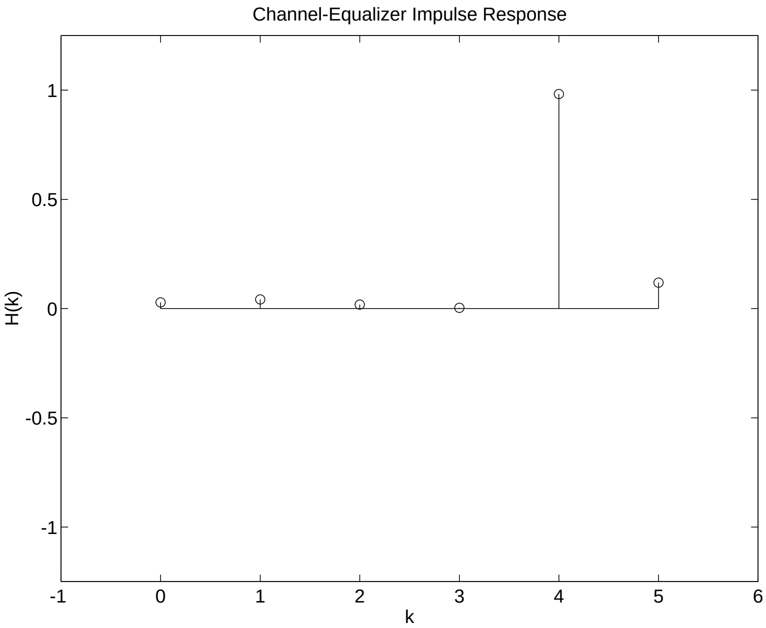

Figure 1.4: Combined Channel-Equalizer Impulse Response

all times there would be little need for performing equalization). Hence, to differentiate our problem from those that have the desired output available at least intermittently (also known as a training sequence), the term *blind* is used to denote the absence of a known transmitted sequence. Thus, the term *blind adaptive equalization* refers to performing equalizer adaptation without the use of a training signal. The lack of need for such a training signal is an advantage of blind equalization schemes since the use of training signals may become cumbersome in broadcast mode and does not make efficient use of available bandwidth.

A variety of blind equalization algorithms may be used during the initial phase of adaptive equalization. After any of these have converged to appropriately low ISI equalization settings (i.e. open-eye), then the equalization scheme may be switched to a specific blind algorithm known as the "decision directed" approach to eke out maximum performance of the equalizer [6]. The switch over to a decision directed equalization may yield better performance (in terms of convergence rates, excess error, residual ISI, etc.) than many blind techniques. However, to benefit from these attractive qualities the decision directed approach often needs to be started from a low ISI setting. Failure to do so may cause the equalizer to diverge to a poor equalization setting. In other words, it may not be as robust with respect to initialization as other blind equalization schemes which are frequently used in the initial phase. The drive for better equalization performance is motivated by the increasing use of higher-order alphabets (bigger/denser constellations) wherein maximum ISI reduction is needed due to smaller intersymbol distances. Notice that for the proper working of such schemes, it is crucial that the blind equalizers have convergent behavior to low ISI channel-equalizer settings. Hence, the study of the convergent behavior of blind equalization algorithms and their properties has been the focus of much research by the blind equalization community (a sampling of these includes [10], [34], [21], [23], [30], [38], [40], [52], [70]).

There are a variety of blind equalization schemes utilizing different approaches: some using linear equalization, some using other methods. An excellent tutorial on the subject of adaptive equalization in general may be found in [58]. In the recent literature one finds methods such as: various adaptive linear equalization error function formulations (Bussgang [7], Sato [60], and CMA/Godard [34], [69]); Decision Feedback Equalization [4], [5], [43]; Viterbi like schemes [53], [61]; cumulants and higher order moments methods [64], [76]; lattice filter implementations [72]; and hidden markov models [45]. However, as many applications demand computational efficiency, we choose to focus on one particular equalization method which is commonly used and remains of high interest. Herein, we consider an adaptive linear feedforward equalizer with tap weights updated by the Godard [34] or Constant Modulus Algorithm (CMA) [69] which uses a specific memoryless polynomial error function for parameter update. Although we focus specifically on CMA in this thesis, it is the polynomial nature of the error function that allows application of the methods described herein. Thus, the formulation and methodology presented herein then are not limited strictly to CMA, but may be applicable to any Bussgang-style scheme using a memoryless, polynomial error function.

To date, *infinitely* long baud rate equalizers adapted by CMA have been shown to be globally convergent to a perfect equalization setting for an independent and uniformly distributed source with an *infinitely* long equalizer, [34], [6], and [30]. However, to reflect the situation in which many equalizers are actually used, more recent work has regarded fractionally spaced equalizers (FSEs) in which the received waveform is sampled at a rate higher than the baud rate. FSEs have been shown to be able to "perfectly equalize" (i.e. provide an equalizer setting for which the combined channel-equalizer system exhibits no ISI) moving average (MA) channels provided certain conditions on *finite* length moving average equalizer and channel are met [66]. Moreover, lacking channel noise and assuming a uniformly distributed, independent source then CMA is known to be globally convergent to this perfect equalization setting [50].

We consider a novel formulation defining the stationary points of a fractionally spaced equalizer adapted by the constant modulus algorithm (FSE-CMA). The stationary points are interpreted as the solution set of a system of multivariate polynomial equations. Standard analysis techniques of the resulting equations revisits some of the known results with CMA under uniform, independent source. Later, they are then extended to yield further results for other distributions of an independent, identically distributed (iid) source. Through this, an improved characterization of the error surface is garnered. Later sections consider the case where the source sequence is temporally correlated (i.e. dropping the assumptions on source sequence independence). Application of some recent results and tools developed within the algebraic geometry community prove useful in this investigation. The use of such tools (e.g. Groebner Bases and Homotopy Methods) is relatively new to the signal processing community (e.g. [42], [19], [47]).

This thesis is organized into seven chapters. Chapter 2 presents a more detailed overview of the blind equalization problem. With many references to known results, it is meant also to serve also as a literature review ending with a section differentiating known results from the problem considered herein. Included are numerical examples of FSE-CMA which exhibit different behavior for source sequences having different statistics which serve to motivate the analytic work. Next, Chapter 3 introduces the mathematical framework of the problem which will be used extensively. The main results of the research are contained in Chapters 4, 5, and 6. Chapter 4 addresses the problem formulated in Chapter 3 in the case of source independence. A topological view of the CMA error surface is included in Chapter 5 which serves as a bridge between the independent source case and the temporally correlated source case. Interestingly, topology deals with deformations, a concept critical in homotopy methods which prove useful in our study of the correlated source case found in Chapter 6. Two methods, one algebraic and one numerical are presented in the investigation of CMA under correlated sources. Finally, Chapter 7 concludes with a review of concepts introduced and their relation to the new results, followed by a discussion of possible extensions to this work.

Chapter 2

The Blind Equalization Problem

2.1 Problem Description

Blind equalization is a form of signal estimation used in digital communications where the transmitted signal has been corrupted by channel effects that introduce inter-symbol interference (ISI). It has been a topic of much study and analysis recently. In fact, the latest ICASSP (May, 1995) conference held a blind equalization tutorial and effectively had two entire sessions dedicated to it. In addition to the many journal articles and conference papers on the subject one finds a fine tutorial which appeared in *Proceedings of the IEEE* [58] as well as a book devoted to the subject [35].

Although there are various solutions to this problem as noted in Chapter 1, in this thesis work we focus on the use of an adaptive linear equalizer that attempts signal reconstruction through the reduction of ISI. An important aspect of this problem is that the channel model is unknown to the receiver. Additionally, the channel may be time-varying, so an adaptive solution is sought. Specifically, the notation used throughout and reflected in Figure 2.1 uses a baseband model. Here

$s(k)$ denotes the elements of the source sequence at time k. Although we investigate the effects of various distributions of s in this thesis, we will strictly limit ourselves to the case of zero mean source. The samples of the received waveform are denoted as $r(k)$, and the equalizer output as $y(k)$. The channel impulse response is denoted by C, the adaptive equalizer parametrization at time k by $D(k)$, and the combined channel-equalizer (or system response) response is denoted by $H(k)$. The time index k present in $H(k)$ and $D(k)$ formally denote that these are time varying quantities, whereas the lack of such an index on C implies that the channel is considered to be non-varying in time for the purposes of our analysis. That is, we invoke the standard concept of "time scale separation" wherein the time variation of the channel is considered to be slow compared to the equalizer adaptation rate.

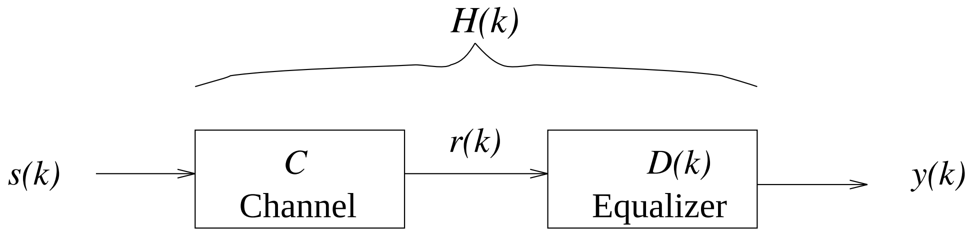

Figure 2.1: Block Diagram

Blind adaptive equalization may be thought of as a specialization of a standard adaptive filtering scenario wherein "blind" signifies that no training signal is used (or available for use) in adjusting the equalizer's tap weights. This contrasts non-blind forms of adaptive filtering algorithms, such as the Least Mean Squares (LMS) algorithm given a training signal. The lack of a need for such a training signal is a great advantage of the blind equalization algorithms, due to the cost associated with transmission of training signals. However, due to the close relationship between blind and non-blind adaptive filtering, we first introduce a non-blind approach.

2.1.1 LMS Non-Blind Adaptive Equalization

In the non-blind setting the transmitter sends a known sequence, called a "training sequence". Of course, if the transmitter were to send only this known sequence, there would be little need to perform equalization at all, since this a priori known signal would carry no information. In actual practice however, this training sequence may be transmitted only during a start-up phase (mostly in point-to-point communications) or periodically transmitted (as used in broadcast mode communications). Equalizer tap adaptation may be performed during reception of this training sequence using the difference between the equalizer output and the known transmitted sequence. Figure 2.2 depicts the situation, wherein the "straight wire" connection between the transmitter and receiver denotes the availability of a known training sequence. A version of this form of adaptive equalization was discussed in some of the earliest works in adaptive equalization roughly thirty years ago ([51] for example).

A standard solution to this problem formulation is the use of the LMS algorithm in a equalization setting. The simplest form of the LMS algorithm uses the difference between the equalizer output $y(k)$ and training sequence $s(k)$ to form an error signal $e(k)$ which is used to update the taps. Let the column vector $R(k)$ represent the equalizer regressor (i.e. the present and previous received samples and the $n+1$ length column vector $D(k)$ represent the n^{th}-order equalizer's tap

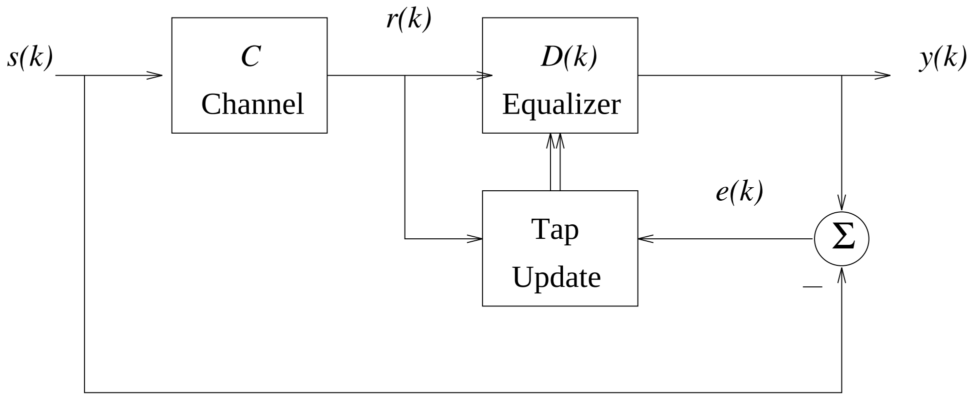

Figure 2.2: LMS Block Diagram

weights at time k,

$$R(k) = [\,r(k) \quad r(k-1) \quad \ldots \quad r(k-n)\,]^{\mathrm{T}} \tag{2.1}$$

$$D(k) = [\,d_0(k) \quad d_1(k) \quad \ldots \quad d_n(k)\,]^{\mathrm{T}}. \tag{2.2}$$

With

$$y(k) = R^{\mathrm{T}}(k)D(k) \tag{2.3}$$

$$e(k) = y(k) - s(k), \tag{2.4}$$

the standard LMS algorithm tap adjustment is

$$D(k+1) = D(k) + \mu e(k)R(k) \tag{2.5}$$

where μ is the (small) adaptation step-size.

Although LMS has been the subject of much study, there are many issues regarding its behavior that are still under investigation such as: step-size effects, tracking ability convergence rate, measurement noise, temporal correlation of source, etc. (A plethora of such articles is available in the literature, more recently

— [3], [15], [65], [28], [13], and [41] — to randomly select a few.). It is well known that LMS adaptation, in the absence of measurement noise and finite arithmetic effects, drives the equalizer taps (on average) to the optimal (least-squares) solution. This important property of global convergence is often lost without access to the training signal, as happens in blind equalization.

2.1.2 Decision-Directed Blind Adaptive Equalization

A close cousin to the LMS non-blind equalization above is the decision directed approach. In fact, the decision-directed approach is often used after successful convergence of a blind equalization algorithm, or after the convergence of the LMS algorithm when training has ended. Here, the equalizer output is passed through a decision device which estimates the source symbol (by a nearest neighbor decision). This estimated source element $\hat{s}(k)$ is then used to generate the error signal as $e(k) = y(k) - \hat{s}(k)$ as in Figure 2.3. Tap weight update then proceeds as in (2.5). Notice, that if $\hat{s}(k) = s(k)$, then this is identical to LMS. Moreover, under this assumption, this scheme may adaptively track slowly varying changes in the channel without the explicit need for a training sequence. In [52] it is shown that decision-directed equalizers converge to the optimal equalizer setting when initialized at an open-eye setting. This means that the equalization setting from a blind equalization algorithm need only be marginally open-eye (depending on SNR) for a successful switch to a decision-directed mode which asymptotically guarantees the optimal equalization setting. The requirement that $\hat{s}(k) = s(k)$ for all time is not really needed, as long as agreement occurs "often enough", the algorithm behaves similarly.

Due to its similarity to LMS (with LMS's attractive qualities: convergence,

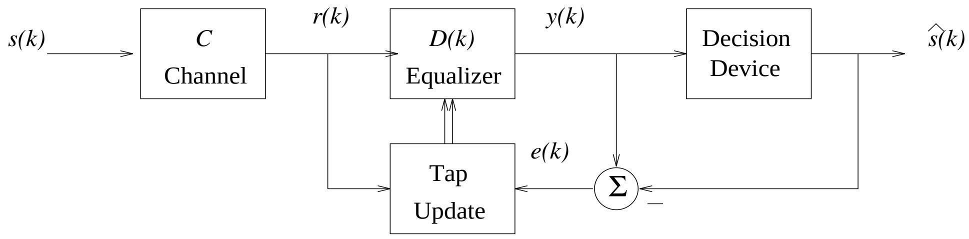

Figure 2.3: Decision Directed Block Diagram

simplicity, tracking ability, etc) decision directed equalization is often switched to after the training period has finished. Moreover, it may also be used after (approximate) convergence of a variety blind equalization algorithm wherein $y(k) \approx s(k)$ (hence $\hat{s}(k) = s(k)$ with high probability).

2.1.3 Error-Function Style Blind Adaptive Equalization

In blind equalization schemes, the error signal $e(k) = y(k) - s(k)$ is not available (since $s(k)$ is unknown). Thus, one attempts to replace the error signal of LMS ($e(k)$) with some other error signal that does not require access to $s(k)$, typically the error signal is some function strictly of the equalizer output $y(k)$, represented by $\Psi(y)$.

The tap update rule for such blind equalizers is analogous to the LMS update rule (merely replace $e(k)$ with $\Psi(y(k))$) yielding,

$$D(k+1) \quad = \quad D(k) + \mu\Psi(y(k))R(k) \tag{2.6}$$

Since the output of the function Ψ effectively replaces the error term in the LMS it is often called the "error function". Its implementation is seen in Figure 2.4.

These algorithms may be viewed as a gradient descent algorithm in which an instantaneous estimate of the gradient of some chosen cost function is used in

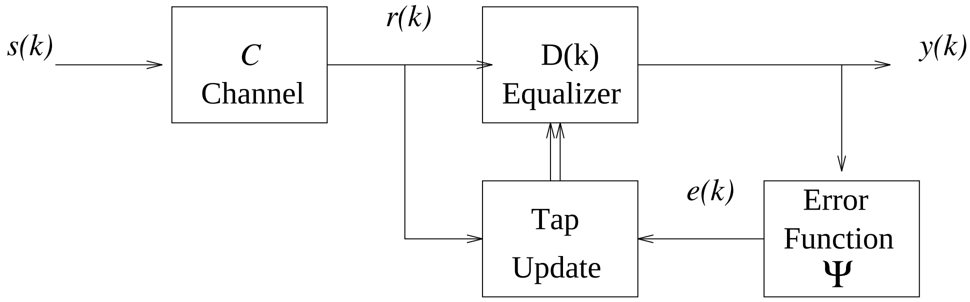

Figure 2.4: Blind Equalization Block Diagram

place of the actual gradient. There are a variety of choices of the cost functions available, and there is a relation between this cost function in terms of the equalizer parametrization (written as $J(D)$) and the associated *error function* (written as $\Psi(y)$). Typically, we have $\Psi(y) = \frac{\partial J}{\partial y}$. It is noted that since it is precisely the term $\Psi(y)$ which is used by the adaptive in the equalizer tap update, and the cost function J is never explicitly calculated.

Blind equalization techniques of this form are known as "Error Function Formulations". Such formulations are attractive due to their computational simplicity (on the order of LMS). Furthermore, due to the high throughput demands of many applications which utilize blind equalization techniques, the error functions need to be simple and efficiently computed. As such, we limit our discussion here to memoryless error functions (although there is some recent research of blind equalization with error functions with memory [17]). Some popular members of this family are: the Godard Algorithm [34] (a.k.a. the Constant Modulus Algorithm — CMA [69]), the Sato Algorithm [60], and Stop-and-Go [57]. The motivations of theses particular members are described below.

Sato Error Function

One of the earliest error function formulations found is the *Sato* algorithm. The concept of this algorithm is to "break off statistical relation [sic]" between samples of the equalizer output [60]. Note that the independence of source sequence elements is critical in the problem formulation. The measure of the statistical relation considered is the "one-side polarity correlation" given as $\mathrm{E}\{y(k+\ell)\mathrm{sign}(y(k))\}$. This leads to the cost function (J_{SATO}) and error function (Ψ_{sato}) of

$$J_{\mathrm{SATO}} = \mathrm{E}\left\{(y(k) - \gamma \mathrm{sign}(y(k)))^2\right\} \tag{2.7}$$

$$\Psi_{\mathrm{SATO}}(y(k)) = y(k) - \gamma \mathrm{sign}(y(k)) \tag{2.8}$$

where $\gamma = \frac{\mathrm{E}\{a^2\}}{\mathrm{E}\{|a|\}}$ for $a \in \mathcal{A}$ (the source alphabet). The cost and error functions associated with the Sato algorithm are depicted in Figure 2.5 for a unit variance 4-PAM alphabet (e.g. $\mathcal{A} = \{-3\Delta, -\Delta, +\Delta, +3\Delta\}$ where $\Delta = \sqrt{\frac{1}{5}}$ is the real valued scalar which sets the alphabet variance to unity).

A detailed analysis of the Sato Algorithm (and generalizations thereof) is found in [10]. This work demonstrates the global convergence of the algorithm to a combined channel-equalizer to a parametrization that is a pure delay (modulo a phase shift) for an *infinite* tap equalizer. The analysis includes work indicating some requirements of the source distributions (e.g. *super-Gaussian*, and *sub-Gaussian*). The distributions are considered to be continuous and differentiable, whereas discrete distributions are more appropriate in the digital communications setting.

Ding et. al. [24] considers the more practical case of finite order equalizers adapted by the Sato algorithm within the finite alphabet setting of digital communications. It is demonstrated that Sato equalizers possess ill-performing lo-

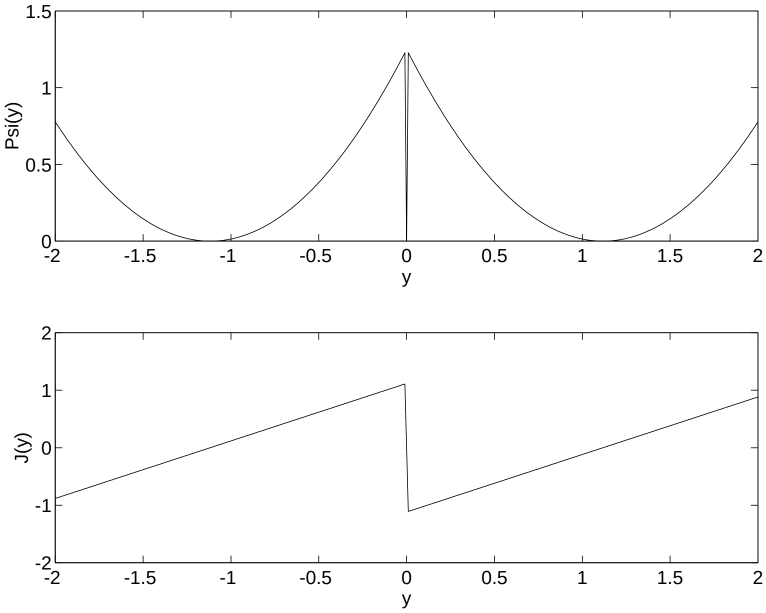

Figure 2.5: Sato Cost and Error Functions

cal minima, and thus can fail to properly equalize a channel. Two mechanisms of such failure are suggested. One due to finite alphabet effects, and the other due to finite equalizer effects. Specifically, it is shown that combined channel-equalizer parametrizations in which all non-zero elements have equal value (e.g. $H = [\,0 \quad \ldots \quad 0 \quad t \quad t \quad \ldots \quad t \quad 0 \quad \ldots \quad 0\,]^{\mathrm{T}}$ for $t \neq 0$) are *stable* stationary points under Sato update. This allows for convergent points associated with very high ISI settings. Although the Sato algorithm's error function is very computationally efficient, due to the rather unattractive property of local minima, the algorithm was not considered for further study in this thesis.

Stop-and-Go Error Function

The Stop-and-Go Algorithm [57] represents a twist on the Decision Directed technique. The basic idea is to use an error function which causes no update if the output is too far from an alphabet member. Such outputs are regarded as too unreliable. In this manner, only outputs which are "reliably" close-enough to a true alphabet member are used in computing tap updates. Looking at the stop-and-go error function in Figure 2.6 (shown for a 4-PAM source), it is seen that the error function is zero in a small neighborhood between the elements of $\mathcal{A}$.

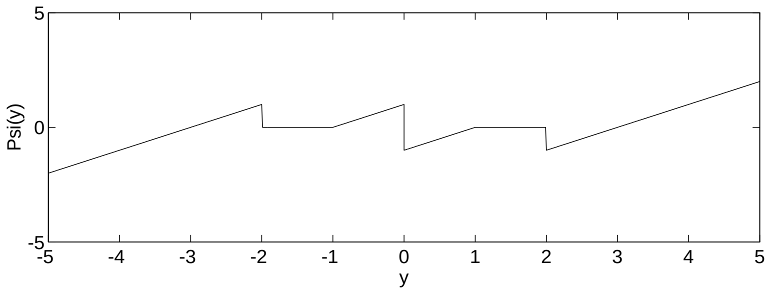

Figure 2.6: Stop-And-Go Error Function

Due to the definition of the error function, the stop-and-go algorithm itself becomes more decision-directed as more of the equalizer outputs fall in the neighborhood of a valid alphabet member. However, this supposed benefit may be offset by a possibly slower convergence since that many equalizer outputs far from a valid alphabet member are not used for tap weight updates.

Shalvi and Weinstein's "Universal Method"

In [62] a stochastic gradient based blind equalization for complex signals method given the name of "universal method" by its authors is presented. It is proposed that the method compares favorable with other blind equalization schemes and is compared directly with the Godard algorithm (CMA). In this algorithm the cost function reduces to (using the notation of this thesis),

$$J_{\mathrm{UNI}} \;=\; \mathrm{sign}(K(s))\mathrm{E}\left\{|y|^4\right\} \tag{2.9}$$

where $K(s) = \mathrm{E}\left\{|s|^4\right\} - 2\mathrm{E}\left\{|s|^2\right\}^2 - \left|\mathrm{E}\left\{s^2\right\}\right|^2$. Updating the taps by the instantaneous estimate of the gradient of J_{UNI} yields the algorithm as,

$$\begin{aligned} d_\ell(k+1) \;=\;& d_\ell(k) + \\ & \delta \mathrm{sign}(K(a)) \left[(|y(k)|^2 + \gamma_1 \hat{\eta}_p(k) + \gamma_2) y(k) - \hat{\eta}_\epsilon(k) y(k)^* \right] yk - \ell \end{aligned}$$

where the quantities $\hat{\eta}_\epsilon$ and $\hat{\eta}_p$ are the empirical averages of $\mathrm{E}\left\{y^2\right\}$ and $\mathrm{E}\left\{|y_i|^2\right\}$ respectively. Formally, these are defined as,

$$\hat{\eta}_\epsilon(k) \;=\; (1-\delta_\epsilon)\hat{\eta}_\epsilon(k-1) + \delta_\epsilon y(k)^2 \tag{2.10}$$

and,

$$\hat{\eta}_p(k) \;=\; (1-\delta_p)\hat{\eta}_p(k-1) + \delta_p |y(k)|^2 \tag{2.11}$$

where δ_ϵ and δ_p are the step-sizes used to estimate $\mathrm{E}\left\{y^2\right\}$ and $\mathrm{E}\left\{|y_i|^2\right\}$. The connection to CMA is made under certain conditions about the source sequence and alphabet (namely $\mathrm{E}\left\{s^2\right\} = 0$ and $K(a) < 0$). Setting $\alpha = -\mathrm{E}\left\{|s|^4\right\}/K(a)$ and $\gamma_1 = 0$ reduces this "universal algorithm" to CMA (which is introduced formally in Section 2.1.4). As such, it may be considered as a generalization of CMA. The claimed benefits of such a generalization is that these algorithms "do not impose any restrictions on the probability distribution of the (unobserved) source sequence". Such, benefits come at the cost of knowing a priori the value of $K(a)$ as well as the increased algorithmic complexity added by the estimation of the quantities $\mathrm{E}\left\{y^2\right\}$ and $\mathrm{E}\left\{|y_i|^2\right\}$. However, later in [68] several additional questions are raised regarding the algorithm. In the case considering noise, it is not clear that the algorithm will achieve proper equalization performance. The original authors acknowledge in [63] that in the noisy case, proper performance can only be guaranteed if the channel is "spectrally white" (e.g. has unity magnitude response). Barring this, then the second and fourth order statistics of the noise must be known. Due to the analytic complexity of the algorithm, its computational complexity, and questioned robustness this particular algorithm has not become as pervasive in the literature as some of the simpler algorithms. As such it was not considered for further study.

Godard/CMA Error Function

Another blind equalization scheme based on a memoryless nonlinear error function is known as the Godard or Constant Modulus Algorithm (CMA). As this particular algorithm is the focus of the thesis research work, it is more fully introduced in the following section.

2.1.4 Introduction to Godard/CMA Algorithm

> "The most widely tested and used in practice blind equalizer is probably the Godard or constant modulus algorithm (CMA)" — *Proakis and Nikias* [35]

Due to CMA's popularity, it is chosen as the algorithm for investigation. However, many of the concepts and results presented herein have analogies under use of other polynomial memoryless error functions. The blind adaptive equalization algorithm that is the focus of this thesis work was independently developed by Godard [34] and Treichler [69] and is known as the Godard Algorithm, or Constant Modulus Algorithm (CMA). Although Godard and Treichler took differing views of the aspects of the blind equalization problem and different approaches in algorithm development, there independent work converges to result in the same algorithm.

Godard's approach focused on the minimization of non-convex cost functions which are shown to characterize ISI. The choice of functions for minimization are called *dispersions* of order p defined as,

$$\mathcal{D}^{(p)} = \mathrm{E}\left\{(|y|^p - R_p)^2\right\} \tag{2.12}$$

where R_p is a positive real function. Note that $\mathcal{D}^{(p)}$ inherently uses higher order statistics of the equalizer output.

With the error function defined as the term of the instantaneous gradient estimate of this function with respect to equalizer taps weights due to the equalizer output, the Godard (or CMA) error function is written as,

$$\Psi_{\mathrm{GODARD}-p} = y|y|^{p-2}(|y|^p - R_p) \tag{2.13}$$

Often, $p = 2$ is chosen and this becomes,

$$\Psi_{\mathrm{GODARD}-2} = y(|y|^2 - R_2). \tag{2.14}$$

Alternatively, Treichler and co-workers work stems initially from an interest in the waveform equalization of frequency modulated (FM) or phase modulated (PM) signals. Such signals inherently have a constant modulus (i.e. envelope). As such, a cost function may be based on the variance of the difference of the equalizer output modulus and some positive real constant γ,

$$J_{\mathrm{CMA}} = \frac{1}{4}\mathrm{E}\left\{(|y|^2 - \gamma)^2\right\}. \tag{2.15}$$

It is pointed out that due to the modulus operator on y in J_{CMA}, that any phase shift of y produces the identical cost. That is, since $|y| = |e^{j\phi}y|$ we have $J_{\text{CMA}}(y) = J_{\text{CMA}}(e^{j\phi}y)$ for any phase shift ϕ. While this apparent shortcoming (i.e. phase ambiguity) may seem bothersome, it is easily overcome by the use of a differential source encoding scheme. In differential encoding the message is carried by the *transitions* between the source sequence elements, not the elements themselves. Such techniques are commonly used in communication systems to overcome polarity (phase) and synchronization difficulties [16]. In light of this, the term "perfect equalization" may be interpreted as removal of all ISI without regard to sign or phase shift of combined channel-equalizer (i.e. in our notation H may be any vector with a single non-zero entry).

Differentiating J_{CMA} with respect to y yields the error function as,

$$\Psi_{\text{CMA}} = y(|y|^2 - \gamma). \tag{2.16}$$

Note the equivalence of (2.14) and (2.16) with appropriate definitions of γ and R_p. The associated cost and error functions are plotted for 4-PAM alphabets in Figure 2.7. The tap update law then follows as,

$$D(k+1) = D(k) + \mu\Psi_{\text{CMA}}(k)R(k) \tag{2.17}$$

where $R(k)$ is the vector containing samples of the received signal (i.e. the equalizer *regressor*).

In [69] it is noted that CMA may be expanded beyond the equalization of constant modulus analog signals and successfully applied to the problem of equalizing multi-modulus signals in a digital communications setting.

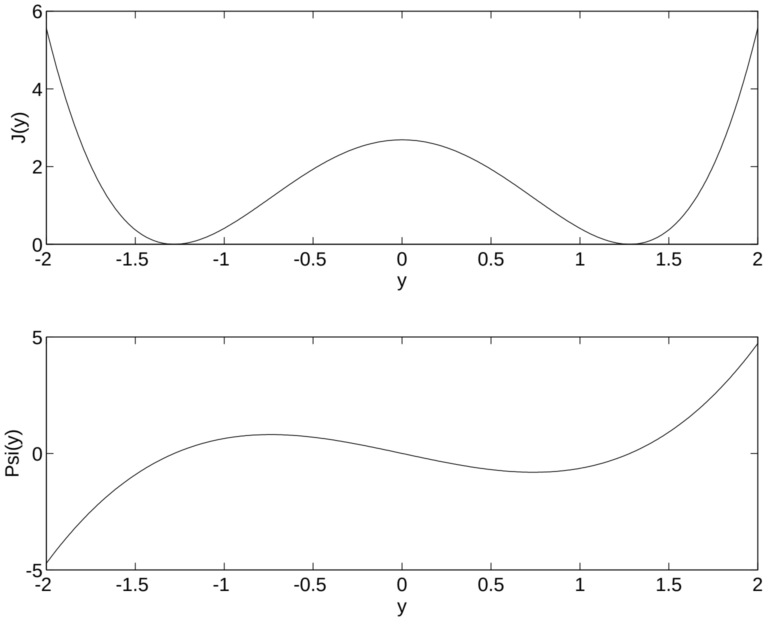

Figure 2.7: CMA Cost and Error Functions

2.1.5 Known Results of CMA

The following sections discuss the results for baud-space blind equalizers adapted by Godard/CMA procedures (simply denoted CMA throughout the rest of this work) that have appeared in the recent literature.

Godard

In [34] a technique for blind equalization is presented within the framework of carrier tracking/equalization for quadrature modulated communications systems. Here, a "new class of ... cost functions" is discussed enabling removal of ISI independent of the source constellation. The assumptions made here are the standard assumptions often found in the blind equalization field, namely the source is considered to be a zero-mean independent, uniformly distributed sequence produced from a known source alphabet. The development of what is today known as the

CMA algorithm is presented, along with a discussion of its convergence properties. Of particular note is the comment that "The problem raised by the existence of local minima is also shown to be soluble by simple initialization of the equalizer...The equalizer will also be assumed infinite". This assumption simplifies analysis greatly but weakens the result considerably since there is no proof that the (realizable) finite tap equalizer will exhibit the same behavior as the (unrealizable) infinite tap equalizer, nor if the "simple" initialization strategy is appropriate for the finite tap case.

Foschini

Foschini [30] presents work in which the Godard adaptation scheme is shown to be globally convergent. That is, convergence to a global minimum occurs regardless of the initialization (initial parametrization) of the equalizer. Unfortunately, this analysis also assumes that the equalizer is of infinite order. The infinite tap equalizer is analyzed because "it is very awkward to deal analytically with the finite tap case". However, it is also stated that "There is some evidence that the infinite tap — finite tap contrast is nearly as tame as it is with MMSE equalization."

It is conveyed that in the finite equalizer case we must limit our analysis to more restricted cases of the equalization problem. We must accept that we are not intending to equalize "pathological" channels with severe nulls in the frequency response. A modification to the Godard algorithm is proposed. Since a finite equalizer is used, a tap-centering strategy is presented to avoid a lop-sided or tail heavy tap weight distributions.

The tap-centering strategy consists of computing the center of gravity of the tap weights and then shifting the taps to balance the tap weights about the center of the equalizer. It is stated that “The centering helps approximate the effect of infinitely many taps that the theory has required”. A numerical example is presented in lieu of proof of such a statement. This omission is addressed, “...with a sufficiently large number of taps (and employing a weight centering procedure), the convergence properties of the Godard algorithm differ negligibly from what is predicted for the infinite tap equalizer. However cogent the supporting evidence, a mathematically rigorous argument has not been given.”

Ding, Johnson, Kennedy

Ding et. al. [22] provide a proof of the existence of multiple local minima for the Godard Algorithm (and other, related error functions) for the *finite* order equalizer. The argument uses a perturbation of an ideal channel with continuity arguments due to the continuous cost function. Realize that with an ideal channel (no ISI), setting any of the equalizer taps to 1 while the other taps have value zero, provides equivalent error to the Godard error function allowing m minima (where m= number of equalizer taps). The case is made that perturbations in the ideal channel may still allow m local minima, and furthermore some of these minima will fail to provide complete ISI removal. This theme is then precisely explored for the case of an IIR channel followed by an FIR equalizer of high enough order to provide perfect equalization.

The importance of such a result is that it points out the need for a proper initialization strategy for finite order equalizers. It also highlights some of the issues in applying results based on infinite order equalizers to implementations requiring finite order equalizers.

Effects of Source Statistics

A critical assumption upon which the Godard (and related algorithms) is based is the assumption of a temporal independence and non-Gaussian distribution of the source signal. Analysis in almost all of the literature, utilizes this assumption. To our knowledge little published work ([1], [18], [37], [39], [70], [75]) has appeared addressing how critical this assumption is for the proper behavior of blind equalization schemes. Some of the other methods mentioned earlier (e. g. hidden Markov models, direct source sequence estimation, Viterbi-like methods) are possibly analyzable and applicable to source sequences which are correlated. However, as they may be computationally formidable, they are considered to be in a different class of algorithm than the one studied herein. Also, some of these methods require a priori knowledge of the source statistics which is not necessarily available. We address the *effect* of source distributions on a computationally simple adaptive blind equalization algorithm, CMA.

<u>Effects of Source Distribution.</u> Chan et. al. [18] attempt to address some aspects of distributional aspects of the received sequence $r(k)$. Unfortunately, their presentation may easily mislead the casual reader. They cite [73], in which a Gaussian model of the received signal is considered to simplify convergence analysis of blind equalization algorithms. The original justification for this model is provided by recognizing that the received signal consists of the sum of a very large number of iid source sequence elements (through the channel convolution sum). Invocation of the central limit theorem then concludes that the received signal's distribution approaches a Gaussian.

The problem arises when the authors use a Gaussian *source* sequence to guarantee a Gaussian received sequence. By doing so they place a condition on the source, but draw conclusions concerning the received signal. From [18], "when the *received* signal is a zero-mean, real Gaussian process ... CMA generally cannot equalize a communication channel. [emphasis added]"

There are fundamental problems with this conclusion. First, it can be shown that the received signal due to a non-Gaussian source may be arbitrarily close to Gaussian (see Appendix D), and yet CMA is able to properly equalize. Secondly, the only way to guarantee that the received signal (being a sum of past input sequence elements) be *truly* Gaussian is to use a Gaussian *source* which places this outside the realm of digital communications. That is, a Gaussian process has a dense and infinite range of values, while only a finite, discrete set of values makes sense in digital communications. In essence, they effectively place conditions on the source and then state their conclusions as properties due to features of the received signal. (It appears that the authors are aware of such logical incongruities by stating in their conclusion "The results in this correspondence support the conclusion that CMA may not be effective when the received signal is *unconditionally* Gaussian [emphasis added].")

Most disturbing is that others seem to have drawn erroneous conclusions from [18]. In [75] an investigation of the effect of constellation shaping (i.e. non-uniform source distributions) on blind equalizers appears. It is commented that CMA may perform poorly on heavily shaped constellation, "It was shown in [10] [referring to [18] herein] that for Gaussian *received* signal [sic], all forms of the CMA algorithm are ineffective in equalizing the channel [emphasis added].". Because of this (mis)-interpretation most of the work focuses on non-CMA blind equalization schemes.

Effects of Source Correlation. Several situations in which CMA fails to converge are documented in [70]. These examples show the behavior of a CMA equalizer when the source sequence is drawn from a variety of cyclostationary, periodic, and non-white inputs. Plots of the convergent equalizer output constellations are presented as experimental evidence of ill-convergence and offers some assessment of the potential causes. It does not attempt any analysis of such behavior. The relevancy of such failure modes is then presented. It is noted that there are a variety of ways in practical telecommunications systems that such signals causing poor CMA behavior can appear. One such situation is when the source is generated by a pseudo-random (PN) sequence generator. To keep an otherwise idle channel properly equalized (open-eye), a PN sequence is transmitted and the equalizer taps may be updated by CMA. Experimental evidence of failure is presented which shows that such sequences can cause ill-convergence. A relation between the sequence length and equalizer order is also noted. Higher-order equalizers may be effected by longer sequences.

In an initial correlated source investigation [39] an interpretation for correlated sources is made by considering the regressor probabilities resulting from a correlated source passing through the channel. By changing the source correlation, the probabilities of various regressors are changed. This may be interpreted as changing the locations of some (perhaps all) of the stationary points of the Godard algorithm.

In [37] and [1] methods of accommodating the presence of a *known* source correlation is considered for a more complicated (non-CMA) method. However, its dependence on knowing the source statistics and its computational complexity places it in a different class than the problem considered here.

2.2 Fractionally Spaced CMA

Much of the analytic work on blind equalization algorithms (such as that cited above) considered the baud spaced equalization problem (wherein the received signal is sampled at the baud rate). This was despite the fact that many equalizers built today use a technique known as "fractional sampling". Historically fractional sampling equalizers were implemented for baud synchronization considerations ([32], [71]) more so than equalization aspects. However, more recent analysis of the effect of this fractional sampling has shown it to have profound influence on equalization performance. Hence, much of the most recent blind equalization literature incorporates the effects of fractional sampling (as does this thesis).

2.2.1 Known Results of FSE-CMA

One of the more useful (and perhaps surprising) results of fractional sampling in a digital communications setting is the ability to "perfectly equalize" a moving average channel with a *finite* order equalizer, under certain conditions. Under these conditions, many of the results obtained in the infinite length baud-spaced equalizers translate to similar results with a finite length equalizer. Analysis in a finite dimensional setting is often easier (and in fact critical to the thesis work presented here). Before presentation of the equalizability conditions, we give a brief synopsis of the fractionally-spaced equalizer setting.

Fractionally Spaced Models

Consider the adaptive fractionally spaced equalizer in the system block diagram in Figure 2.8. Here the path from discrete source sequence $s(k)$ with baud spacing of T seconds to the received (analog) signal $r(t)$ is modeled as the cascade of a discrete-to-continuous device (D/A) and a continuous time channel impulse response $c(t)$. The received waveform is then sampled at intervals of T/L seconds (where L is a positive integer). This sampled sequence is then filtered through a discrete-time equalizer whose output is then desampled by L to produce the baud-space output sequence $y(k)$. Equalizer taps are then updated based on the output of the error function Ψ as described earlier.

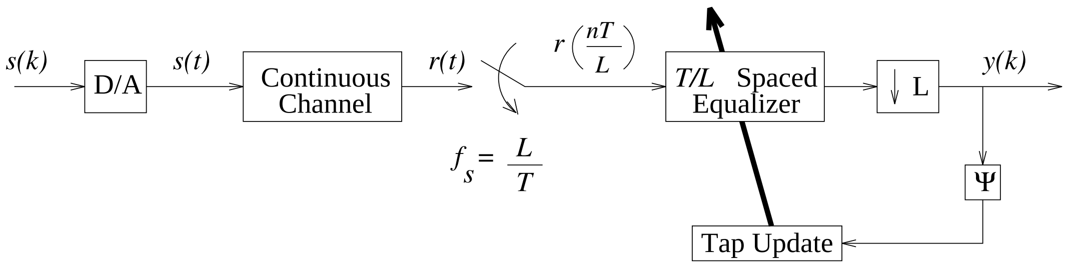

Figure 2.8: Fractionally-Spaced Adaptive Equalization Block Diagram

It is shown in Appendix B that the fractionally-spaced system may be alternatively described by the sub-channel model in Figure 2.9, in which all sub-blocks are considered as baud-spaced discrete-time systems. This formulation eases introduction of the aforementioned “equalizability” conditions allowing perfect equalization. With

C1 Time-Span of equalizer exceeding the time-span of the channel

C2 Sub-channels (as polynomials in z) having no common roots then there exists an equalizer parametrization capable of setting the combined channel-equalizer system to a pure delay with no intersymbol interference [66].

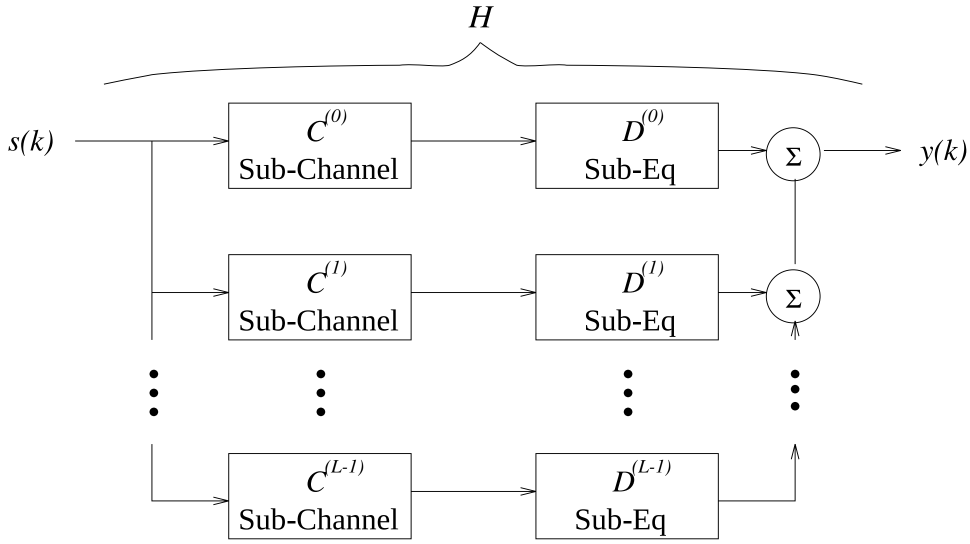

Figure 2.9: Associated Sub-Channel Model

To see this, consider the following simple example where the oversampled channel $C(z)$, and equalizer $D(z)$ (with z^{-1} as the $\frac{T}{2}$ delay operator),

$$\begin{aligned} C(z) &= c_0 + c_1 z^{-1} + c_2 z^{-2} + c_3 z^{-3} \\ D(z) &= d_0 + d_1 z^{-1} + d_2 z^{-2} + d_3 z^{-3} \end{aligned}$$

Then the half-baud combined channel-equalizer response (denoted $H_{\frac{T}{2}}$) is represented by the product of the channel convolution matrix and the equalizer tap column vector,

$$H_{\frac{T}{2}} = \begin{bmatrix} c_0 & 0 & 0 & 0 \\ c_1 & c_0 & 0 & 0 \\ c_2 & c_1 & c_0 & 0 \\ c_3 & c_2 & c_1 & c_0 \\ 0 & c_3 & c_2 & c_1 \\ 0 & 0 & c_3 & c_2 \\ 0 & 0 & 0 & c_3 \end{bmatrix} \begin{bmatrix} d_0 \\ d_1 \\ d_2 \\ d_3 \end{bmatrix} \tag{2.18}$$

Decimation of the equalizer output yields a baud spaced channel-equalizer combination (denoted H_T and resulting from striking out every other row of $H_{\frac{T}{2}}$),

$$H_T = \begin{bmatrix} c_0 & 0 & 0 & 0 \\ c_2 & c_1 & c_0 & 0 \\ 0 & c_3 & c_2 & c_1 \\ 0 & 0 & 0 & c_3 \end{bmatrix} \begin{bmatrix} d_0 \\ d_1 \\ d_2 \\ d_3 \end{bmatrix} \tag{2.19}$$

Now, the matrix H_T is full rank if subchannels ($C^{(0)}(z) = c_0 z + c_2$, $C^{(1)}(z) = c_1 z + c_3$) have no common root [29], [12]. With all of H space reachable, a parametrization realizing strictly a delay is possible. This relates to the Bezout Equation in which we seek finite order polynomials $D^{(0)}(z)$ and $D^{(1)}(z)$, given finite order polynomials $C^{(0)}(z)$ and $C^{(1)}(z)$, so that $C^{(0)}(z)D^{(0)}(z)+C^{(1)}(z)D^{(1)}(z) = 1$. This is solvable iff $C^{(0)}$ and $C^{(1)}$ share no common roots.

More specifically related to CMA equalizers is the result that with the additional conditions of,

C3 Independent, Uniformly Distributed Source

C4 No Channel Noise

then, the fractional equalizer adapted under the CMA algorithm is globally convergent to perfect equalization setting (no ISI) [29], [50].

2.2.2 Numerical Example of FSE-CMA

Example A: An illustrative example of "proper" CMA behavior in a fractionally spaced equalization setting is presented. The source sequence elements $s(k)$ are independently drawn from a uniform distribution. The over sampling factor is $L = 2$, with a 5 tap (half baud spaced) channel and 5 tap (half baud spaced) equalizer. For this example (as well as following Examples B, and C) the parameters are:

- 8 PAM, unit variance alphabet,
  $\mathcal{A} = \{-7\Delta, -5\Delta, -3\Delta, -\Delta, +\Delta, +3\Delta, +5\Delta, +7\Delta\}$ with $\Delta = \frac{\sqrt{84}}{2}$
- adaptive stepsize, $\mu = 8 \times 10^{-5}$
- channel taps, $c = [\,-0.5735 \quad 1.0000 \quad -0.2802 \quad -0.8203 \quad -0.5027\,]^{\mathrm{T}}$
- equalizer initialization, $d(0) = [\,0 \quad 0 \quad 1 \quad 0 \quad 0\,]^{\mathrm{T}}$

Figure 2.10 plots the baud spaced equalizer output y versus time. Initially the equalizer output is "smeared" over the range from -2 to 2. As tap adaptation takes place the smearing is reduced, appearing finally as very tight clusters about the true alphabet member values. Here, the equalizer has removed ISI to allow source sequence recovery by the use of a quantizer (nearest-neighbor decision device).

Figures 2.11, and 2.12 show the equalizer tap vector (D), and combined channel-equalizer tap vector (H) parametrization trajectories, respectively. The final combined channel-equalizer parametrization is plotted in Figure 2.13 demonstrating that the achieved system is very nearly a delay.

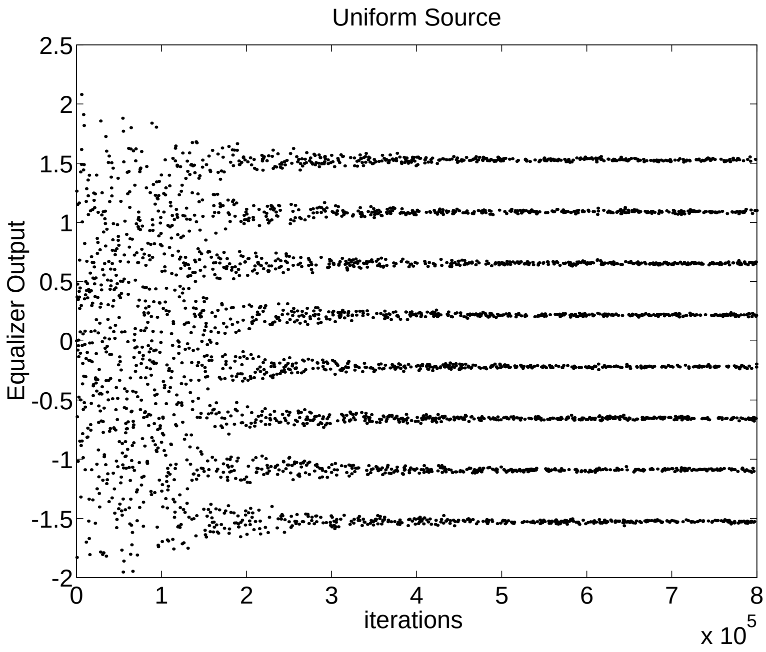

Figure 2.10: Example A: Equalizer Output

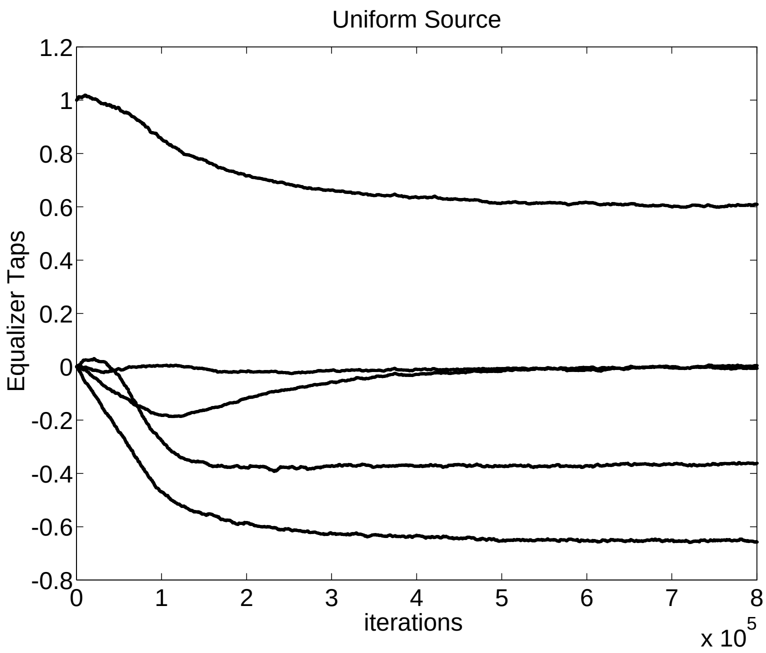

Figure 2.11: Example A: Equalizer Tap Trajectories

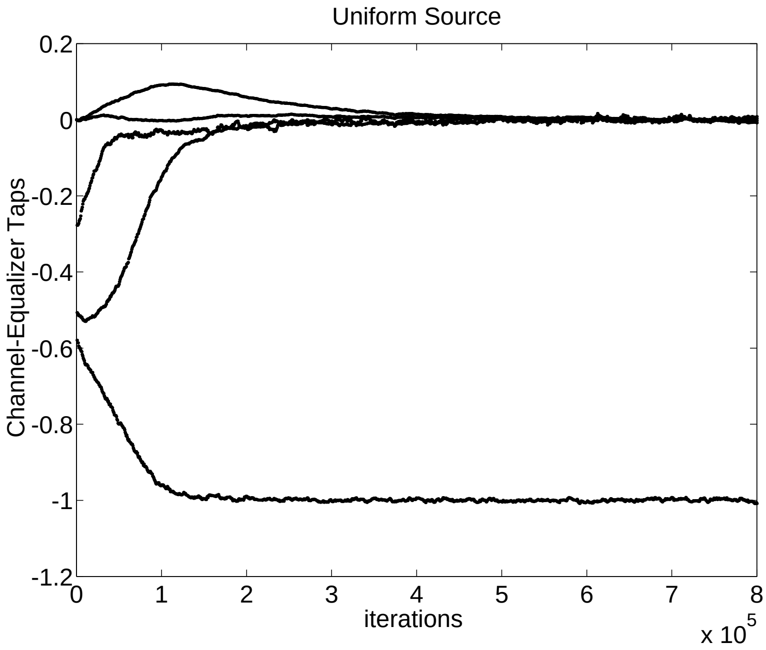

Figure 2.12: Example A: Channel-Equalizer Parameter Trajectories

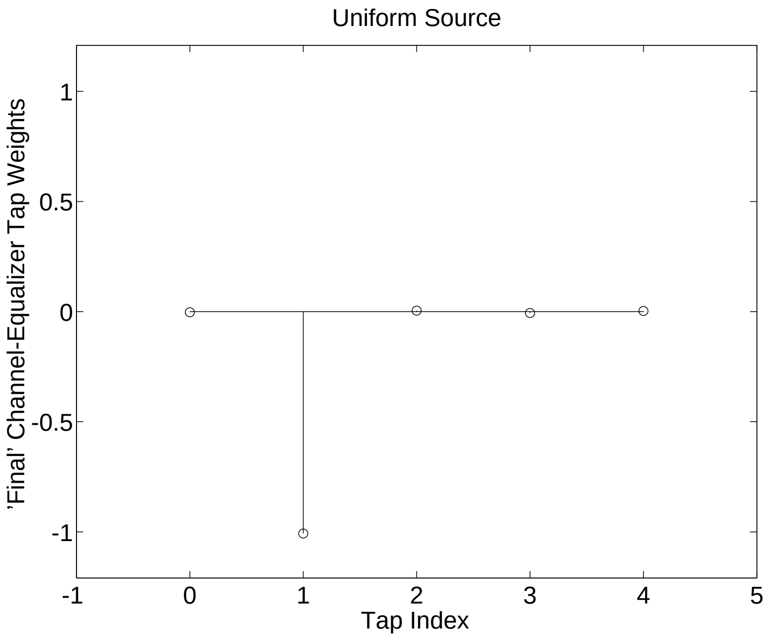

Figure 2.13: Example A: Chan. -Eq. Parametrization after 800,000 iterations

We introduce a quantitative measure of ISI, introducing $\mathcal{ISI}$ as,

$$\mathcal{ISI} \;=\; \frac{\sum_i |h_i| - \max_i |h_i|}{\max_i |h_i|} \tag{2.20}$$

also known as the *peak distortion* [33]. This a measure of the maximum intersymbol interference present. For an m-PAM source, when $\mathcal{ISI} < \frac{1}{m-1}$ then the channel equalizer combination is considered to be "open-eye". That is, the decision device will successfully reconstruct the source in the absence of noise. Figure 2.14 shows the evolution of $\mathcal{ISI}$ during equalizer adaption. This example demonstrates a fractionally spaced equalizer update by CMA successfully removing ISI.

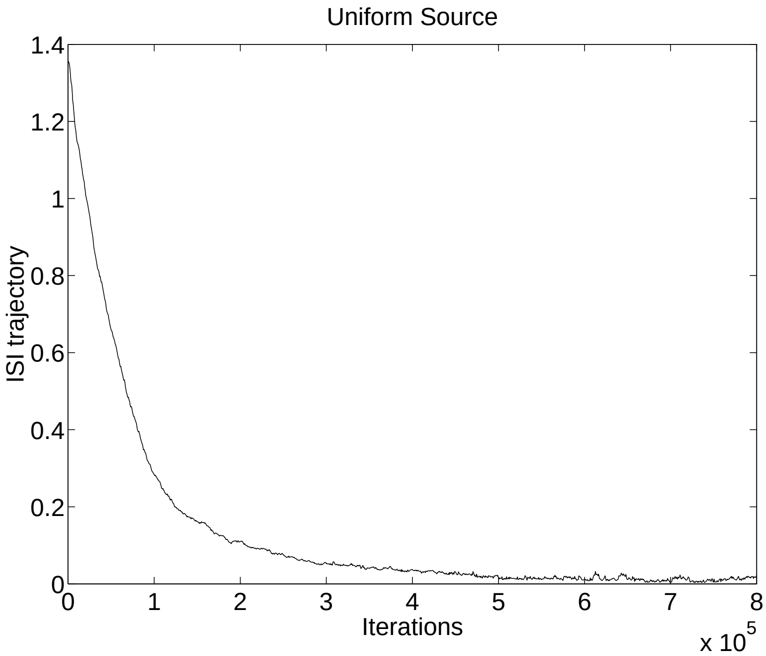

Figure 2.14: Example A: $\mathcal{ISI}$ evolution

2.3 Thesis Focus

The review of previous work regarding FSEs and CMA, details a set of conditions which guarantee perfectly equalizing asymptotic performance of FSE-CMA; appropriate equalizer length, sub-channel disparity (no common channel zeros), no channel noise, and uniformly distributed independent source sequence. The focus of the thesis work investigates what happens under violation of the last condition. Results regarding global convergence of CMA ([50],[29] — for finite order fractionally spaced equalizers ; [30], [34], [6] — for infinite order baud spaced equalizers) critically hinge on the assumption that the source is iid, and often further assumed to be uniformly distributed. The limitations of analysis which requires iid source may have limited utility when the (uniformly) iid assumption is invalid. To wit,

> "most important ... is ... what happens if the input sequence is not white. Little work has been done on this matter. Usually one tries known methods and hopes they are robust enough to perform acceptably even if the basic assumption of independence is not met. Often this approach works, indeed, but we cannot predict its performance."
> — *Bellini* [35]

Specifically, we investigate the effect of relaxing assumptions on distributions and temporal correlations on CMA convergence. The investigation focuses determining CMA behavior by identification of CMA stationary points locations. This work follows two avenues.

First, we investigate effects of the distribution that the independent source is drawn from. Through standard linear algebra, we show that the non-degenerate stationary point parametrization of CMA remains unchanged for any independent source distribution. However, the stationary point categorization (stable, unstable, or saddle) may change. Such categorization relies strictly on a single quantity, namely the source *kurtosis*. New results here include: evaluation of the Hessian at all stationary points, quantification of the error surface *structure*, presentation of the loss of error surface curvature due to source distributions (analytic, and simulations which demonstrate effect on convergence time). Relations between these new results and previously known results found in the literature are noted.

Next, we explore case of temporal source correlation. As this situation is not amenable to the standard techniques used in the iid source case, more novel techniques were applied. A bridge is formed between the iid and temporally correlated source cases by regarding the topology of the error surface. The new results here provide a framework in which to view the correlated case, and recognize limits to which source correlation can effect CMA behavior. More quantitative descriptions of stationary points locations under source correlation are attempted through use of algebraic geometry techniques (Groebner Bases). The limited success of these techniques lead to the use of some numerical *continuation methods* to identify stationary points under specific sources. From these methods, examples of CMA (mis-)behavior are identified. Furthermore, a semi-quantitative view of the robustness of CMA under source correlation is gleaned from the accumulated data.

Two motivational examples are offered before presentation of the mathematical formulation of the problem addressed and the new results obtained. Each of the examples delineates CMA from the "proper" behavior of Example A. Effects of the distribution of an iid source on CMA's convergent behavior is depicted in Examples B, while effects of source correlation are found in Example C.

2.3.1 Source Distributions

Chapter 4 considers the stationary point locations of CMA under the assumption of independence of the source sequence. Later, the effects of the source distribution are considered in terms of the error surface curvature.

Example B: As a preview, consider the following numerical example of CMA. Here, all parameters are the same as in Example A, except that the probabilities of occurrence of alphabet members are unequal; $p(\pm\Delta) = 0.75$, $p(\pm 3\Delta) = 0.05$, $p(\pm 5\Delta) = 0.05$, $p(\pm 7\Delta) = 0.15$ (yielding a *leptokurtic* source — a term to be defined late). Figures 2.15, 2.16, and 2.17 display the results below which demonstrate dismal performance. In fact, in this case CMA yields ISI enhancement! A detailed analysis of the situation is presented in Chapter 4.

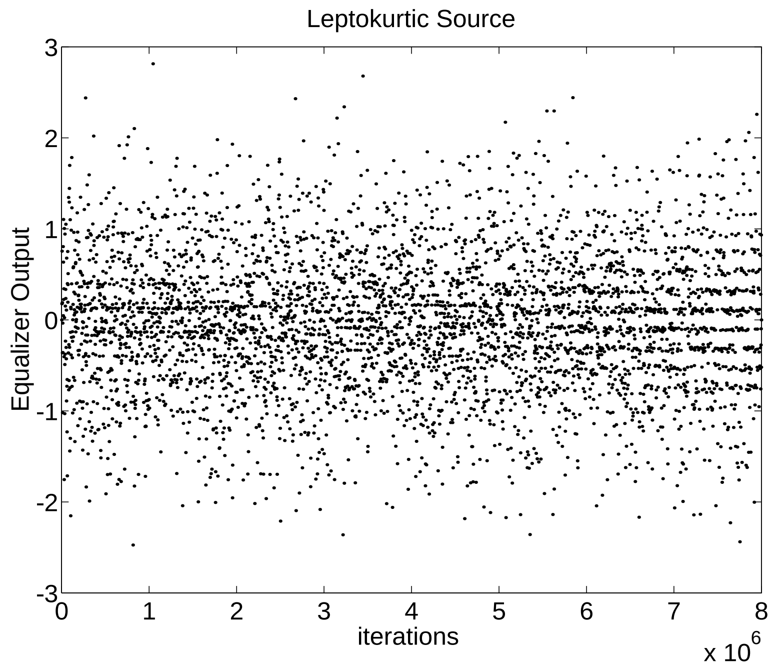

Figure 2.15: Example B: Equalizer Output

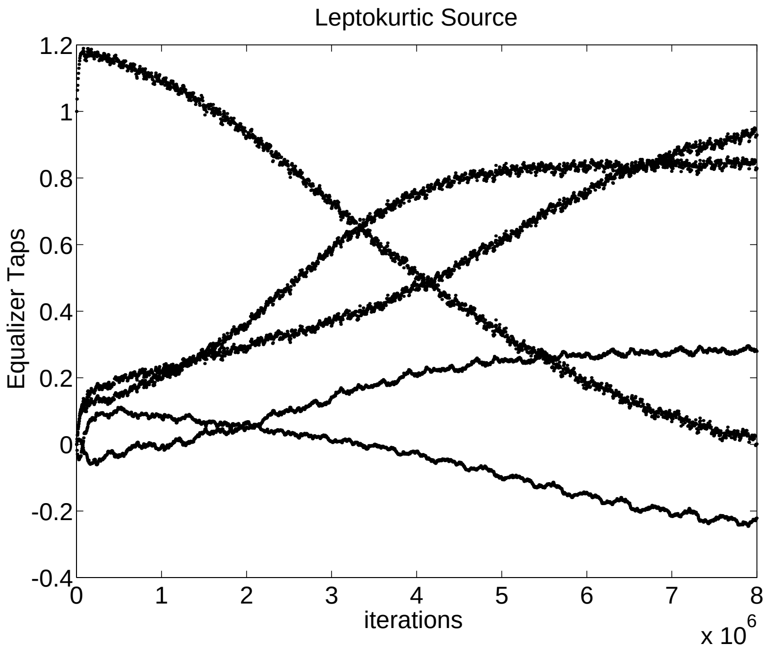

Figure 2.16: Example B: Equalizer Tap Trajectories

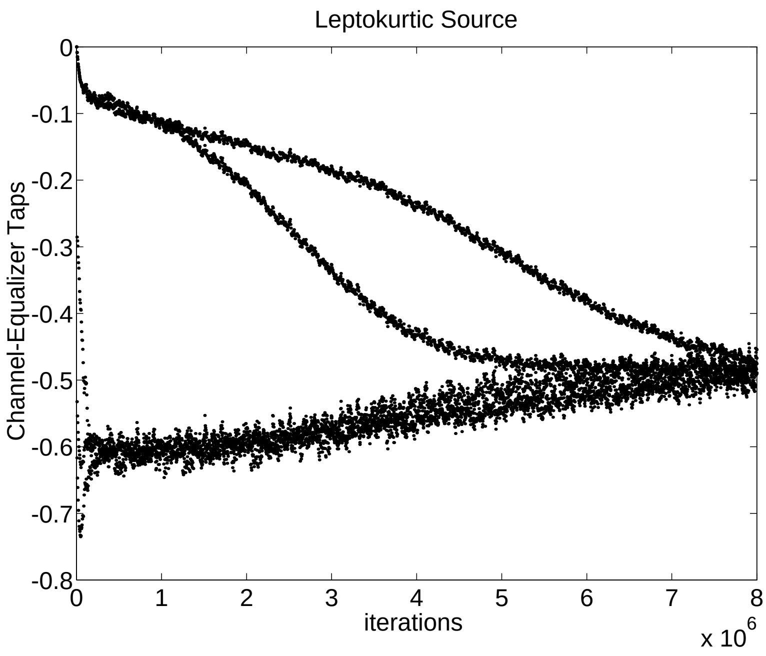

Figure 2.17: Example B: System Parameter Trajectories

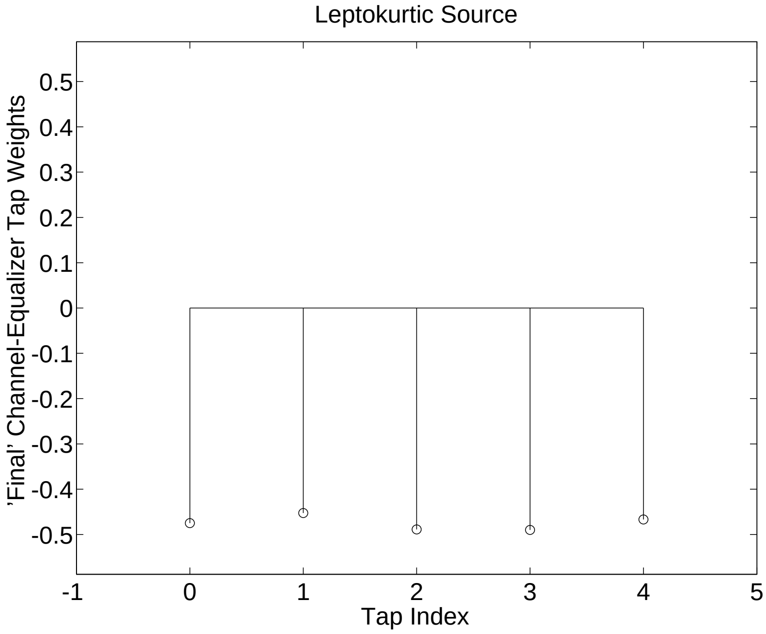

Figure 2.18: Example B: Chan. -Eq. Parametrization after 800,000 iterations

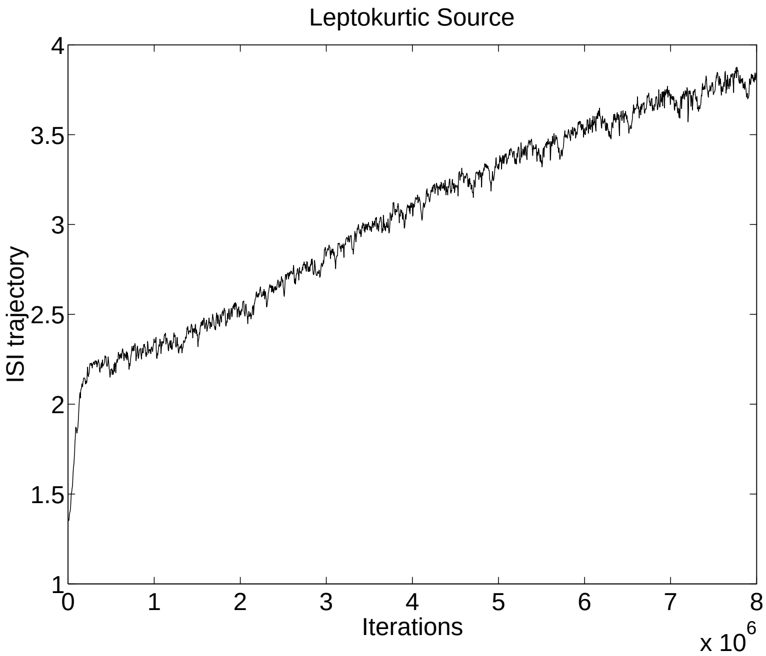

Figure 2.19: Example B: $\mathcal{ISI}$ evolution

Also in Chapter 4 is a discussion on more subtle effects of the source distribution which, while yielding acceptable ISI reduction, reduce error surface curvature resulting in slower equalizer convergence rates. The implication of this will be tradeoff between source coding (which may effect source distributions) and equalizer convergence rates.

2.3.2 Topological Aspects

The other main thesis theme focuses on temporal source correlation. It will be shown that due to the nature of the CMA error function, that source correlation effects may be viewed as a *deformation* of the iid CMA error surface. As deformations are the realm of topology, Chapter 5 looks at some of the topological aspects connected with CMA source correlation. Some general characteristics of CMA under iid source are presented, pulling in relations to Morse Theory, polytopes, and Euler Characteristics. Later these relations to the temporally correlated source case is examined.

2.3.3 Temporal Correlation

Source correlation may have a profound effect on the performance of the CMA blind equalizer.

Example C: Consider a temporally correlated source sequence generated by a Markov model (discussed in Appendix A) under similar parameters as in the earlier presented examples A and B. The deleterious effects are found below in Figures 2.20 2.21 2.22.

Under the chosen Markov source the equalizer output shown never coalesces into bands about the alphabet members, but remain a blur across the values from

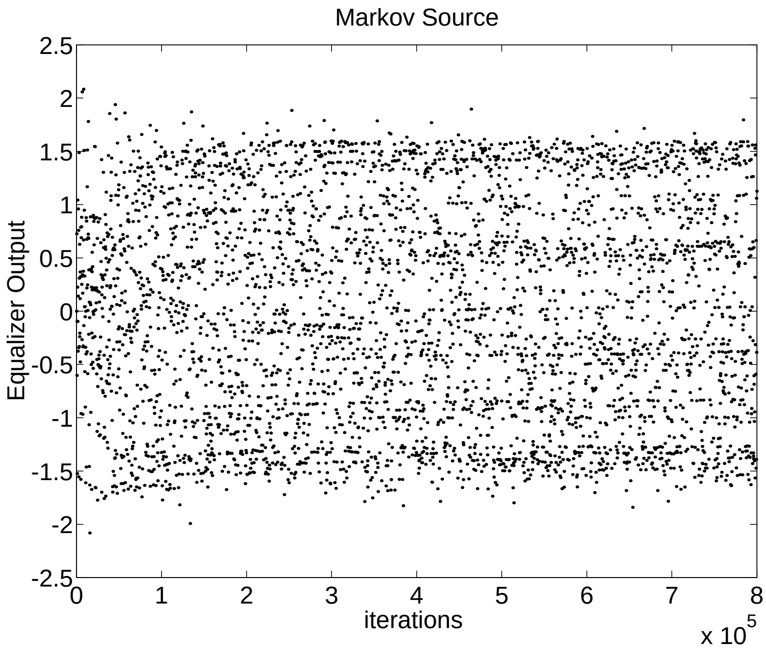

Figure 2.20: Example C: Equalizer Output

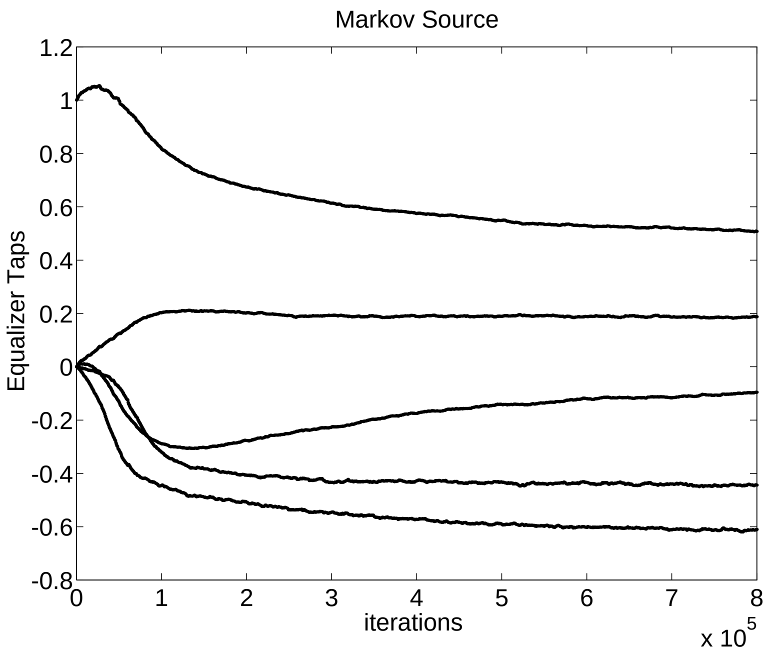

Figure 2.21: Example C: Equalizer Tap Trajectories

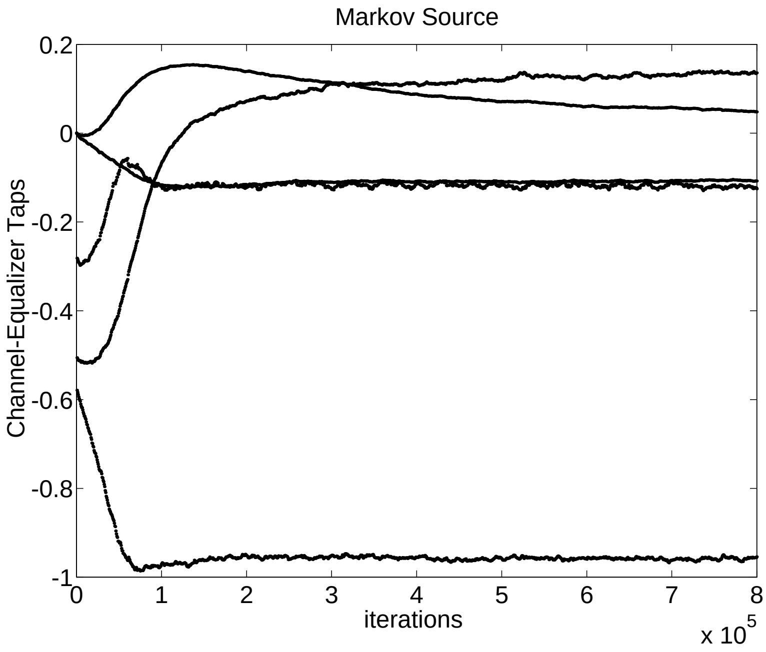

Figure 2.22: Example C: Channel-Equalizer Parameter Trajectories

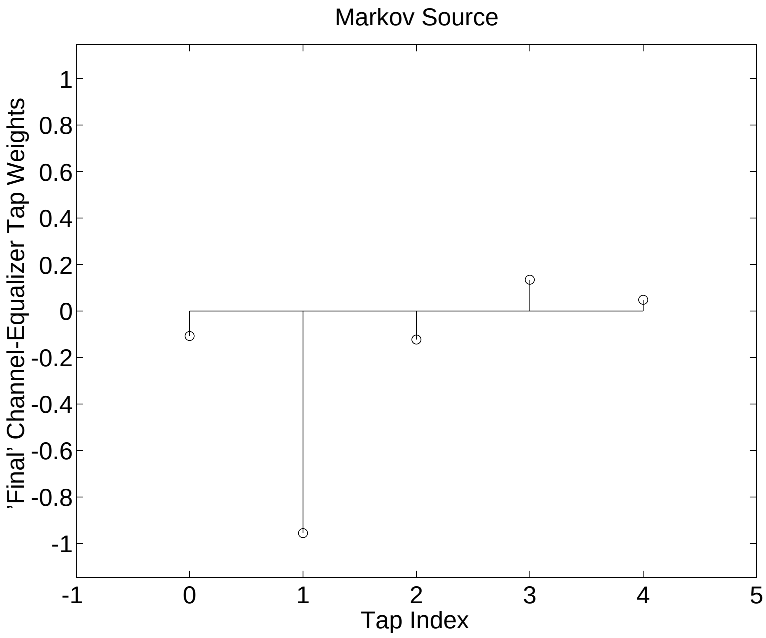

Figure 2.23: Example C: Chan. -Eq. Parametrization after 800,000 iterations

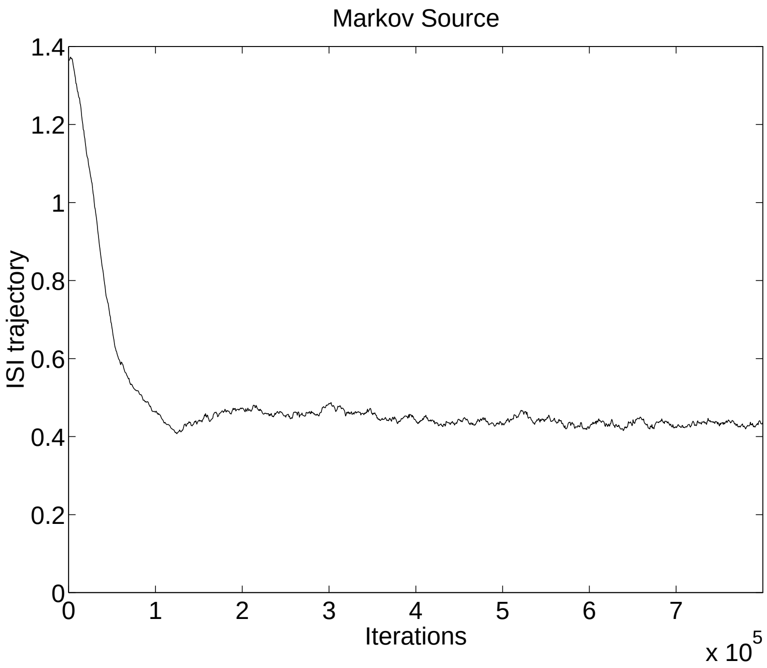

Figure 2.24: Example C: $\mathcal{ISI}$ evolution

-2 to 2 as in Figure 2.20. The system parametrization after 800,000 iteration are seen to have significant ISI(Figure 2.22). (Although such simulations of adaptive systems provide insight to the convergence, due to the slow convergence of such systems, it is often unwise to draw conclusions about the asymptotic convergent parametrizations. However, such poorly performing settings will be later shown to exemplify CMA minima under correlated sources.) The ISI trajectory of Figure 2.24 levels out at about a $\mathcal{ISI} = 0.4$ which is significantly closed eye (a level of $\mathcal{ISI} = \frac{1}{8}$ would be marginally open-eye).

Chapter 6 contains a study of the correlation effects in terms of CMA stationary point locations. Inherently, this is a difficult problem as it requires the solution of a system of multivariate polynomial equations. Techniques applied to this problem are drawn from recent results in the algebraic geometry community. Namely, *Groebner Basis* techniques are applied. A successful algebraic solution of stationary point parametrizations is shown for a low dimensional case. Unfortunately, for higher dimensional cases their success is limited by the dimensionality of the problem and computational complexity of the Buchberger algorithm associated with Groebner Bases. Furthermore, even when an explicit solution can be found, the number of terms are staggering, making interpretation of the results quite difficult.

Due to this difficulty, a numerical avenue is pursued. Homotopy Methods (or Continuation Methods) are introduced. This method may be used to find *all* stationary points of the CMA error surface given specific correlation statistics. Stationary point computations are performed for two models of temporally correlated sources (e.g. periodic and Markov sources).

Chapter 3

Mathematical Framework

This chapter presents the mathematical framework used throughout this thesis. A discussion of the use and implications of fractional spacing in CMA equalizers is followed by a description of the relevant equations used in studying CMA. Behavior of the algorithm can be understood through a study of the error surface. As asymptotic behavior may be attributed to the location of stable stationary points, a system of equations which define stationary points of CMA is presented. Study of this system forms the main avenue of investigation. Such analysis of adaptive algorithms and their convergent points is often pursued through the investigation of stationary points and Hessian evaluation and may be found in many of the texts on the subject applied to a variety of adaptive algorithms.

3.1 Specifically FSE-CMA

The work herein addresses specifically the use of fractionally spaced CMA equalizers assumed operating under the condition of equalizability. Such an assumption allows analysis of CMA to take place in the combined channel-equalizer space (H-

space) rather than in strictly the equalizer tap space (D-space). The importance of this is that our results are general to any channel (meeting equalizability). Without such an assumption, since all of H is then not reachable, any results would be germane only to a particular choice of channel.

Also, although CMA is often used for two-dimensional signal constellations (i.e. complex alphabet members), we limit our discussion to situations using strictly real alphabets (e.g. M-PAM — Pulse Amplitude Modulation with M discrete amplitude values). This is fairly common in the literature of CMA analysis. The major motivation behind our limitation to strictly real alphabets is to maintain differentiability of the cost function and keep notation simple. (Strictly speaking the absolute value operator in (2.15) does not meet the Cauchy-Riemann criterion and hence is not differentiable. To work around this it is possible to regard analysis as taking place in $\mathcal{R}^{2N}$ instead of $\mathcal{C}^N$ with a change in the cost function definition, but this carries excessive notational baggage. A discussion of this issue is found in [59].) Instead of viewing the FSE as a multirate, mixed-time base systems (continuous-time channel, fractionally-spaced equalizer with desampled output) we use the multichannel baud rate description as in Figure 2.9.

3.2 CMA Cost: Source and Channel-Equalizer Taps

The CMA cost as a function of equalizer output y under the use of a strictly real alphabet is developed here. It is noted that in the strictly real alphabet case that the term $|y|^2$ in (2.15) may be replaced by y^2 yielding,

$$J = \frac{1}{4}\mathrm{E}\left\{\left(y^2(k) - \gamma\right)^2\right\} \tag{3.1}$$

where $\gamma = \frac{\mathrm{E}\{a^4\}}{\mathrm{E}\{a^2\}}$ for $a \in \{\mathcal{A}\}$ and $\mathcal{A}$ is a strictly real alphabet. Note that the phase ambiguity of the complex alphabet case simplifies to a sign ambiguity here. With the combined channel-equalizer tap weights defined as $H = [\, h_0 \quad h_1 \quad \ldots \quad h_n \,]^{\mathrm{T}}$ and $S(k) = [\, s(k) \quad s(k-1) \quad \ldots \quad s(k-n) \,]^{\mathrm{T}}$ as the column vector containing source sequence elements, then we have $y(k) = H^{\mathrm{T}} S(k)$. Rewriting (3.1) in terms of the combined channel-equalizer parametrization yields,

$$J \;=\; \frac{1}{4}\mathrm{E}\left\{((H^{\mathrm{T}} S(k))^2 - \gamma)^2\right\}. \tag{3.2}$$

As H is the combined channel-equalizer response, it may be written as the matrix product of the L-multichannel convolution matrix $\mathbb{C}$ and the equalizer tap weight vector D as,

$$H = \mathbb{C}^{\mathrm{T}} D \tag{3.3}$$

where,

$$\mathbb{C} = \begin{bmatrix} c_0^{(0)} & \ldots & c_n^{(0)} & & \\ \vdots & & \vdots & & \\ c_0^{(L-1)} & \ldots & c_n^{(L-1)} & & \\ & \ddots & & \ddots & \\ & & c_0^{(0)} & \ldots & c_n^{(0)} \\ & & \vdots & & \vdots \\ & & c_0^{(L-1)} & \ldots & c_n^{(L-1)} \end{bmatrix} \tag{3.4}$$

and $[\, c_0^{(i)} \quad c_1^{(i)} \quad \ldots \quad c_n^{(i)} \,]$ is the baud spaced impulse response of sub-channel i. Now, the CMA cost function may be written in terms of the channel and equalizer parametrizations as

$$J \;=\; \frac{1}{4}\mathrm{E}\left\{\left(((\mathbb{C}^{\mathrm{T}} D)^{\mathrm{T}} S(k))^2 - \gamma\right)^2\right\}. \tag{3.5}$$

Invoking the assumptions of equalizability, yields the matrix $\mathbb{C}$ to be full rank [29], meaning that all of H-space is reachable by choice of equalizer D.

3.3 Formulation of Stationary Points

3.3.1 Use of Equalizability Condition

The error surface stationary points are given by $\frac{\partial J}{\partial D} = \vec{0}$. With $H = \mathbb{C}^{\mathrm{T}} D$, we then have $y(k) = H^{\mathrm{T}} S(k) = D^{\mathrm{T}} \mathbb{C} S(k)$, and may write,

$$\begin{aligned} \frac{\partial J}{\partial D} &= \mathrm{E}\left\{\left((D^{\mathrm{T}}\mathbb{C}S)^3 - \gamma D^{\mathrm{T}}\mathbb{C}S\right)\mathbb{C}S\right\} && (3.6) \\ &= \mathbb{C}\mathrm{E}\left\{\left((H^{\mathrm{T}}S)^3 - \gamma H^{\mathrm{T}}S\right)S\right\}. && (3.7) \end{aligned}$$

With $\mathbb{C}$ full column rank (i.e. lacking a non-trivial right nullspace), $\frac{\partial J}{\partial D} = \vec{0}$ necessarily implies

$$\mathrm{E}\left\{\left((H^{\mathrm{T}}S)^3 - \gamma H^{\mathrm{T}}S\right)S\right\} = \vec{0}, \tag{3.8}$$

obtaining $\frac{\partial J}{\partial D} = \vec{0} \Leftrightarrow \frac{\partial J}{\partial H} = \vec{0}$. Hence, the stationary points of the FSE-CMA equalizer correspond to stationary parametrizations of the global system, and are affected only by the source statistics. To see this recognize that (3.7) is a function of the channel ($\mathbb{C}$), the combined channel-equalizer parametrization (H), and the source statistics (fourth and second moments of S). But, (3.8) removes any consequence of the channel (assuming equalizability) leaving the combined parametrization (H) affected only by source statistics. Due to this we focus the error surface investigation in terms of the global channel-equalizer system or H space.

3.3.2 H-Space

There are a variety of reasons to investigate the error surface in terms of H space. First, it is precisely the *combined* channel-equalizer parametrization which determines the equalizer output which is then used to estimate the source sequence. In turn, any meaningful performance metric must be considered in terms of the equalizer output (e.g. bit error rate, ISI level).

More importantly, in certain situations there may be a variety of different equalizer parametrizations that yield identical combined channel-equalizer responses. In [29] it is noted that in cases where the equalizer time support sufficiently exceeds the channel time support, a dense subspace in D corresponds to a point in H space. As such, it is difficult to discuss stationary *points* in equalizer space.

3.3.3 Stationary Points in H-Space

Given perfect equalizability, differentiation of the cost function with respect to the combined channel-equalizer parametrization H and equating with zero defines the CMA stationary points in terms of the combined channel-equalizer parametrization. Expanding the inner products of (3.8) for clarity we have,

$$\frac{\partial J}{\partial H} = \mathrm{E}\left\{\Big((s(k)h_0+\ldots+s(k-n)h_n)^3 - \gamma(s(k)h_0+\ldots+s(k-n)h_n)\Big)\begin{bmatrix} s(k) \\ \vdots \\ s(k-n) \end{bmatrix}\right\}.$$

Taking the expectation operator with respect to the source regressor elements s_i leads to $n+1$ multivariate polynomial equations in H space with monomials having coefficients given by the fourth and second moments of the source signal. Denote these moments of a symmetrically distributed source as,

$$\begin{aligned} \mathcal{R}^{\substack{i\\j}}_{\substack{k\\ \ell}} &= \mathrm{E}\left\{s(m-i)s(m-j)s(m-k)s(m-\ell)\right\} \\ \mathcal{R}^i_j &= \mathrm{E}\left\{s(m-i)s(m-j)\right\}. \end{aligned} \tag{3.9}$$

We are assuming a symmetric distribution wherein $\mathrm{E}\{s\} = \mathrm{E}\left\{s^3\right\} = 0$. It should be noted that since we are considering correlations of stationary processes, keeping all four (two) lag indices for the fourth (second) moments is unnecessary. However, these indices are kept here since they aid in showing the structure of the resulting system of equations.

The resulting system of equations F may then be written as

$$F(H) = \begin{bmatrix} f_0(H) \\ f_1(H) \\ \vdots \\ f_n(H) \end{bmatrix} = \begin{bmatrix} \sum_i \mathcal{R}^{\substack{0\\i}}_{\substack{i\\i}} h_i^3 + 3\sum_{i\neq j} \mathcal{R}^{\substack{0\\i}}_{\substack{i\\j}} h_i^2 h_j + \sum_{i\neq j\neq k} \mathcal{R}^{\substack{0\\i}}_{\substack{j\\k}} h_i h_j h_k - \gamma \sum_i \mathcal{R}^0_i h_i \\ \\ \sum_i \mathcal{R}^{\substack{1\\i}}_{\substack{i\\i}} h_i^3 + 3\sum_{i\neq j} \mathcal{R}^{\substack{1\\i}}_{\substack{i\\j}} h_i^2 h_j + \sum_{i\neq j\neq k} \mathcal{R}^{\substack{1\\i}}_{\substack{j\\k}} h_i h_j h_k - \gamma \sum_i \mathcal{R}^1_i h_i \\ \vdots \\ \sum_i \mathcal{R}^{\substack{n\\i}}_{\substack{i\\i}} h_i^3 + 3\sum_{i\neq j} \mathcal{R}^{\substack{n\\i}}_{\substack{i\\j}} h_i^2 h_j + \sum_{i\neq j\neq k} \mathcal{R}^{\substack{n\\i}}_{\substack{j\\k}} h_i h_j h_k - \gamma \sum_i \mathcal{R}^n_i h_i \end{bmatrix}. \quad (3.10)$$

Values of H for which $F(H) = \vec{0}$ define the CMA stationary points. For an $n+1$ tap system, this yields a set of $n+1$ equations in the $n+1$ unknowns (h_m, $0 \leq m \leq n$).

3.3.4 Categorization by Hessian

Each of the stationary points (solutions of $F(H)$) may be categorized as a saddle, local minimum, or local maximum of the error surface depending on the eigenvalues of the Hessian matrix evaluated at the stationary point. Calculations similar to those in (3.8) verify that the sign of the eigenvalues of the cost function Hessians with respect to D and H agree. Denote the error surface Hessian by the matrix

$\mathbb{M}$, with

$$\mathbb{M}(i,j) = \frac{\partial f_i}{\partial h_j}. \tag{3.11}$$

i.e.,

$$\mathbb{M} = \begin{bmatrix} \frac{\partial f_0}{\partial h_0} & \frac{\partial f_0}{\partial h_1} & \cdots & \frac{\partial f_0}{\partial h_n} \\ \frac{\partial f_1}{\partial h_0} & \frac{\partial f_1}{\partial h_1} & \cdots & \frac{\partial f_1}{\partial h_n} \\ \vdots & \vdots & \ddots & \vdots \\ \frac{\partial f_n}{\partial h_0} & \frac{\partial f_n}{\partial h_1} & \cdots & \frac{\partial f_n}{\partial h_n} \end{bmatrix}. \tag{3.12}$$

For a local minima (maxima), $\mathbb{M}$ is positive (negative) definite. $\mathbb{M}$ having both positive and negative eigenvalues denotes a saddle point. In cases where $\mathbb{M}$ is singular, the stationary points are degenerate (i.e. a dense neighborhood satisfies $\frac{\partial J}{\partial H} = \vec{0}$).

Chapter 4

IID Source Case: Distributional Aspects

In this chapter, we assume that source symbols are drawn independently from some distribution (iid). The system of equations defining the stationary points is solved. Classification of the stationary points by the number of non-zero elements in the tap vector is presented. Categorization of stationary points into minima, saddles, and maxima is shown to be dependent on class membership and the source *kurtosis* (a quantity to be introduced). Analytic results are meshed with computer simulations describing the disappearance of error surface curvature (and related equalizer convergence rate issues) as the source kurtosis approaches that of a Gaussian distribution.

4.1 Kurtosis

A useful concept that appears repeatedly in the stability analysis of the CMA stationary points contained herein, having a profound effect on the error surface, is the dimensionless quantity known as *kurtosis* [1]. Denote the central moments by

$$\mathrm{M}_n = \mathrm{E}\left\{(x-\mu)^n\right\}$$

where $\mu = \mathrm{E}\{x\}$. Then kurtosis is defined to be the ratio,

$$\kappa_{\mathrm{X}} = \frac{\mathrm{M}_4}{\mathrm{M}_2^2} . \tag{4.1}$$

In a sense, kurtosis forms a measure of the "peakedness" of the distribution. The minimum possible kurtosis value is $\kappa = 1$ which corresponds to a symmetric uniform distribution of only two values (i.e. a binary phase shift keying (BPSK) source). The continuous uniform distribution has $\kappa = 1.8$. The Gaussian distribution has $\kappa = 3$ and is regarded as forming the boundary between platykurtic (low kurtosis, $\kappa_{\mathrm{S}} < 3$) distributions and leptokurtic (high kurtosis, $\kappa_{\mathrm{S}} > 3$) distributions.

4.2 CMA Cost Function in terms of kurtosis

The importance of kurtosis in CMA can be seen by rewriting the CMA cost function in terms of the equalizer output kurtosis

$$\begin{aligned}
J_{\mathrm{CMA}} &= \frac{1}{4}\mathrm{E}\left\{(y^2-\gamma)^2\right\} \\
&= \frac{1}{4}\left(\mathrm{E}\left\{y^4\right\} - 2\gamma\mathrm{E}\left\{y^2\right\} + \gamma^2\right) \\
&= \frac{1}{4}\left(\kappa_{\mathrm{Y}}\mathrm{E}\left\{y^2\right\}^2 - 2\gamma\mathrm{E}\left\{y^2\right\} + \gamma^2\right) \\
&= \frac{1}{4}\left((\kappa_{\mathrm{Y}}-1)\mathrm{E}\left\{y^2\right\}^2 + (\mathrm{E}\left\{y^2\right\} - \gamma)^2\right) \qquad (4.2)
\end{aligned}$$

[1]The reader is cautioned that some texts define kurtosis a bit differently as $\kappa = \frac{\mathrm{M}_4}{\mathrm{M}_2^2} - 3$. We shall however follow the definition above as found in [14].

4.3 Tap Constraints

Note that for the iid source all the correlation coefficients of (3.10) are zero, except $\mathcal{R}^{\substack{i\\i}}_{\substack{i\\i}} = \mathrm{E}\left\{s^4\right\}$, $\mathcal{R}^{\substack{i\\i}}_{\substack{j\\j}} = (\mathrm{E}\left\{s^2\right\})^2$ for $i \neq j$ and $\mathcal{R}^{i}_{i} = \mathrm{E}\left\{s^2\right\}$. Defining the zero mean source sequence moments by,

$$\mathrm{M}_n \quad = \quad \mathrm{E}\left\{s^n\right\} \tag{4.3}$$

yields (3.10) as

$$\begin{bmatrix} \mathrm{M}_4 h_0^3 + 3\mathrm{M}_2^2 \sum\limits_{i \neq 0} h_i^2 h_0 - \gamma \mathrm{M}_2 h_0 \\ \\ \mathrm{M}_4 h_1^3 + 3\mathrm{M}_2^2 \sum\limits_{i \neq 1} h_i^2 h_1 - \gamma \mathrm{M}_2 h_1 \\ \\ \vdots \\ \\ \mathrm{M}_4 h_n^3 + 3\mathrm{M}_2^2 \sum\limits_{i \neq n} h_i^2 h_n - \gamma \mathrm{M}_2 h_n \end{bmatrix} = \begin{bmatrix} 0 \\ \\ 0 \\ \vdots \\ \\ 0 \end{bmatrix}. \tag{4.4}$$

Each of the $n+1$ equations of F can be rewritten as f_m, for $0 \leq m \leq n$,

$$\begin{aligned} f_m &= \mathrm{M}_4 h_m^3 + 3\mathrm{M}_2^2 \sum_{i \neq m} h_i^2 h_m - \gamma \mathrm{M}_2 h_m \\ &= \mathrm{M}_2^2 h_m \left(\kappa_{\mathrm{S}} h_m^2 + 3 \sum_{i \neq m} h_i^2 - \kappa_{\mathrm{S}} \right) \end{aligned} \tag{4.5}$$

The CMA stationary points are the values of H solving each $f_m = 0$. It is seen that any $h_m = 0$ trivially solves $f_m = 0$. So, only f_m for which $h_m \neq 0$ need be further considered. Now, for any $h_m \neq 0$ we have the condition,

$$\kappa_{\mathrm{S}} h_m^2 + 3 \sum_{i \neq m} h_i^2 - \kappa_{\mathrm{S}} \quad = \quad 0. \tag{4.6}$$

In the case that $\kappa_{\mathrm{S}} = 3$, all the f_m equations are the same. That is, our system is degenerate and we truly have only one equation to satisfy which has the solution $\sum_i h_i^2 = 1$. In this case, the stationary points in H are not a discrete set but a dense set corresponding to a unit sphere. Thus, for $\kappa_{\mathrm{S}} = 3$ CMA adaptation will converge to this sphere and then will wander about the sphere.

Alternatively, when $\kappa_{\mathrm{S}} \neq 3$ each non-zero h_m in a solution set must solve *each* equation f_m, we then have that the value of h_m^2 for all non-zero h_m in this solution must be the same (i.e. all h_m have the same magnitude). This is a generalization of a similar result in [38] pertaining to a uniformly distributed BPSK source. Also found in [38] is a classification of stability of the equalizer stationary points. All stationary points are shown to reside in the nullspace of one of three matrices. The stability of a solution is determined by which of the three nullspaces the solution resides. Here, the classification concept is also used, albeit in a different manner. Herein classification takes place in the combined channel-equalizer space (H-space) and is extended, defining many more classes which allows a finer view of the structure of the solutions.

4.4 Classes of Solutions

For the iid source case, the *value* of each non-zero h_m will depend on the total *number* of non-zero elements of H for any $F(H) = \vec{0}$. A useful construct is to divide the set of solutions of (3.10) into classes. Define the class,

$$\mathcal{C}_N = \left\{ H : F(H) = \vec{0} \text{ where } H \text{ has exactly} N \text{ non-zero elements} \right\}. \quad (4.7)$$

Furthermore, denote the size of the class (i.e. the number of its members) by $|\mathcal{C}_N|$.

Of the total $n+1$ elements of H, since each of its N non-zero elements may have one of two values and there are $\binom{n+1}{N}$ ways to group N elements we have,

$$|\mathcal{C}_N| = 2^N \binom{n+1}{N}. \tag{4.8}$$

Thus, the total number of CMA stationary points under iid source is 3^{n+1} (using the binomial theorem, $\sum_{i=0}^{n+1} |\mathcal{C}_i| = \sum_{i=0}^{n+1} 2^i \binom{n+1}{i} = \sum_{i=0}^{n+1} 2^i 1^{n-i} \binom{n+1}{i} = (2+1)^{n+1} = 3^{(n+1)}$(or from recognizing each of the $n+1$ elements may take one of 3 values, hence 3^{n+1}.

To see that class membership defines the magnitude of the non-zero taps, note that for $H \in \mathcal{C}_N$ (4.6) becomes

$$\kappa_S h_m^2 + 3(N-1)h_i^2 - \kappa_S \;=\; 0 \tag{4.9}$$

yielding

$$h_m \;=\; \begin{cases} 0 \\ \pm\sqrt{\frac{\kappa_S}{\kappa_S - 3 + 3N}} \end{cases} \qquad 0 \le m \le n. \tag{4.10}$$

4.5 Categorization of Solutions by Hessian

Determination of the Hessian of the CMA error surface for the diagonal elements yields

$$\begin{aligned} \mathbb{M}(m,m) = \frac{\partial f_m}{\partial h_m} &= \mathrm{M}_2^2 \frac{\partial}{\partial h_m}\left(\kappa_S h_m^3 + 3\sum_{i \neq m} h_i^2 h_m - \kappa_S h_m\right) \\ &= \mathrm{M}_2^2 \left(3\kappa_S h_m^2 + 3\sum_{i \neq m} h_i^2 - \kappa_S\right). \end{aligned} \tag{4.11}$$

Similarly for the off-diagonal elements ($m \neq n$),

$$\begin{aligned} \mathbb{M}(m,n) = \frac{\partial f_m}{\partial h_n} &= \mathrm{M}_2^2 \frac{\partial}{\partial h_n}\left(\kappa_S h_m^3 + 3\sum_{i \neq m} h_i^2 h_m - \kappa_S h_m\right) \\ &= 6\mathrm{M}_2^2 h_n h_m. \end{aligned} \tag{4.12}$$

Evaluating these expressions at a stationary point for the case $H \in \mathcal{C}_N$ we consider the three cases $\mathbb{M}(m,m)$ with $h_m \neq 0$, $\mathbb{M}(m,m)$ with $h_m = 0$, and $\mathbb{M}(n,m)$ with $m \neq n$.

All the elements of $\mathbb{M}$ evaluated at a stationary point in $\mathcal{C}_N$ for $N \geq 1$ contain a common factor of $\mathrm{M}_2^2\left(\frac{\kappa_\mathrm{S}}{\kappa_\mathrm{S}-3+3N}\right)$. We factor this out to simplify notation, introducing $\widehat{\mathbb{M}}$ related by,

$$\mathbb{M} \;=\; \mathrm{M}_2^2\left(\frac{\kappa_\mathrm{S}}{\kappa_\mathrm{S}-3+3N}\right)\widehat{\mathbb{M}} \tag{4.13}$$

Notice that the common factor is strictly positive for $N \geq 1$, thus the signs of the eigenvalues of $\mathbb{M}$ and $\widehat{\mathbb{M}}$ agree for $H \in \mathcal{C}_N$ with $N \geq 1$. The diagonal elements $\widehat{\mathbb{M}}$ may be described by,

$$\widehat{\mathbb{M}}(m,m) \;=\; \begin{cases} 3-\kappa_\mathrm{S}, & h_m = 0, \\ 2\kappa_\mathrm{S}, & h_m \neq 0. \end{cases} \tag{4.14}$$

Off-diagonal terms are,

$$\widehat{\mathbb{M}}(m,n) \;=\; \begin{cases} 6, & h_m = h_n \neq 0, \\ -6, & h_m = -h_n \neq 0, \\ 0, & \text{else.} \end{cases} \tag{4.15}$$

The eigenvalues of $\widehat{\mathbb{M}}$ are merely scaled versions of the eigenvalues of $\mathbb{M}$. In this sense, we investigate the eigenvalues of $\widehat{\mathbb{M}}$ to ascertain categorization of a stationary point.

4.5.1 Stationary Point Categorization by Class Membership

$H \in \mathcal{C}_0$

For $H \in \mathcal{C}_0$ (i.e. the origin), we have $\mathbb{M} = -\kappa_\mathrm{S}\mathbb{I}$, where $\mathbb{I}$ is the identity matrix. Since κ_S is strictly positive, $\mathbb{M}$ is negative definite and $H = \vec{0}$ is a local maximum.

$H \in \mathcal{C}_1$

In the case of a single non-zero tap element, $\widehat{\mathbb{M}}$ is a diagonal matrix with elements given by (4.14). The diagonal entry corresponding to the single non-zero h_m is $2\kappa_{\mathrm{S}}$ (which is strictly positive). The remaining diagonal entries have value $3-\kappa_{\mathrm{S}}$. The sign of these entries (and hence, the corresponding eigenvalues) are determined by the kurtosis of the source signal, κ_{S}. The cases are:

> $\boldsymbol{\kappa_{\mathrm{S}} < 3}$: For platykurtic source distributions, all diagonal entries of $\widehat{\mathbb{M}}$ are positive and these channel-equalizers parametrizations are stable (i.e. local minima).
>
> $\boldsymbol{\kappa_{\mathrm{S}} > 3}$: For leptokurtic source distributions, there is the one positive diagonal entry of $2\kappa_{\mathrm{S}}$ and all remaining diagonal entries of $\widehat{\mathbb{M}}$ are $3-\kappa_{\mathrm{S}}$ which are negative and these parametrizations are saddle points (i.e. 1 positive eigenvalue, rest negative).

$H \in \mathcal{C}_N, \quad 2 \leq N \leq n$

Stationary points in this class are found to be saddle points, regardless of the distribution of the iid source. To demonstrate this, we will first define a few terms and note some properties of $\widehat{\mathbb{M}}$. Define the ordered index lists,

$$\mathcal{I} = \{i : h_i \neq 0\} \quad \text{and} \quad \mathcal{O} = \{i : h_i = 0\} \tag{4.16}$$

Concatenating these ordered list, we form $\mathcal{IO}$. That is, $\mathcal{IO}$ lists the ascending indices of the non-zero h_m followed by the ascending indices of the zero valued h_m.

To evaluate the eigenvalues of $\widehat{\mathbb{M}}$ we make use of the fact that similarity transformations do not change the eigenvalues of a matrix. (In other words, for $\mathbb{B} = \mathbb{P}^{-1}\widehat{\mathbb{M}}\mathbb{P}$, then $\mathbb{B}$, and $\widehat{\mathbb{M}}$ have the same eigenvalues.) Furthermore, scaling these by the common factor in (4.13) yields the eigenvalues of $\mathbb{M}$. Form the transformation matrix $\mathbb{P}$ as,

$$\mathbb{P}(m, \mathcal{IO}_m) \quad = \quad \mathrm{sign}(h_{\mathcal{IO}_m}) \tag{4.17}$$

and note that $\mathbb{P}$ is unitary ($\mathbb{P}\mathbb{P}^{\mathrm{T}} = \mathbb{I}$).

A quick example for the case $H^{\mathrm{T}} = \sqrt{\frac{\kappa_{\mathrm{S}}}{\kappa_{\mathrm{S}}+6}}\,[\,0 \quad 1 \quad 1 \quad 0 \quad -1 \quad 0\,]$ follows. The index list is $\mathcal{IO} = \{1, 2, 4, 0, 3, 5\}$. We then write,

$$\mathbb{B} \quad = \quad \mathbb{P}^{-1}\widehat{\mathbb{M}}\mathbb{P} \tag{4.18}$$

as

$$\begin{bmatrix} 2\kappa_{\mathrm{S}} & 6 & 6 & & & \\ 6 & 2\kappa_{\mathrm{S}} & 6 & & & \\ 6 & 6 & 2\kappa_{\mathrm{S}} & & & \\ & & & 3-\kappa_{\mathrm{S}} & 0 & 0 \\ & & & 0 & 3-\kappa_{\mathrm{S}} & 0 \\ & & & 0 & 0 & 3-\kappa_{\mathrm{S}} \end{bmatrix} =$$

$$\mathbb{P}^{-1} \begin{bmatrix} 3-\kappa_{\mathrm{S}} & 0 & 0 & 0 & 0 & 0 \\ 0 & 2\kappa_{\mathrm{S}} & 6 & 0 & -6 & 0 \\ 0 & 6 & 2\kappa_{\mathrm{S}} & 0 & -6 & 0 \\ 0 & 0 & 0 & 3-\kappa_{\mathrm{S}} & 0 & 0 \\ 0 & -6 & -6 & 0 & 2\kappa_{\mathrm{S}} & 0 \\ 0 & 0 & 0 & 0 & 0 & 3-\kappa_{\mathrm{S}} \end{bmatrix} \mathbb{P} \tag{4.19}$$

where

$$\mathbb{P} = \begin{bmatrix} 0 & 1 & 0 & 0 & 0 & 0 \\ 0 & 0 & 1 & 0 & 0 & 0 \\ 0 & 0 & 0 & 0 & -1 & 0 \\ 1 & 0 & 0 & 0 & 0 & 0 \\ 0 & 0 & 0 & 1 & 0 & 0 \\ 0 & 0 & 0 & 0 & 0 & 1 \end{bmatrix} \tag{4.20}$$

For $H \in \mathcal{C}_N$ the similarity transformation of $\widehat{\mathbb{M}}$ into $\mathbb{B}$ yields a block form matrix, wherein one block is $(3 - \kappa_{\text{S}})\mathbb{I}$ of dimension equal to the number of h_m which are zero. The other block is an $N \times N$ circulant matrix with strictly positive elements. Such structure allows easy identification of the eigenvalues. Interestingly, the signs of the eigenvalues of both sub-matrices are determined by the source kurtosis κ_{S}.

Diagonal Sub-Matrix: The diagonal sub-matrix eigenvalues are $3-\kappa_{\text{S}}$. For $\kappa_{\text{S}} < 3$, this sub-matrix is positive definite. However, for $\kappa_{\text{S}} > 3$ we have a negative definite sub-matrix. The case $\kappa_{\text{S}} = 3$, this sub-matrix becomes singular with all elements zero.

Circulant Sub-Matrix: The circulant block's eigenvalues are identified by the Discrete Fourier Transform (DFT) of a column (a well-known property of circulant matrices, see [74]). Thus,

$$\begin{aligned} \text{Upper Block Eigenvalues} &= \mathcal{DFT}([2\kappa_{\text{S}} \quad 6 \quad \ldots \quad 6]) \\ &= \mathcal{DFT}([2\kappa_{\text{S}} - 6 \quad 0 \ \ldots \ 0]) + \mathcal{DFT}([6 \quad 6 \ \ldots \ 6]) \\ &= [2\kappa_{\text{S}} - 6 \quad 2\kappa_{\text{S}} - 6 \ \ldots \ 2\kappa_{\text{S}} - 6] + [6N \quad 0 \ \ldots \ 0] \\ &= [2\kappa_{\text{S}} + 6(N-1) \quad 2\kappa_{\text{S}} - 6 \quad \ldots \quad 2\kappa_{\text{S}} - 6] \end{aligned} \tag{4.21}$$

Where $\mathcal{DFT}(\cdot)$ represents the discrete Fourier operator. The first term $2\kappa_S + 6(N-1)$ is always positive and can be shown to correspond to the radial direction eigenvector (related through the transformation matrix $\mathbb{P}$). The signs of the remaining eigenvalues will depend on the value of κ_S. For:

> $\boldsymbol{\kappa_S < 3}$: Here, $2\kappa_S - 6 < 0$. So, this block has one positive eigenvalue, and the remaining $N-1$ eigenvalues being negative.
>
> $\boldsymbol{\kappa_S > 3}$: Here, the sub-block has all N eigenvalues being positive.

In any case, whenever $\kappa_S \neq 3$, $\widehat{\mathbb{M}}$ has mixed eigenvalues with the diagonal submatrix and circulant sub-matrix always containing eigenvalues of opposing signs.

$H \in \mathcal{C}_{n+1}$ (all non-zero)

In this case, we have the entire matrix $\widehat{\mathbb{M}}$ being circulant, with eigenvalues of $2\kappa_S + 6(N-1)$ and $2\kappa_S - 6$. For $\kappa_S < 3$, this is corresponds to H being a saddle point. However, for $\kappa_S > 3$, we have that all H in this class are minima (with maximal ISI!).

4.6 CMA as Kurtosis Minimizer

For both platykurtic and leptokurtic sources the CMA error surface minima coincide with minimum kurtosis of equalizer output. It will be shown that in the platykurtic source case kurtosis reduction realizes ISI *reduction*, while for leptokurtic sources this yields ISI *enhancement*. Herein, we demonstrate a specific connection between ISI and kurtosis in CMA which follows along ideas regarding "partial ordering" of random variables as presented in [27].

Consider the kurtosis of a non-trivial weighted sum, y, of two iid random variables (herein considered as source sequence elements), having forth and second moments given by M_4 and M_2,

$$y = h_0 s_0 + h_1 s_1, \quad h_i \neq 0. \tag{4.22}$$

The kurtosis of y is given by,

$$\begin{aligned}
\kappa_{\mathrm{Y}} &= \frac{\mathrm{E}\left\{y^4\right\}}{\mathrm{E}\left\{y^2\right\}^2} = \frac{\mathrm{E}\left\{(h_0 s_0 + h_1 s_1)^4\right\}}{\mathrm{E}\left\{(h_0 s_0 + h_1 s_1)^2\right\}^2} \\
&= \frac{(h_0^4 + h_1^4)\mathrm{M}_4 + 6h_0^2 h_1^2 \mathrm{M}_2^2}{(h_0^4 + h_1^4 + 2h_0^2 h_1^2)\mathrm{M}_2^2} \\
&= \kappa_{\mathrm{S}} + (3 - \kappa_{\mathrm{S}}) \left(\frac{2h_0^2 h_1^2}{h_0^4 + h_1^4 + 2h_0^2 h_1^2} \right)
\end{aligned} \tag{4.23}$$

We see that $\kappa_{\mathrm{Y}} > \kappa_{\mathrm{S}} \Leftrightarrow \kappa_{\mathrm{S}} > 3$, and $\kappa_{\mathrm{Y}} < \kappa_{\mathrm{S}} \Leftrightarrow \kappa_{\mathrm{S}} < 3$. Summing two iid platykurtic signals increases the kurtosis (with an upper bound on the resulting kurtosis being 3). Considering the equalizer output y as a sum of iid random variables, then the partial sums of the convolution have monotonically increasing kurtosis value, asymptotically approaching 3 in agreement with the central limit theorem.

Consider the case $\kappa_{\mathrm{S}} < 3$, in which the received signal consists of the sum of independent random variables. The received signal's distribution is "more Gaussian" than the source. In effect, the channel has increased the signal's kurtosis. Removal of ISI, hence removing components of the sum of independent random variables, reduces the kurtosis. Here, any amount of ISI will increase the kurtosis of the equalizer output. So, minimizing the kurtosis indeed represents the minimization of the ISI.

Alternatively, with a leptokurtic source the kurtosis of the partial sums is strictly *decreasing*. Minimization of kurtosis is achieved by maximizing the num-

Table 4.1: Summary of Stationary Point Analysis

CLASS	$\|\mathcal{C}_i\|$	$\kappa_S < 3$			$\kappa_S > 3$			COMMENT
		# pos. eigvals	# neg. eigvals	type	# pos. eigvals	# neg. eigvals	type	
$H \in \mathcal{C}_0$	1	0	$n+1$	max	0	$n+1$	max	Origin
$H \in \mathcal{C}_1$	$2(n+1)$	$n+1$	0	min	1	n	saddle	Perfect Eq.
$H \in \mathcal{C}_N$	$2^N \binom{n+1}{N}$	$n-N$	$N+1$	saddle	$N+1$	$n-N$	saddle	for $2 \leq N \leq n$
$H \in \mathcal{C}_{n+1}$	2^{n+1}	1	n	saddle	$n+1$	0	min	Max ISI

ber of non-zero weight h_i (hence maximizing ISI). This is reflected in the stability point analysis for $H \in \mathcal{C}_{n+1}$ when $\kappa_S > 3$ which is shown to maximize ISI.

4.7 Summary of Results

A summary of the stationary point stability analysis is tabulated in Table 4.7 for $H \in \mathbf{R}^{n+1}$:

4.7.1 Platykurtic

It has been demonstrated that only the solutions $H \in \mathcal{C}_1$ are stable points of the FSE-CMA error surface under an iid source with $\kappa_S < 3$. Furthermore, as any $H \in \mathcal{C}_1$ is a perfect equalization setting we have that CMA is globally convergent to a perfect equalization setting in this case, duplicating the results of [29] [50].

4.7.2 Leptokurtic

However, in cases with $\kappa_S > 3$, CMA is globally convergent to settings in which all taps have equal, non-zero values. Such parametrizations correspond to maximal

ISI settings, providing disastrous equalization performance.

4.7.3 Meso-Kurtic

A Gaussian source is known to be a source which causes ill-behavior of CMA and other blind equalization schemes [10] and we note that a Gaussian source distribution has $\kappa_{\mathrm{S}} = 3$. Our work here has shown that in the case of $\kappa_{\mathrm{S}} = 3$, CMA will adapt to any parametrization on the sphere which, in general, does not provide adequate equalization. However, the class of sources for which this behavior occurs is much broader than the oft-cited Gaussian class. There are many other distributions which may attain $\kappa_{\mathrm{S}} = 3$ (e.g. let $s_i = \pm 1$ with probability $p(\pm 1) = \frac{79-\sqrt{97}}{90}$, $s_i = \pm 4$ with probability $p(\pm 4) = \frac{11+\sqrt{97}}{90}$) which have this extreme effect on CMA. We propose a name of *meso-kurtic* to denote them. The point being that even non-Gaussian source distributions may cause problems with blind equalizers. In light of the potential for misinterpretation, it is worth pointing out again that we are referring to the *source* distribution, not the received signal distributions. This distinction is important since often the received distribution looks Gaussian after a non-Gaussian source signal is distorted through a channel with a large amount of ISI.

4.7.4 Error Surface Curvature and Convergence

The important, desired quality of global convergence to perfect equalization settings for platykurtic sources is almost transparent through the above stability analysis. However, a potentially disturbing quality surfaces as well. The vast number of saddle points (on the order of 3^{n+1}) might lead to slow convergence. This concern is heightened in cases where the source kurtosis increases towards 3. From (4.19) and (4.21) it is seen that as κ_S approaches 3, *all but one* (the one in the radial direction) eigenvalues of all stationary points approaches zero. The neighborhood of all saddle points becomes "flatter". This warns of prolonged convergence times. This should be especially noted in cases where CMA equalizers are used in conjunction with constellation shaping which increases the Gaussianity of the source (e.g. the v.34 modem standard). In [46] it is shown that optimal shaping for a large two-dimensional constellation is close to a Gaussian distribution. So, improved source coding may hinder blind equalization ability and the tradeoff should be considered in the design of a communication system.

Example D: An example of convergence rate decrease due to curvature reduction resulting from source kurtosis increasing towards $\kappa_S = 3$ is demonstrated in Figure 4.1. Here the ISI trajectories are plotted for a variety of source kurtosis values. The equalizers are initialized with a center tap initialization ($d = [0 \quad 0 \quad 1 \quad 0 \quad 0]^T$ as in Examples A, B, and C.) All other parameters are the same as earlier examples except for the source distributions which have a kurtosis ranging within $1.76 < \kappa_S < 5.04$. Generalizations that one might draw from this plot is that ISI is reduced by CMA-FSE if $\kappa_S < 3$, while ISI is enhanced when $\kappa_S > 3$, which has just been shown earlier in this chapter. Furthermore, for $\kappa_S < 3$, the larger the source kurtosis, the slower the convergence. In fact, this generalization was hinted at earlier. It was seen that *all* but one of the eigenvalues of the Hessian evaluated at *all* of the stationary points diminish as $\kappa_S \to 3$ from below.

Example E: Another experiment is performed in order to view the effect of kurtosis on convergence time. In this example a different initialization was used. The

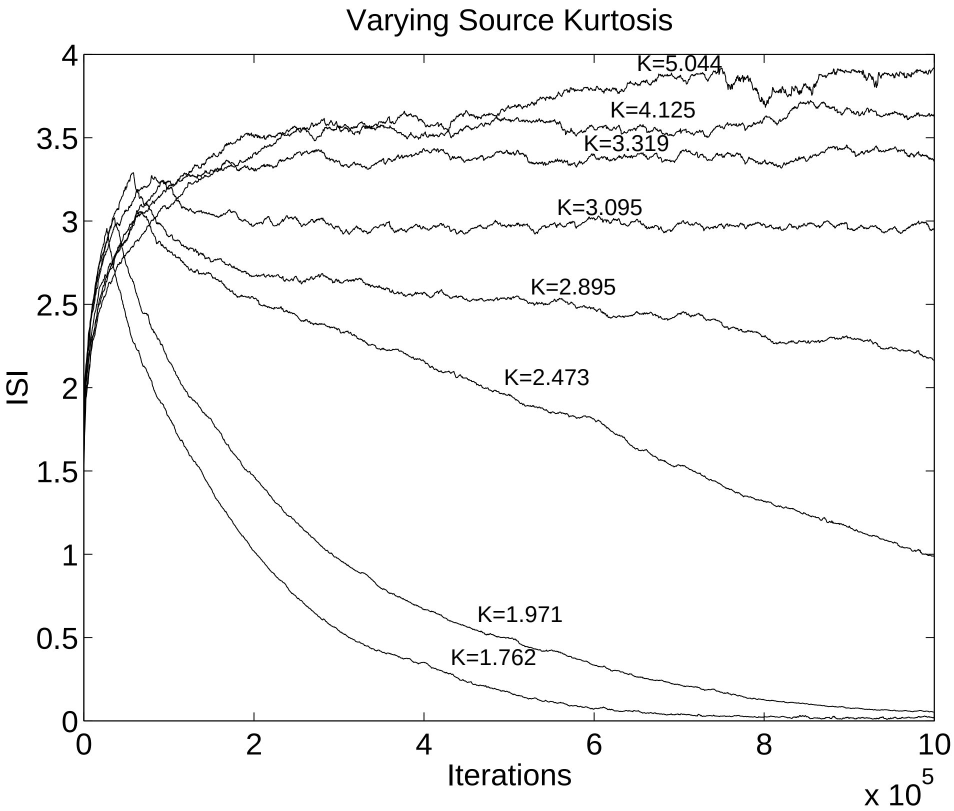

Figure 4.1: Example D: ISI trajectories for various source kurtoses

equalizer is initialized so that the combined channel-equalizer setting has maximal ISI (i.e. $H = [1 \quad 1 \quad 1 \quad 1 \quad 1]^{\mathrm{T}}$). By doing so our trajectories start at a maximum on the γ manifold, and in some sense, we may traverse "more" of the manifold than if we had chosen a center tap initialization for the given channel. Using the same channel and stepsize μ as in examples A through D, the number of iterations needed to reduce ISI to an open-eye setting (e.g. $\mathcal{ISI} = 1/(M-1)$ where $M = 8$ and is the number of levels in PAM alphabet) is computed for a variety of source kurtosis values ($\kappa_{\mathrm{S}} < 3$). The reason for computing the convergence to this ISI level is that this represents the *earliest* time for a switch to decision directed is guaranteed to produce no decision errors (in the absence of channel noise).

Figure 4.2 reflects the dependence of convergence time on source kurtosis and highlights the necessity of avoiding a source kurtosis too close to $\kappa_{\mathrm{S}} = 3$. Thus, we have an apparent tradeoff between source coding gains (driving $\kappa_{\mathrm{S}} \to 3$) and blind equalizer convergence (preferring κ_{S} away from value 3).

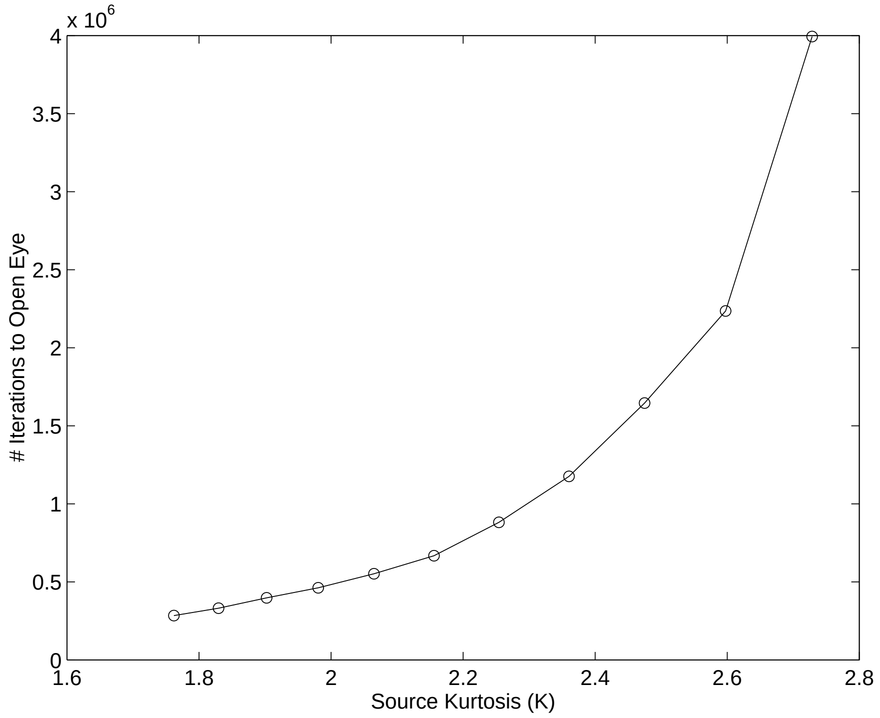

Figure 4.2: Eye-opening Time vs. Kurtosis

Chapter 5

Topological Viewpoint

> "If your head were a doughnut, you could comb your hair without leaving a bald spot."
>
> *Differential Topology*, V. Guillemin, A. Pollack.

In this chapter we present a look at the CMA error surface from a topological viewpoint. Recognizing topology as the study of deformational invariants, and viewing correlation as inducing a deformation of the iid error surface, this section serves as a bridge between the distributional aspects of iid source considered in the previous chapter and temporally correlated sources to be discussed in following chapter. First, source invariant properties which are due to the topological manifold are presented. This manifold will be shown to induce specific properties on the CMA error surface. Connections are made to Morse Theory, as well as polytopes and their relation to vector fields on manifolds. A further look at the iid results are presented detailing these connections.

5.1 Source Invariant Properties of CMA Error Surface

5.1.1 γ Non-Effect

In the case of an unknown constellation, or source distribution, a priori knowledge of the true value of γ is impossible (and perhaps seemingly irrelevant if the receiver includes automatic gain control), hence there may be some concern as to the improper selection of this constant. It is shown here that the choice of γ's value is somewhat unimportant, in the sense that it only introduces a scaling effect on the achieved system parametrization (and hence equalizer output y). In other words, the ability to remove (or reduce) ISI is unaffected.

Consider the effect of differing values of γ on the cost function. Here, the original CMA cost function, $J(H)$ from (3.1) is compared with a cost function using a version of γ which has been scaled by a positive scalar λ,

$$J_\lambda(H) \;=\; \frac{1}{4}\mathrm{E}\left\{\left((H^{\mathrm{T}}S)^2 - \lambda\gamma\right)^2\right\}. \tag{5.1}$$

Notice that,

$$J_\lambda(H) \;=\; \lambda^2 J\left(\frac{H}{\sqrt{\lambda}}\right). \tag{5.2}$$

Thus, the value of γ effects the error surface only by a scaling of the range and a dilation in the domain. No qualities of the error surface (e.g. number of minima, maxima, etc) are changed. The "shape" remains the same. Hence, the equalizer output y is merely scaled, ISI levels are unaffected.

5.1.2 γ Matching Manifold is n-Sphere

There exists a closed, bounded manifold of the error surface to which CMA converges regardless of initialization. In a general sense, the algorithm's convergent behavior can be described by characterization of this manifold which will be denoted $\mathcal{M}_\gamma$.

To develop this concept, note that along any ray extending from the origin in H space, there is one and only one minimum. This has been demonstrated for uniformly iid sources ([23], [38]) but is extended here to include any distribution and temporal source correlation.

Consider the ray given by $\lambda \bar{H}$ for some $\bar{H} \in \mathbf{R}^{n+1}$ with $\lambda \geq 0$. Let $\bar{y}$ be the output resulting from $\bar{H}$ (i.e. $\bar{y} = \bar{H}^{\mathrm{T}} S$), and consider the output y resulting from any parametrization along the ray (i.e. $y = \lambda \bar{y} = \lambda \bar{H} S$, $\lambda \geq 0$). The CMA error surface in terms of λ may be written,

$$\begin{aligned} J(\lambda) &= \frac{1}{4} \mathrm{E}\left\{ \left((\lambda \bar{y})^2 - \gamma \right)^2 \right\} \\ &= \frac{1}{4} \left(\lambda^4 \mathrm{E}\left\{ \bar{y}^4 \right\} - 2\gamma\lambda^2 \mathrm{E}\left\{ \bar{y}^2 \right\} + \gamma^2 \right) \end{aligned} \tag{5.3}$$

Differentiating to find the extrema along this ray yields,

$$\frac{\partial J(\lambda)}{\partial \lambda} = \lambda^3 \mathrm{E}\left\{ \bar{y}^4 \right\} - \gamma \lambda \mathrm{E}\left\{ \bar{y}^2 \right\}. \tag{5.4}$$

There are only two solutions,

$$\lambda = \left\{ 0, \quad +\sqrt{\gamma \frac{\mathrm{E}\{\bar{y}^2\}}{\mathrm{E}\{\bar{y}^4\}}} \right\} \tag{5.5}$$

with corresponding second derivative values of,

$$\left\{ -\gamma \mathrm{E}\left\{ \bar{y}^2 \right\}, \quad +2\gamma \mathrm{E}\left\{ \bar{y}^2 \right\} \quad \right\}. \tag{5.6}$$

Hence, the origin is a local maximum, and the other stationary point is the only minimum along that ray, in agreement with [23], [38].

Furthermore, the output at this radial minimum has the property that its ratio of fourth to second moments match γ. To see this, substitute the value of λ at this ray minimum yielding,

$$y = \lambda \bar{y} = \sqrt{\frac{\gamma \mathrm{E}\{\bar{y}^2\}}{\mathrm{E}\{\bar{y}^4\}}}\bar{y}. \tag{5.7}$$

The ratio of the resulting equalizer outputs' fourth and second moment is seen to match γ by,

$$\begin{aligned} \frac{\mathrm{E}\left\{y^4\right\}}{\mathrm{E}\{y^2\}} &= \frac{\mathrm{E}\left\{(\lambda\bar{y})^4\right\}}{\mathrm{E}\{(\lambda\bar{y})^2\}} \\ &= \lambda^2 \frac{\mathrm{E}\left\{\bar{y}^4\right\}}{\mathrm{E}\{\bar{y}^2\}} \\ &= \left(\gamma \frac{\mathrm{E}\left\{\bar{y}^2\right\}}{\mathrm{E}\{\bar{y}^4\}}\right) \frac{\mathrm{E}\left\{\bar{y}^4\right\}}{\mathrm{E}\{\bar{y}^2\}} \\ &= \gamma \end{aligned} \tag{5.8}$$

The union of all such radial minima is the manifold of interest and denoted the "γ manifold", or $\mathcal{M}_\gamma$. This manifold is topologically equivalent to the sphere $\mathcal{S}^n$. The continuity of the manifold is guaranteed due to the polynomial, and hence continuous nature, of the error surface. All points on this "distorted" sphere have been shown to correspond to equalizer output whose ratio of fourth moment to second moment match γ. The concept is that all stationary points necessarily lie on this manifold, since it is comprised of all points having zero gradient in the radial direction, and stationary points must have zero gradient in *all* directions.

Benveniste ([10]) uses the notion of a manifold in his analysis of the Sato (and extensions thereof) under iid source. The manifold under consideration is the unit sphere (for a unit energy input). Stationary points of the vector field restricted to this unit sphere are identified. In such a formulation however, these are *not* stationary points of the algorithm itself, as there may exist a radial component orthogonal to the manifold. In contrast, herein we use the γ manifold which, while being topologically equivalent to the sphere has the property that stationary points on this manifold are indeed stationary points of the CMA algorithm.

Another important point is that the radial gradient is seen to be positive whenever $\mathrm{E}\left\{y^4\right\}/\mathrm{E}\left\{y^2\right\} < \gamma$, hence, on average, the update term has a component in a radial expanding direction (likewise a contracting radial component whenever the ratio exceeds γ.) The upshot of this is that initial settings residing within the topological sphere have trajectories which increase in norm to approach $\mathcal{M}_\gamma$, and vice versa for settings outside this manifold. In a general sense, the convergence to the γ-matching manifold may be quite quick due to the quartic nature of the error surface in the radial direction. After reaching the neighborhood of the manifold it remains there and convergence is governed by the vector field existing on the manifold. This vector field may be influenced greatly by source distributions and temporal correlation.

In [38] a presentation of the expanding/contracting radius is found. However, the work there considers strictly a Bernoulli source (binary, zero-mean iid source), as opposed to the results here which hold for arbitrary distributions and correlations. Furthermore, the actual convergent radius (the γ manifold) is not specifically identified, but recognized as a region:

> "... parametrizations sufficiently distant from the origin ... motion along any gradient descent path decreases the distance to the origin. Conversely, ... parametrizations sufficiently near the origin, motion ... increases the distance from the origin." — *Johnson, Anderson* [38]

A quantitative assessment of this region is derived in [38] for the white binary source as,

$$\frac{1}{\lambda_{\min}(\mathbb{R}_{rr})} > D^{\mathrm{T}} D > \frac{1}{3\lambda_{\max}(\mathbb{R}_{rr})} \tag{5.9}$$

where $\lambda_{\min}(\mathbb{R}_r r)$ is the minimum eigenvalue of the autocorrelation matrix of the received signal r.

5.1.3 Symmetries

It has been noted that since every monomial appearing in $F(H)$ has an odd total degree, whenever $F(H) = \vec{0}$, then also we have $F(-H) = \vec{0}$. This is mentioned earlier within the context of a sign ambiguity caused by the y^2 term in the cost function. However, the point is meant to be extended here beyond just a property at the stationary points. The property that $F(H) = -F(H)$ is true everywhere in H space. One manifestation of this is that the error surface will always have an even number of minima, an even number of maxima, and an even number of saddle points (discounting the origin).

5.2 Introduction to Topology

The existence of a manifold on which all stationary points must exist (i.e. the γ manifold), coupled with the fact that CMA is a gradient algorithm, places some restraints on the relation of stationary points due to the topology of the manifold. In this section we introduce some terms necessary for consideration of the topological aspects of our investigation and then present resulting information about the error surface.

The seemingly unrelated quote about doughnut shaped heads at the beginning of this chapter turns out to have some relevance here. The connection to CMA may be realized by

- Relating "hair combing" of "doughnut head" to assigning *vector field* on *torus*.
- Recognize that the structure of the torus allows a vector field with no critical points.
- Note that structure of the sphere disallows a vector field with no critical points.

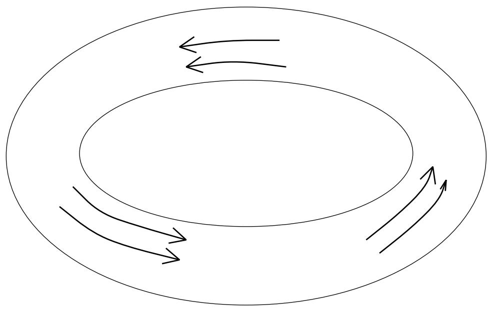

Figure 5.1: Torus Allows Vector Field With No Critical Points

This demonstrates that there is a qualitative difference between the torus and the sphere. Moreover this difference remains even if these objects are bent or twisted (i. e. it is the "structure" of the object, not the "shape"). Topology is the study and identification of such qualities which remain unchanged under deformations.

We have seen that all critical points (except the one at origin) of CMA lie on the γ matching manifold. The "topology" of this γ manifold places constraints on CMA behavior, by limiting the combinations of types of stationary points (in the same manner that the torus and sphere have differing constraints). We can

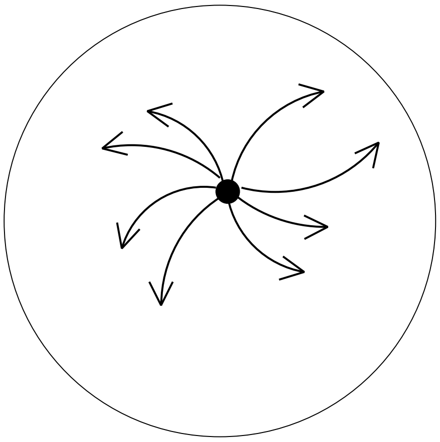

Figure 5.2: Sphere Forces Vector Field to Have Critical Points

recognize that source correlation can be viewed as imparting a deformation of the error surface. To see this, note that a temporally correlated source will effect the correlations coefficients of (3.10) and due to its polynomial nature this may be viewed as a deformation. In this manner, topology yields some description of what may or may not happen under source correlation.

5.3 Definitions

It is necessary to present definitions of the topological terms used herein before proceeding with the material specific to our CMA investigation. The tone hear tends to be informal, a more formal presentation of these same concepts may be found in Appendix F.

Topological Space: A set with a collection of subsets (called neighborhoods), Such that:

1. every point is in some neighborhood,

2. intersection of any two neighborhoods of a point contains a neighborhood of the point.

Manifold: A topological space in which every point has a neighborhood that is topologically equivalent to an n-dimensional open disc. Two distinct points have disjoint neighborhoods.

The 2-manifolds (e.g. $n = 2$) are known as *surfaces*, some common examples are: a plane, surface of a ball (known as $\mathcal{S}^2$), a torus. Here though, we are specifically considering the topological space to be the γ manifold. This is really just a dense, closed, connected subset of the space $\mathbf{R}^{n+1}$.

Deformation: (Non-mathematically) A bending, twisting, or reshaping of a topological space which leaves neighborhoods intact. "Cutting" is allowed only if severed neighborhoods are later rejoined.

A (trite) example of this is that a coffee cup may be deformed into a doughnut as figure 5.3 (from [44]).

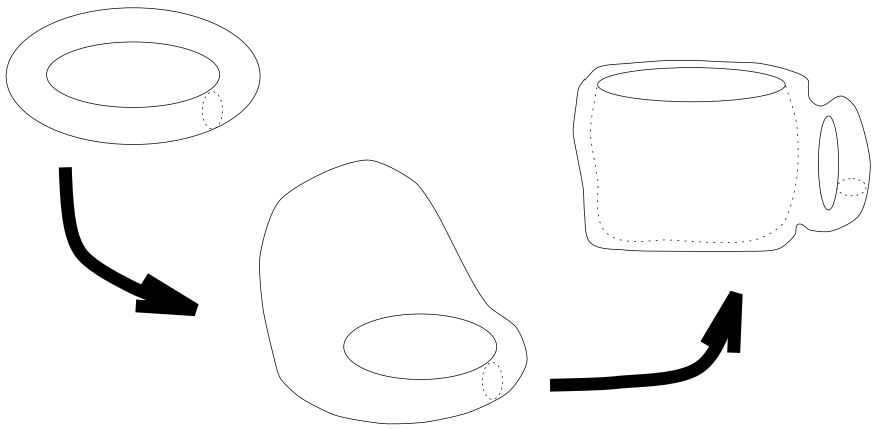

Figure 5.3: Doughnut deformed into Coffee Cup

Topological Equivalence: Two Structures are considered equivalent if one may be deformed into the other, denoted by "$\approx$"

That is to say (based on the example above) that a doughnut is topologically equivalent to the coffee cup (doughnut $\approx$ coffee cup).

Vector Field: A vector field on a manifold $X \in \mathbf{R}^N$ assigns a vector tangent to X at each point in x. That is, a smooth map $\vec{v} : X \to \mathbf{R}^N$

Critical Point: A critical point of a vector field $\vec{v}$ on a manifold X is a point where $\vec{v}(x) = \vec{0}$.

We view the vector field to the that of the CMA cost function gradient restricted to the γ manifold.

5.4 Connection to CMA Effort: γ Manifold

It has been pointed out in section 5.1.2 that all CMA Stationary Points lie on the γ manifold which has been identified as topologically equivalent to the sphere $\mathcal{S}^{\mathbf{n}}$. As all trajectories from inside or outside this manifold converge monotonically towards it, it is the vector field on the manifold that will govern asymptotic behavior. In this manner, we consider only this manifold and view the CMA error surface as a vector field on this manifold. Specifically, let the topological space be defined as the union of all points with zero gradient in the radial direction (excluding the origin),

$$\mathcal{M}_\gamma \ \approx \ \bigcup \left\{ H \neq 0 \ : \ \frac{\partial J(H)}{\partial |H|} = 0 \right\} \tag{5.10}$$

Due to the continuity of J in H, $\mathcal{M}_\gamma$ will be connected. Also, due to nature of CMA cost function to become infinite at infinite radius in H (or realizing that all radial minima occur at a finite radius) , we have that $\mathcal{M}_\gamma$ is necessarily compact.

Note that on $\mathcal{M}_\gamma$, the CMA gradient has no radial component (seen trivially by definition of $\mathcal{M}_\gamma$), and hence the CMA gradient is tangent to $\mathcal{M}_\gamma$ at all points $H \in \mathcal{M}_\gamma$. Then, the CMA gradient suits the definition of a vector field on a manifold topologically equivalent to a sphere.

5.4.1 Interesting Parts of Vector Field

In a vector field, there are large regions which may be deemed "uninteresting". That is, uninteresting in the sense that have little to do with the asymptotic behavior of the gradient algorithm. For $x \in X$ not near a critical point, $\vec{x}$ is nearly constant as in Figure 5.4 (from [31]). Contrarily the interesting parts of the vector

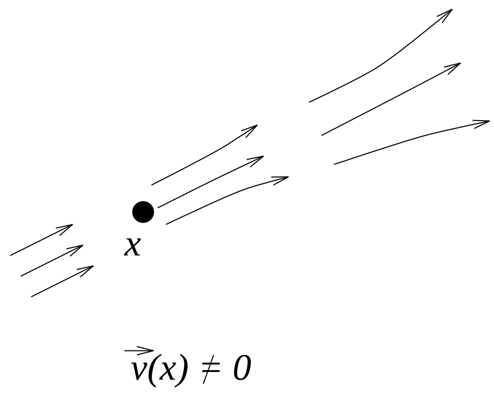

Figure 5.4: Vector Field Away from Critical Points

field are those in the neighborhood of a critical point. For this reason we focus on describing the vector field in the neighborhood of critical points. Near critical points a variety of behaviors are possible. CMA, being a gradient system (i.e.

curl-free), precludes some of these, leaving the only critical points to be saddles, minima (sinks), or maxima (sources). (See Figure 5.5, modified from [31].)

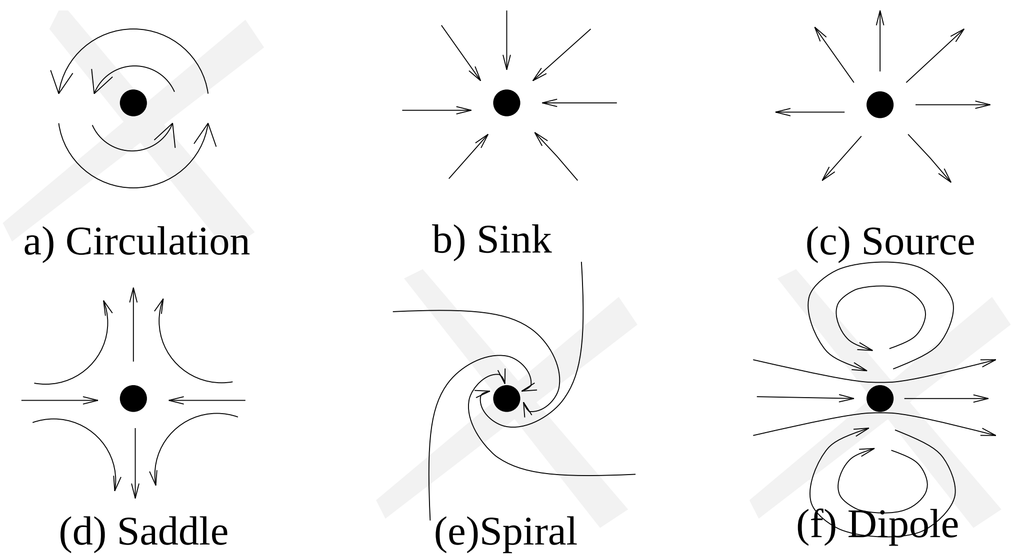

Figure 5.5: Categorization of Critical Points

5.4.2 $\mathcal{M}_\gamma$ for Platykurtic IID Source

Using the results from the iid source section, the CMA minima for $H \in \mathbf{R}^3$ (under a platykurtic source) are the parametrizations containing only one non-zero element of $+1$ or -1. These points are associated with the axes of Figure 5.6 and labeled N, S, E, W, F, B and denoted by a "$*$". In this figure we also have the other stationary points. The saddle points with two non-zero elements are denoted by a "o", and those associated with three non-zero elements are denoted by a "$+$".

One might consider painting arrows on the sphere to represent the CMA flow lines (i. e. vector field), similar to Figure 1 [10]. Of course, such painting must agree with results on the number of attractive (dispersive) directions which is related to the number of positive (negative) eigenvalues of the Hessian at the stationary

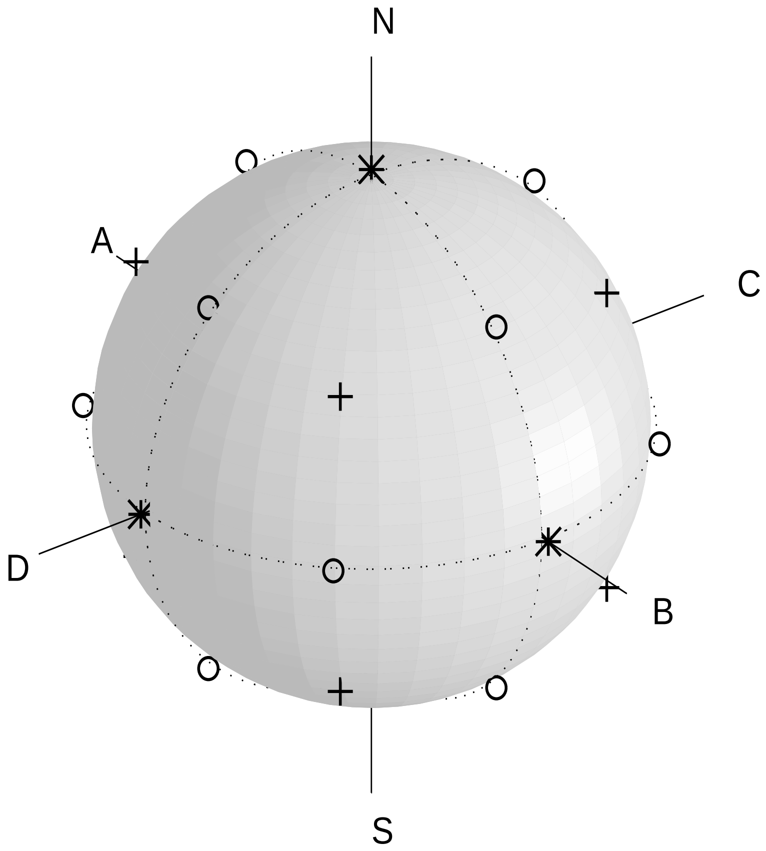

Figure 5.6: Manifold of CMA Error Surface Containing Stationary Points

points. In the typical blind equalization setting the combined channel-equalizer order exceeds three and the γ manifold may be of high dimensions which makes visualization difficult. Nonetheless, we proceed with this low dimension example.

5.4.3 Painting $\mathcal{M}_\gamma$ for Platykurtic IID Source

$\underline{H \in \mathcal{C}_1}$: first consider the neighborhoods around each of these minima points. The "$*$" in Figure 5.6 denote such minima (e. g. are in $\mathcal{C}_1$) and have 3 positive eigenvalues and hence three attractive "directions". One of the three attractive directions is seen to be the radial direction. To verify this note that the Hessian evaluated at $H_* = [\,1 \quad 0 \quad 0\,]^{\mathrm{T}}$ is,

$$\begin{bmatrix} 2\kappa_{\mathrm{S}} & 0 & 0 \\ 0 & 3-\kappa_{\mathrm{S}} & 0 \\ 0 & 0 & 3-\kappa_{\mathrm{S}} \end{bmatrix} \tag{5.11}$$

which has eigenvectors and associated eigenvalues,

$$\begin{array}{ccc} v_0 = \begin{bmatrix} 1 \\ 0 \\ 0 \end{bmatrix} & v_1 = \begin{bmatrix} 0 \\ 1 \\ 0 \end{bmatrix} & v_2 = \begin{bmatrix} 0 \\ 0 \\ 1 \end{bmatrix} \\ \lambda_0 = 2\kappa_{\mathrm{S}} & \lambda_1 = 3-\kappa_{\mathrm{S}} & \lambda_2 = 3-\kappa_{\mathrm{S}} \end{array} \tag{5.12}$$

The unique eigenvalue of $2\kappa_{\mathrm{S}}$ is in the radial direction from our example point of interest here H_* (i.e. has associated eigenvalue $[\,1 \quad 0 \quad 0\,]^{\mathrm{T}}$). As the other two eigenvalues are equal their associated eigenvectors may be any linear combination of v_1 and v_2 (which is necessarily orthogonal to the radial vector v_0). The point being that the vector field on the manifold is attractive to the point H_* in the same manner in *all* directions (on the manifold). Similar results hold for all other stationary points in $\mathcal{C}_1$.

$\underline{H \in \mathcal{C}_2}$: these are the stationary points marked by "o". Consider $H_o = [1 \quad 1 \quad 0]^{\mathrm{T}}$ and its associated Hessian,

$$\begin{bmatrix} 2\kappa_{\mathrm{S}} & 6 & 0 \\ 6 & 2\kappa_{\mathrm{S}} & 0 \\ 0 & 0 & 3-\kappa_{\mathrm{S}} \end{bmatrix} \tag{5.13}$$

which has eigenvectors and associated eigenvalues,

$$\begin{array}{ccc} v_0 = \begin{bmatrix} 1 \\ 1 \\ 0 \end{bmatrix} & v_1 = \begin{bmatrix} 1 \\ -1 \\ 0 \end{bmatrix} & v_2 = \begin{bmatrix} 0 \\ 0 \\ 1 \end{bmatrix} \\ \lambda_0 = 2\kappa_{\mathrm{S}} + 6 & \lambda_1 = 2\kappa_{\mathrm{S}} - 6 & \lambda_2 = 3 - \kappa_{\mathrm{S}} \end{array} \tag{5.14}$$

Notice again that the radial direction (from our point of interest, H_o) is an eigenvector. Its associated eigenvalue is positive showing attraction in the radial direction. (as necessitated demonstrated convergence to the manifold). Furthermore, it is the strongest direction of attraction, as shown by $2\kappa_{\mathrm{S}} + 6 > 3 - \kappa_{\mathrm{S}}$. Again, by orthogonality of eigenvectors, the eigenvectors v_1 and v_2 must lie on $\mathcal{M}_\gamma$. One direction is repulsive (v_1), the other attractive (v_2).

$\underline{H \in \mathcal{C}_3}$: these are the stationary points marked by "+". Consider $H_+ = [1 \quad 1 \quad 1]^{\mathrm{T}}$ and its associated Hessian,

$$\begin{bmatrix} 2\kappa_{\mathrm{S}} & 6 & 6 \\ 6 & 2\kappa_{\mathrm{S}} & 6 \\ 6 & 6 & 2\kappa_{\mathrm{S}} \end{bmatrix} \tag{5.15}$$

which has eigenvectors and associated eigenvalues,

$$\begin{array}{ccc} v_0 = \begin{bmatrix} 1 \\ 1 \\ 1 \end{bmatrix} & v_1 = \begin{bmatrix} 1 \\ 0 \\ -1 \end{bmatrix} & v_2 = \begin{bmatrix} 1 \\ -1 \\ 0 \end{bmatrix} \\ \lambda_0 = 2\kappa_{\mathrm{S}} + 12 & \lambda_1 = 2\kappa_{\mathrm{S}} - 6 & \lambda_2 = 2\kappa_{\mathrm{S}} - 6 \end{array} \tag{5.16}$$

Table 5.1: Directions of Flow on γ Manifold

Stationary Point	Repulsive Directions on γ Manifold	Attractive Directions on γ Manifold	Comment
$H \in \mathcal{C}_1$	0	2	Sink
$H \in \mathcal{C}_2$	1	1	Saddle
$H \in \mathcal{C}_3$	2	0	Source

The radial direction (from our point of interest, this time H_+) is again an eigenvector, with a positive associated eigenvalue (hence, attractive in radial direction). The other eigenvectors have equal, strictly negative eigenvalues. So, the vector field is equally repulsively in all directions on the manifold at H_+. As before, we have the radial component at all stationary points is the strongest direction of attraction. A summary of these points for our 3 tap example under platykurtic iid source is found in Table 5.4.3. Which lead to the γ manifold "painting" in Figure 5.7.

5.4.4 Generalized Results for IID sources

For any iid source where $\kappa_S \neq 3$, by applying similar stationary point Hessian analysis we have,

- The radial direction is always attractive, and it is always the strongest attractive direction.

For any platykurtic iid sources,

- The number of repulsive directions on the manifold equals the $N-1$ for stationary point $H \in \mathcal{C}_N$.

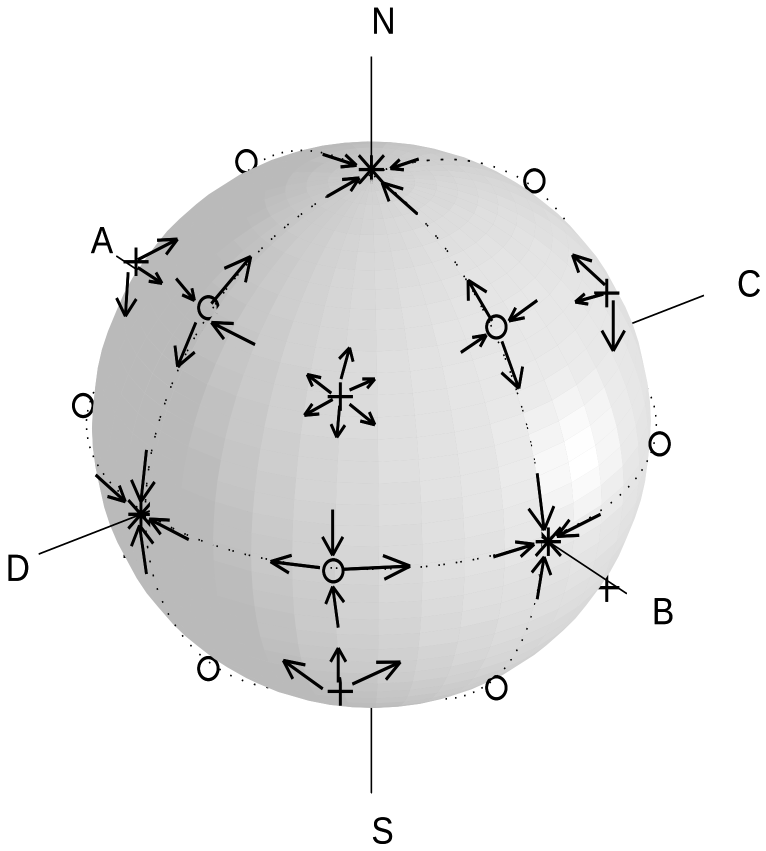

Figure 5.7: Vector Field Assigned at Stationary Points

- The number of attractive directions on the manifold equals the $n+1-N$ for stationary point $H \in \mathcal{C}_N$.

Since, *all* of the non-radial Hessian eigenvalues for $\kappa_S < 3$ have opposite signs when $\kappa_S > 3$ we see that the vector field at critical points (on the manifold) is the negative (reversed) for a leptokurtic source. Thus, the minima and maxima are exchanged. Hence, for any leptokurtic iid sources,

- The number of repulsive directions on the manifold equals the $n+1-N$ for stationary point $H \in \mathcal{C}_N$.
- The number of attractive directions on the manifold equals the $N-1$ for stationary point $H \in \mathcal{C}_N$.

5.4.5 Euler Characteristic

An important topological invariant on compact manifolds is the *Euler Characteristic*. This is perhaps the most elementary of topological invariants and may be defined in a number of ways. In [31] we find the rather abstract:

Euler Characteristic: If Y is a compact, oriented manifold, its *Euler Characteristic* $\chi(Y)$ is defined to be the self-intersection number of the diagonal Δ in $Y \times Y$: $\chi(Y) = I(\Delta, \Delta)$.

However, most of us are introduced to a simpler form of this concept in the setting of polyhedra in 3 space by the name of the *Euler Equation* written as,

$$2 = V - E + F \tag{5.17}$$

where V is the number of vertices, E is the number of edges, F is the number of faces of a polyhedron. Actually, since all polyhedra in three space may be deformed to a sphere ($\mathcal{S}^2$), they are topologically equivalent to a sphere, and the "2" in (5.17) refers to the Euler Characteristic of $\mathcal{S}^2$. Furthermore, the vertices V are merely faces of dimension 0, the edges E are faces of dimension 1, and the F are merely faces of dimension 2. So, we may rewrite (5.17) in a slightly more abstract form as,

$$\chi(\mathcal{S}^2) = \sum_{i=0}^{2} (-1)^i \, |\mathcal{F}_i| \tag{5.18}$$

where $|\mathcal{F}_i|$ denotes the number of faces of dimension i. Carrying this a bit further we define the Euler Characteristic for "polyhedra" in $n+1$ space to be,

$$\chi(\mathcal{S}^n) = \sum_{i=0}^{n} (-1)^i \, |\mathcal{F}_i|. \tag{5.19}$$

Where the Euler Characteristic of the sphere $\mathcal{S}^n$ is (see [44], for example),

$$\chi(\mathcal{S}^n) = \begin{cases} 0 & n \text{ odd} \\ 2 & n \text{ even} \end{cases} \tag{5.20}$$

Admittedly, these polytopes and their Euler Characteristic seem rather far removed from our interest in the vector field on $\mathcal{M}_\gamma$. We address this in the next section which bridges the concepts of polytopes and vector fields on manifolds.

5.4.6 Morse Theory

Morse Theory deals with smooth mappings on manifolds. Specifically, it details how functions with no degenerate critical points can yield insight into the topology of the manifold of their domain and vice versa. A fine technical reference is found in [54]. However, Marston Morse has created a film [56] which provides a gentle introduction to the topic. A basic tenet of Morse theory is that near a nondegenerate critical point, a function can be "completely" determined by the following lemma [31]:

Morse Lemma: Suppose the point $a \in \mathbf{R}^k$ is a nondegenerate critical point of the function f, and

$$(H_{ij}) = \frac{\partial^2 f}{\partial x_i \partial x_j}(a)$$

is the Hessian of f at a. Then there exists a local coordinate system $(x_1, \ldots, x_k)$ around a such that

$$f = f(a) + \sum h_{ij} x_i x_j$$

So, all neighborhoods of nondegenerate critical points are quadratic in nature.

The connection to polytopes is found in the text entitled *Morse Theory* [54] wherein we find:

Theorem 3.5: If f is a differentiable function on a manifold $\mathcal{M}$ with no degenerate critical points, and if each $\mathcal{M}^a$ is compact, then $\mathcal{M}$ has the homotopy type of a CW-complex, with one cell of dimension λ for each critical point of index λ.

A bit of explanation, $\mathcal{M}^a$ denotes a level set. In the CMA error surface all level sets have finite bound, the compactness is met. The "index" of a critical point is the number of negative eigenvalues of its Hessian. Although the term "CW-complex" is fairly technical in a general topology sense (see [36]), in our setting here (a finite dimensional compact, manifold, with a finite number of stationary points) we may take it to simply mean a polytope.

Here, we finally have a connection between local behavior of the vector field at the critical points and the global structure of the manifold. As this is a rather abstract connection we continue with our example of the $\mathcal{M}_\gamma$ for a three tap channel-equalizer.

5.4.7 CW-Complex of $\mathcal{M}_\gamma$ for Platykurtic IID Source

For platykurtic sources, we had from Figure 5.6 $H_* =$ minima, $H_o =$ saddles, $H_+ =$ maxima. On $\mathcal{S}^2$, this means that H_* has a Morse index of 0, H_o has a morse index of 1, H_+ has a morse index of 2, so construction of the homotopic equivalent CW-complex means that points associated with H_* become a face with dimension 0 (vertex), H_o become a face with dimension 1 (edge), H_+ become a face with dimension 2 (face). The resulting CW-complex forms the octahedron in 3 space (more generally the n-octahedron or cross-polytope). as shown in Figure 5.8 and tabulated in Table 5.4.7.

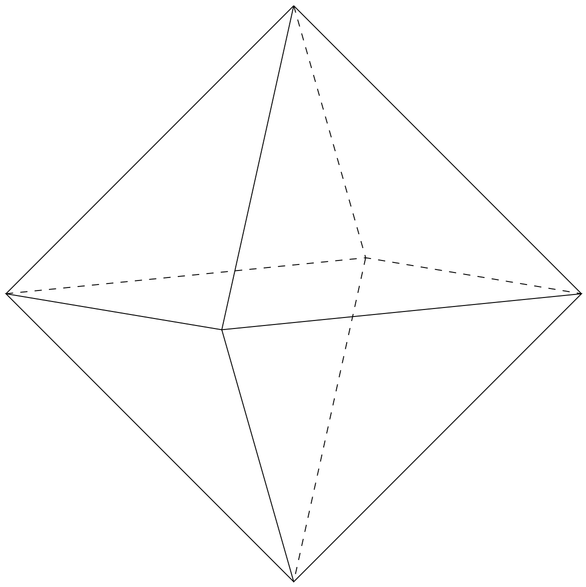

Figure 5.8: CW-Complex of for Platykurtic Source

The relation to Euler Characteristic is then seen to be,

$$\begin{aligned}\chi(\mathcal{M}_\gamma) &= \sum_{i=0}^{2} (-1)^i \, |\mathcal{F}_i| \\ &= 6 - 12 + 8 = 2 \qquad (5.21)\end{aligned}$$

Table 5.2: Relation of Stationary Points to Polytopes

n	# total of faces of dimension n		# of positive e-values on Manifold	Comment
0	6	vertices	0	Min. on $\mathcal{M}_\gamma$
1	12	edges	1	Saddles
2	8	faces	2	Max. on $\mathcal{M}_\gamma$
total	26			

So, we have agreement between the Euler Characteristic of $\mathcal{M}_\gamma$ and the relation of the numbers of types of stationary points.

5.4.8 CW-Complex of $\mathcal{M}_\gamma$ for Leptokurtic IID Source

Interestingly, performing the same for a leptokurtic source (wherein $H \in \mathcal{C}_3$ are minima having a morse index of 0, $H \in \mathcal{C}_2$ are saddles with a morse index of 1, $H \in \mathcal{C}_1$ are maxima with a morse index of 2) we form a cube (more generally an n-cube) as in Figure 5.9 which is the dual polytope (i.e. exchanging faces and vertices) of the octahedron.

5.4.9 CW-Complex of $\mathcal{M}_\gamma$ for Correlated Sources

Up to this point, we have considered only the CW-complexes generated by iid cases. This was because by our earlier analysis we know exactly what the stationary points and their Hessian are for this case. We have that the CW-complexes are the n-octahedron. However, for the correlated case we do not know this information. The point here is that even knowing nothing of the stationary points for a correlated source, we do know the relation that the Euler Characteristic of the CW-complex

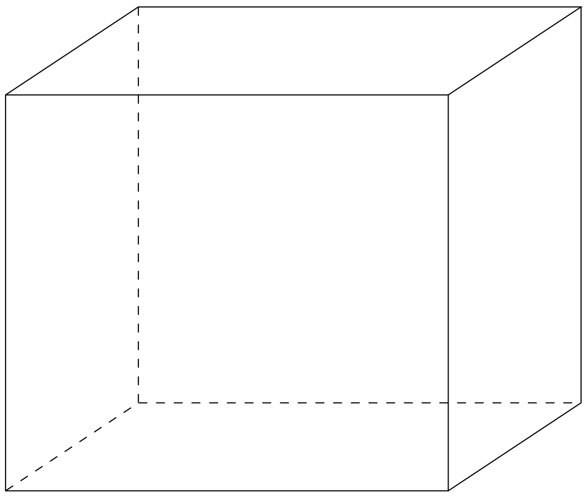

Figure 5.9: CW-Complex of for Leptokurtic Source

formed by them will have the same characteristic as $\mathcal{S}^n$ (as given by (5.20)). This issue will be explained in Chapter 6.

Chapter 6

Temporally Correlated Sources

The global convergence to perfect equalization settings demonstrates a rather attractive property of CMA-FSEs meeting the length, diversity, and platykurtic iid source conditions. Next we relax the condition of the source "whiteness" and investigate CMA stationary points under (a class of) temporally correlated sources. We first recognize that source conditions allowing perfect equalization under CMA are extremely stringent, disallowing perfect equalization for non-white sources. In light of this, methods for determining the stationary point locations are discussed. Algebraic solution methods under arbitrary source correlations are followed by numerical techniques which solve for stationary point locations under specific correlations. Analysis of stationary point parametrizations for 220 periodic sources and a Markov model source are then presented which yield insight into the sensitivity of CMA to source correlation. Connections to the topological discussion are verified and discussed with respect to equalization performance.

6.1 No Perfect Equalization

Henceforth we assume our source to be wide-sense stationary. (As such, the fourth order moments need be only described by three indices. However, since the use of all four indices exhibits the structure of (3.10), for consistent notation all four indices will be kept.) Let $\vec{\mathcal{R}}$ denote the vector containing all such correlations coefficients appearing in (3.10). We can now consider (3.10) as the system $F(H,\vec{\mathcal{R}}) = \vec{0}$. Of particular interest is what happens to the result of global convergence to perfect equalization when temporally correlated source is introduced.

We first turn this result for iid sources around and ask, "for which source correlations do there exist perfect equalization parametrizations which are stationary points?". Denote such perfect equalizing parametrizations by $H^{j\star}$ (i.e. the global system parametrization which has all zero entries, except for a 1 (or -1) in the j^{th} position). Note that $H^{j\star} \in \mathcal{C}_1$. Evaluating $F(H^{j\star},\vec{\mathcal{R}})$ yields the conditions,

$$\overset{0}{\underset{i}{\mathcal{R}}}{}^{i}_{i} - \gamma \mathcal{R}^{0}_{i} \;=\; 0 \quad \text{for } 0 < i < n-1 \tag{6.1}$$

Recall that for an iid source all correlation coefficients are zero except $\mathcal{R}^{0}_{i}$ and $\overset{0}{\underset{i}{\mathcal{R}}}{}^{i}_{i}$ when $i = 0$, which trivially meets the stated conditions for perfect equalization. However, rewriting (6.1) for clarity, we recognize how stringent these conditions may be for non-white sources.

$$h_j \;=\; \pm\sqrt{\frac{\gamma \mathcal{R}^{0}_{0}}{\overset{0}{\underset{0}{\mathcal{R}}}{}^{0}_{0}}} = \pm\sqrt{\frac{\gamma \mathcal{R}^{0}_{1}}{\overset{0}{\underset{1}{\mathcal{R}}}{}^{1}_{1}}} = \ldots = \pm\sqrt{\frac{\gamma \mathcal{R}^{0}_{n}}{\overset{0}{\underset{n}{\mathcal{R}}}{}^{n}_{n}}} \tag{6.2}$$

This is a very tight constraint and appears to admit only "pathological" source sequences (e.g. $s(k)$ constant for *all* k, or $s(k)$ alternating between some constant and its negative). Such signals are considered pathological since they contain no information. In general, it may be said that non-white source correlations do not admit a perfect equalization setting to be a stationary point of CMA. Of course, the real question is "how far from perfect equalization settings are the resulting stable stationary points?"

6.1.1 Metrics of Performance and Correlation

Before describing the results regarding equalization under temporally correlated sources, we must define a metric of equalization performance and source correlation. In addition to the previously introduced performance metric of ISI ($\mathcal{ISI}$) in (2.20), an appropriate metric of equalization performance is the mean squared error (MSE) between source and equalizer output at a stable stationary channel-equalizer parametrization. We quantify the measure of MSE as

$$\text{MSE} \quad = \quad \min_{\delta} \left\{ \mathrm{E}\left\{ \left(s(k-\delta) + y(k) \right)^2 \right\}, \mathrm{E}\left\{ \left(s(k-\delta) - y(k) \right)^2 \right\} \right\} \qquad (6.3)$$

wherein the presence of both the sum and difference terms denotes a toleration of the sign ambiguity (i. e. we are assuming the source is differentially encoded). As we are motivated to show the effect of source correlation on achieved MSE, we define a metric on non-whiteness as,

$$\mu_{\text{COR}}(\vec{\mathcal{R}}) \quad = \quad \|\vec{\mathcal{R}} - \vec{\mathcal{R}}_w\|_1 \qquad (6.4)$$

where $\vec{\mathcal{R}}_w$ is the vector $\vec{\mathcal{R}}$ evaluated for an independent, uniformly distributed source, and $||\cdot||_1$ is the ℓ_1 vector norm. The choice of the ℓ_1 vector norm as opposed to the perhaps more prevalent ℓ_2 norm was somewhat arbitrary. (None of the qualitative results of the experiments to be presented are changed by use of the ℓ_2 norm.)

6.2 Algebraic Solution Method

In the iid source case it was seen that application of standard linear algebra techniques lead to the solution of the stationary point parametrizations. In the correlated source case, with a large number of the correlation coefficients being non-zero, the situation is quite a bit more complex. However, realizing that solving for the stationary points requires solution of a system of multivariate polynomial equations, we may apply some mathematical techniques from slightly more abstract algebra to bear on the problem. Systems of multivariate polynomial equations are often solved using Groebner basis techniques [20]. This approach was attempted here for the CMA equations and is presented in the following sections. In this manner we may find the *algebraic* solution under an arbitrary source correlation. A brief description of concepts relevant to Groebner Basis techniques is presented next.

6.2.1 Ideals, Varieties Defined

The mathematical notions of ideals, and varieties are fundamental concepts of Groebner basis methods. Although more formal definitions of the concepts involved are found in Appendix G, we present the basic ideas here. Polynomials are the elemental concept of both and denoted as:

Polynomial: $f_i =$ polynomial in $k[x_0, ..., x_n]$, where k denotes the field that the monomial coefficients are drawn from and x_i are the polynomial variables.

Herein, we consider k to be the field of real numbers $\mathbf{R}$. Specifically, we have these coefficients determined by the source statistics. As the source alphabet under consideration is strictly real, these statistics are necessarily real. The polynomial variables are given by the combined channel-equalizer taps h_i.

Next, the geometric object of a variety is introduced. In words, a variety is the solution set of a system of polynomial equations. Mathematically,

Variety: $\mathcal{V}(f_0, ..., f_s) = \{(a_0, ..., a_n) \in k^n : f_i(a_0, ..., a_n) = 0 \text{ for all } 0 \leq i \leq s\}$ (i.e. The solution set).

Seeking the stationary points of CMA has been described earlier as solving a system of multivariate polynomial equations. With the introduction of the concept of a variety, the stationary points are seen to be the variety $\mathcal{V}(f_0, ..., f_n)$. As will be seen, there is a close connection between the solution set (variety) and a more abstract algebraic concept known as an ideal, introduced presently.

Ideal: A subset $\mathcal{I} \subset k[x_0, ..., x_n]$ is an ideal if it satisfies the following conditions.

i) $0 \in \mathcal{I}$

ii) $f, g \in \mathcal{I} \quad \Rightarrow \quad f + g \in \mathcal{I}$

iii) $f \in \mathcal{I}$, $h \in k[x_0, ...x_n] \quad \Rightarrow \quad hf \in \mathcal{I}$

One way to form an ideal is to pick some finite set of polynomials as a "basis". Then this ideal consist of all "polynomial consequences" of this chosen set. For example, choosing polynomials $\{f_0(x), \ldots, f_s(x)\}$ as our basis, we see from the definition of an ideal, that it consists of polynomials $h(x)$ of form

$$h(x) = \sum_{i=0}^{s} p_i(x) f_i(x) \tag{6.5}$$

where $p_i(x)$ are any polynomials in ring.

How the concept of an ideal is helpful in solving polynomial equations is seen by noting the if $f_0(a) = \ldots = f_s(a) = 0$, then $h(a) = 0$ also. Now, suppose the existence of a different set of polynomials $\{g_0(x), \ldots, g_s(x)\}$ that was capable of recreating any of the $h(x)$ formed by (6.5). Then, f_i and g_i define the same ideal (written as $\langle f_0, \ldots, f_s \rangle = \langle g_0, \ldots, g_s \rangle$). Since f_i can be written as a linear combination of g_i and vice versa, means that $f_0(a) = \ldots = f_s(a) = 0 \Leftrightarrow g_0(a) = \ldots = g_s(a) = 0$. Hence, $\mathcal{V}(f_0, \ldots, f_s) = \mathcal{V}(g_0, \ldots, g_s)$. The point being that the solution set may be defined by the ideal generated by the equations, not just the equations themselves. A example of how useful this can be is presented.

6.2.2 Change of Basis Example

Consider the example of change of basis below (taken from [20]).

Q: Find x, y that solves $f_0(x, y) = f_1(x, y) = 0$, with

$$\begin{aligned} f_0 &= 2x^2 + 3y^2 - 11 \\ f_1 &= x^2 - y^2 - 3. \end{aligned}$$

A: In other words, we seek $\mathcal{V}(f_0, f_1)$. Notice we can write, a combination of f_0 and f_1 as,

$$\begin{aligned} f_0 + 3f_1 &= (2x^2 + 3y^2 - 11) + 3(x^2 - y^2 - 3) = 5(x^2 - 4) \\ f_0 - 2f_1 &= (2x^2 + 3y^2 - 11) - 2(x^2 - y^2 - 3) = 5(y^2 - 1) \end{aligned}$$

since $x^2 - 4$ and $y^2 - 1$ can be written as a polynomial consequence of f_0 and f_1, then they are in the same ideal (by definition of an ideal). Furthermore, one can say $\langle f_0, f_1 \rangle = \langle x^2 - 4, y^2 - 1 \rangle$. Now the interesting point is since $\langle f_0, f_1 \rangle = \langle x^2 - 4, y^2 - 1 \rangle$. we also have $\mathcal{V}(f_0, f_1) = \mathcal{V}(x^2 - 4, y^2 - 1)$. Notice that the solution of the second variety is "easier" due to the separation of variables yielding, $\mathcal{V}(f_0, f_1) = \{\pm 2 \pm 1\}$.

The points to emphasize from this example are,

- By changing the basis of the ideal, the system was made easier to solve.
- Varieties are determined by *ideals*, not by equations themselves.

The fundamental idea that a system of polynomial equations may be easier to solve after an appropriate change of basis is the basic idea of Groebner basis techniques.

6.2.3 Rings/Vector Space Comparison

As traditional engineering mathematics tend to focus on vector spaces and related techniques more so than algebraic concepts of ideals and varieties, a rough analogy between the structure of a vector space and a polynomial ring is found in Table 6.2.3.

The familiar concept of a finite dimensional vector space has the property of closure under scalar multiplication and vector addition. Furthermore, the vector space may be fully described by a set of *spanning* vectors. That is, all elements of the vector space may be reached by linear combinations (scalar multiplies and vector additions) of some finite set of vectors in this space — called a basis. Finally, there is no unique basis for a vector space, and transformation exists which provide a "change of basis".

Notice that an ideal is an object which also has closure under multiplication and addition. However, here this means something slightly different. Multiplication is by any element of the ring and addition is with any element of the ideal. The vector-space concept of spanning vectors may be associated with the existence of a *finite* set of polynomials from which all the members of the ideal may be attained through multiplication and addition — also called a basis. The change of

Table 6.1: Relation Between Rings and Vector Spaces

Rings	**Vector Spaces**	**Comment**
Ideal	Subspace	Closure under addition and multiplication
generated by $\langle f_0, ..., f_s \rangle$	spanned by $\langle w_0, ..., w_s \rangle$	Spanning sets define structure
$\langle f_0, ..., f_s \rangle = \langle g_0, ..., g_s \rangle \Rightarrow \mathcal{V}(f) = \mathcal{V}(g)$	$\langle w_0, ..., w_s \rangle = \langle u_0, ..., u_s \rangle \Rightarrow \mathcal{W} = \mathcal{U}$	Change of Basis

basis concept here means that, in general, there is no unique generating set for an ideal. There exists a "change of basis" to go from one generating set to another. In vector spaces a useful change of basis is one that transforms the system into upper triangular form, which allows solution of a single variable equations, through the use of backsubstitution. A similar form exists in polynomial rings: An ideal basis can be found which allows single variable polynomial equations to be solved through the use of backsubstitution (as seen in the above example).

6.2.4 Buchberger Algorithm, Elimination Ideal

While the actual issues of determining simplifying change of bases are beyond the scope of this work, it was seen that in the simple example of Section 6.2.2 the variety was easily solved by obtaining a system of univariate equations. In general, there exists an algorithm to reduce (in finite iterations) *all* ideals to forms which are solvable by backsubstitution of a single univariate equation. One such technique employs a (modified) Buchberger Algorithm. While this is a powerful technique there are several caveats to bear in mind.

- Intermediate term swell may make computation infeasible on real-world machines.

- Answer may be ugly, and not easily analyzed.

An example of such problems is presented for the CMA situation.

Example for Two Tap System

Consider using Groebner Basis techniques for solving the a *two*-tap combined channel-equalizer $H = [\, h_0 \quad h_1 \,]^t$. This may be phrased as finding the *variety* $\mathcal{V}(\mathcal{I})$, generated by the ideal $\mathcal{I}$ given by the stationary point equations,

$$\begin{aligned} ah_0^3 + 3bh_0^2h_1 + 3ch_0h_1^2 + dh_1^3 + eh_0 + fh_1 &= 0 \\ bh_0^3 + 3ch_0^2h_1 + 3dh_0h_1^2 + ah_1^3 + fh_0 + eh_1 &= 0 \end{aligned}$$

Here, the variables a, b, c, d, e, f are used as a shorthand notation to represent the fourth and second source sequence moments (i.e. the rather awkward $\mathcal{R}^{\,i}_{\substack{j\\k\\\ell}}$ and $\mathcal{R}^i_j$). Generating the elimination ideal for h_1 using the MACAULAY [1] computer algebra package yields the monovariate equation for h_1,

$$\alpha h_1^9 + \beta h_1^7 + \gamma h_1^5 + \delta h_1^3 + \epsilon h_1 = 0$$

Which can "easily" be solved given the values of $\alpha, \beta, \ldots$ as follows:

$$\alpha = a^6 - 27a^2b^4 + 54a^3b^2c - 18a^4c^2 - 54ab^2c^3 + 81a^2c^4 - 12a^4bd + 108ab^3cd$$

[1] MACAULAY is a computer algebra package developed by D. Bayer (Dept. of Mathematics, Columbia University) and M. Stillman (Dept. of Mathematics, Cornell University) and is available by ftp at `math.harvard.edu`.

$$
\begin{aligned}
& -180a^2bc^2d - 6a^2b^2d^2 + 54a^3cd^2 + 36b^2c^2d^2 - 54ac^3d^2 - 64b^3d^3 \\
& +108abcd^3 - 27a^2d^4 \\
\beta &= 3a^5e + 9a^3b^2e - 54ab^4e - 6a^4ce + 108a^2b^2ce - 36a^3c^2e - 27ab^2c^2e \\
& +54a^2c^3e - 54b^2c^3e + 81ac^4e - 24a^3bde + 18ab^3de - 60a^2bcde \\
& +108b^3cde - 180abc^2de + 9a^3d^2e - 6ab^2d^2e + 54a^2cd^2e \\
& +12b^2cd^2e - 27ac^2d^2e + 18abd^3e - 6a^4bf + 54ab^3cf \\
& -90a^2bc^2f - 6a^2b^2df + 54a^3cdf + 36b^2c^2df - 54ac^3df \\
& -96b^3d^2f + 162abcd^2f - 54a^2d^3f \\
\gamma &= 3a^4e^2 + 18a^2b^2e^2 - 27b^4e^2 - 12a^3ce^2 + 54ab^2ce^2 - 9a^2c^2e^2 \\
& -27b^2c^2e^2 + 54ac^3e^2 - 18a^2bde^2 + 18b^3de^2 - 60abcde^2 + 9a^2d^2e^2 \\
& -3b^2d^2e^2 - 12a^3bef - 18a^2bcef + 54b^3cef - 90abc^2ef + 6a^3def \\
& -6ab^2def + 54a^2cdef + 18b^2cdef - 36ac^2def + 30abd^2ef \\
& +12a^3cf^2 - 36b^3df^2 + 60abcdf^2 - 36a^2d^2f^2 \\
\delta &= a^3e^3 + 10ab^2e^3 - 6a^2ce^3 + 9ac^2e^3 - 6abde^3 - 8a^2be^2f - 18abce^2f \\
& +6a^2de^2f - 4b^2de^2f + a^3ef^2 + 12a^2cef^2 + 6b^2cef^2 - 9ac^2ef^2 \\
& +14abdef^2 - 4b^3f^3 + 6abcf^3 - 10a^2df^3 \\
\epsilon &= b^2e^4 - 2abe^3f + a^2e^2f^2 - b^2e^2f^2 + 2abef^3 - a^2f^4
\end{aligned}
$$

Attempting computation of Groebner Basis for higher order systems quickly exceeded program capacity. One of the problems is that our system of equations is regarded as having dense monomial support. In such cases, performing the Buchberger algorithm may be considered to be difficult due to the large number of terms that are involved in calculation of the elimination ideal. Additionally, we note that the complexity of CMA stationary point description shows that this is indeed a difficult problem. Furthermore, even in small order cases where the computation can be algebraically solved, one must question how much understanding of the problem is gained by the resulting solution. Consider, the solution for the two tap case above. Can one really gain a conceptual understanding of the problem from its reported solution?

Due to both the difficulty and limited usefulness of solving algebraically the system of equations, we adjusted our strategy. We see the need to consider more specific forms of correlation, and seek a different solution method.

6.3 Numerical Solution Method

Direct algebraic solution for the roots of $F(H, \vec{\mathcal{R}})$ is difficult in the general case, as F is a set of multivariate polynomial equations with many monomials. However, the numerical approach of continuation methods [2], [55] may be applied to solve for roots of $F(H, \vec{\mathcal{R}})$ given a *specific* $\vec{\mathcal{R}}$.

6.3.1 Homotopy and Continuation Methods

In this method, one introduces the homotopy

$$\Phi(\lambda) \quad = \quad \lambda F + c(1-\lambda)G \tag{6.6}$$

consisting of the system of interest (here, F), a system G with known roots, a random complex constant c, and a scalar $0 \leq \lambda \leq 1$. As $\Phi(\lambda)$ is a system with one degree of freedom, the solutions breakup into paths almost everywhere. The desired roots of F may be found by "tracing", in a predictor-corrector fashion, the roots of Φ from the known roots of G to the roots of F by varying λ from 0 to 1.

Mathematically, there are three issues of concern. First, in order to perform such root tracing, we must be guaranteed that there are the same number of roots of systems F and G. We construct G such that this is true and follows from Bernstein's Theorem [11] or by recognizing that our system F satisfies the Bezout upper bound. Furthermore, nastiness such as bifurcations (i.e. path crossings during roots tracings) must be ruled out. This is accomplished herein by the use of the random constant c which puts the systems F and G in relatively general position. A detailed presentation may be found in [55]. Specifically, we choose G to be the CMA-FSE system under independent uniformly distributed source, with the known 3^{n+1} solutions derived earlier.

For all homotopy methods calculations we have used PELICAN [2]. Also, to differentiate effects of correlated source investigated in this chapter from the effects of source distributions considered earlier, all source sequences used here have an equiprobable symbol occurrence. That is all periodic sequences used have an equal occurrence of each alphabet member, and the steady state probability vector for the Markov sources results in identical probability of occurrence for each alphabet member.

6.3.2 Experiment I: Periodic Sources

Using continuation methods, the stationary points for CMA-FSE under periodic sources may be computed. To gain some insight into how the MSE at stable stationary points may be effected as the period increases, a Monte-Carlo computation was performed. For each period (P) of length 32, 64, ..., 8192, twenty source sequences with equal symbol occurrence were randomly drawn from a 4-PAM, unit variance alphabet, (i.e. $\mathcal{A} = \{-3\Delta, -\Delta, +\Delta, +3\Delta\}$ with $\Delta = \frac{1}{\sqrt{5}}$). For each sequence, *all*

[2]PELICAN is a software package for polynomial continuation methods under development by Birk Huber at the Dept. of Mathematics, Cornell University. Documentation and release information available at `http://math.cornell.edu/~birk`

81 stationary combined channel-equalizer parametrizations corresponding to a 4 tap (half-baud spaced) channel and 4 tap (half-baud spaced) equalizer when $L = 2$ were computed.

Equalization Performance

The resulting μ_{COR} and MSE for the subset of stable, strictly real, stationary parametrizations resulting from these computations was also computed. (Stationary points with a non-zero imaginary component were not considered to be achievable by a strictly real channel-equalizer excited by a strictly real source. As such they were not included in performance analysis.) Results relating MSE and μ_{COR} are plotted in Figure 6.1 which exhibits a general trend of MSE with increasing correlation. Also plotted is MSE versus the sequence period (P) in Figure 6.2. Here as the period increases, MSE tends to decrease. As $\lim\limits_{P\to\infty} \mathrm{E}\left\{\mathcal{R}(\vec{P}) = \vec{\mathcal{R}}_w\right\}$, one expects that MSE $\to \infty$ as $P \to 0$ since $H \in \mathcal{C}_1$ (with non-zero element equal to one for the proper choice of γ) is a stable, stationary point for white sources.

It is noted that there exists a wide range of equalization performance (about 20dB MSE) for a given period (seen from Figure 6.2). This is not too surprising since for a given period some sequences appear "whiter" than others. For example, compare the period 12, zero mean, 4 PAM sequence S_a with the more random S_b below:

- $S_a = [3 \quad 3 \quad 3 \quad 1 \quad 1 \quad 1 \quad -1 \quad -1 \quad -1 \quad -3 \quad -3 \quad -3]^{\mathrm{T}}$
- $S_b = [1 \quad -1 \quad 3 \quad -3 \quad 1 \quad -1 \quad 3 \quad -1 \quad -3 \quad 3 \quad 1 \quad -3]^{\mathrm{T}}$.

Some sequences of a given period will then deform the error surface stationary points away from perfect equalization parametrizations more than other. However,

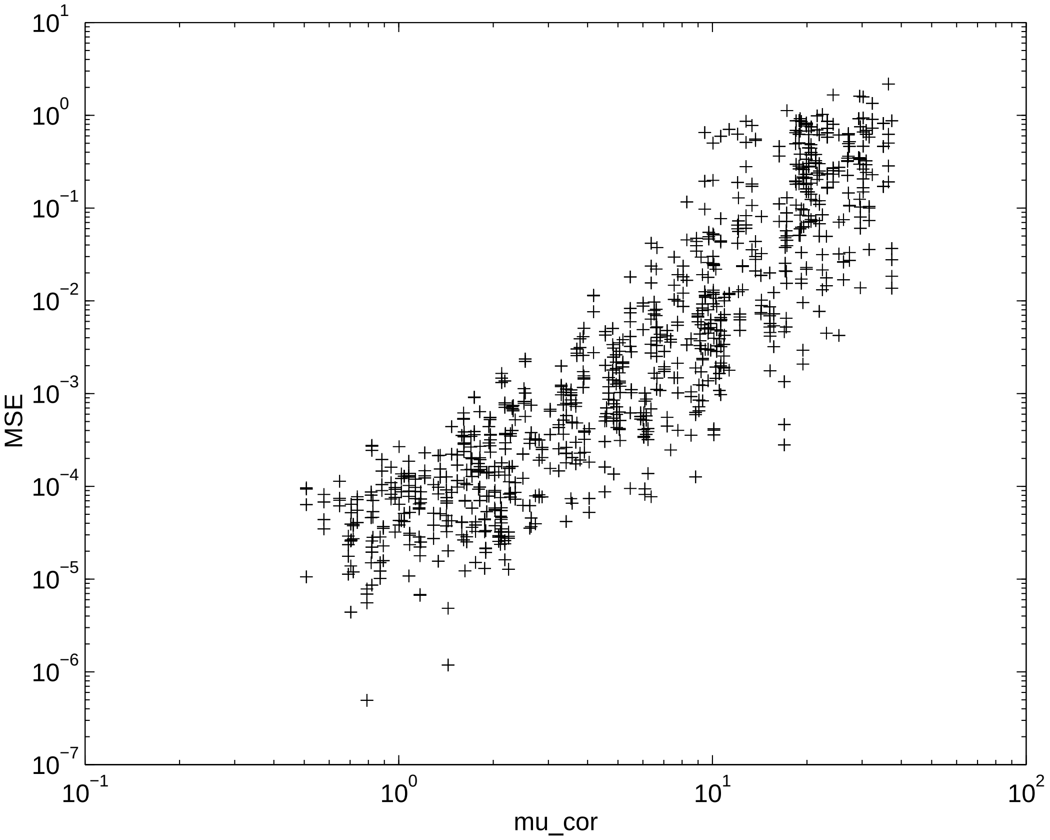

Figure 6.1: Periodic Source: MSE vs Correlation

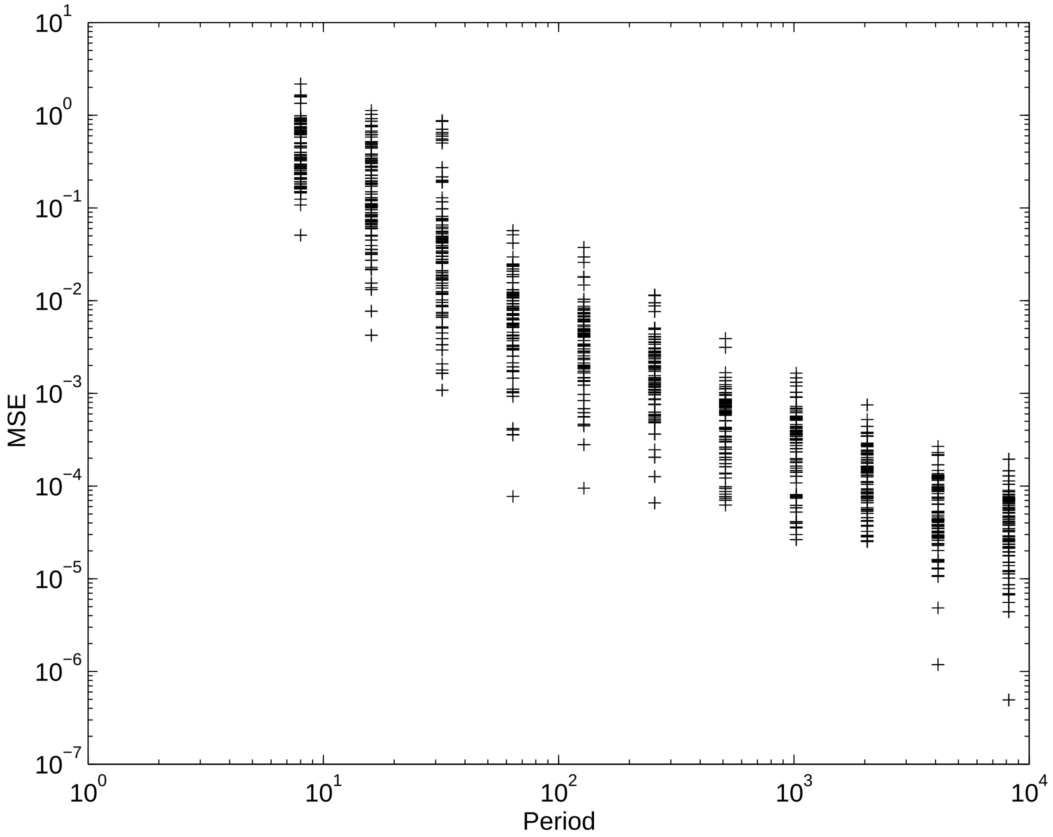

Figure 6.2: Periodic Source: MSE vs. Period

there is another more significant point that may be culled from the continuation method computations.

Changing Number of Minima

For each of the 220 source sequences considered, the number of (possibly complex) stable stationary solutions to $F(H, \vec{\mathcal{R}})$ due to a particular sequence of period P was computed, results shown in Figure 6.3. However, restricting our attention to the strictly real (i.e. achievable) parametrizations results in Figure 6.4. Notice that for sequences of short period, the number of minima may be double of that of sequences of long periods (as well as white). In the white source case the number of minima (all of which are strictly real) is 2^{n+1} (the number of vertices of the N-Octahedron). For $n+1 = 3$ we expect 8 minima. However, under source correlation we see that as many as 16 minima may exist. (It is noted that although our results herein for the 4 tap case shows only increases of number of minima under source correlation, it is also possible for the number of minima to decrease as well [48].)

Such an increase in the number of minima may be alarming. In essence, this means that the error surface has not merely deformed in such a way that resulting stable stationary points are just slightly shifted away from the perfect equalization parametrization. To the contrary, the error surface has deformed to the point that *new* minima have been created. Consider the example of Figure 6.5 which shows all eight stable parametrizations are depicted for a source sequence period of 2048 (four parametrizations are drawn explicitly, the other four are the negatives of those shown). All parametrizations have one significant tap and three taps weights of small magnitude. Hence, they correspond to relatively low ISI settings.

Contrast this to Figure 6.6 in which a sequence of period 32 yields ten stable

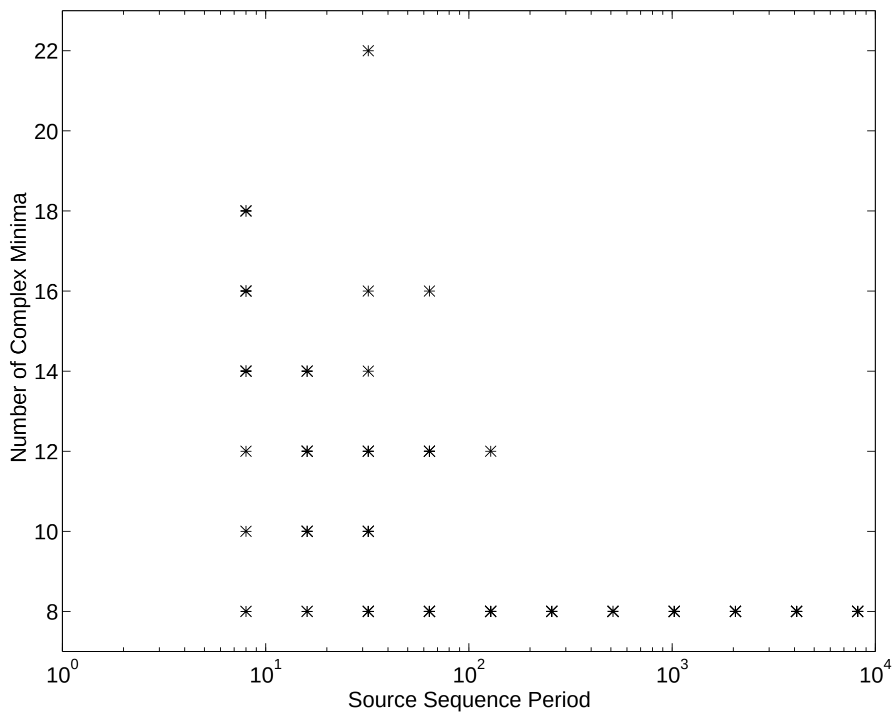

Figure 6.3: Number of Complex Minima under source of Period P.

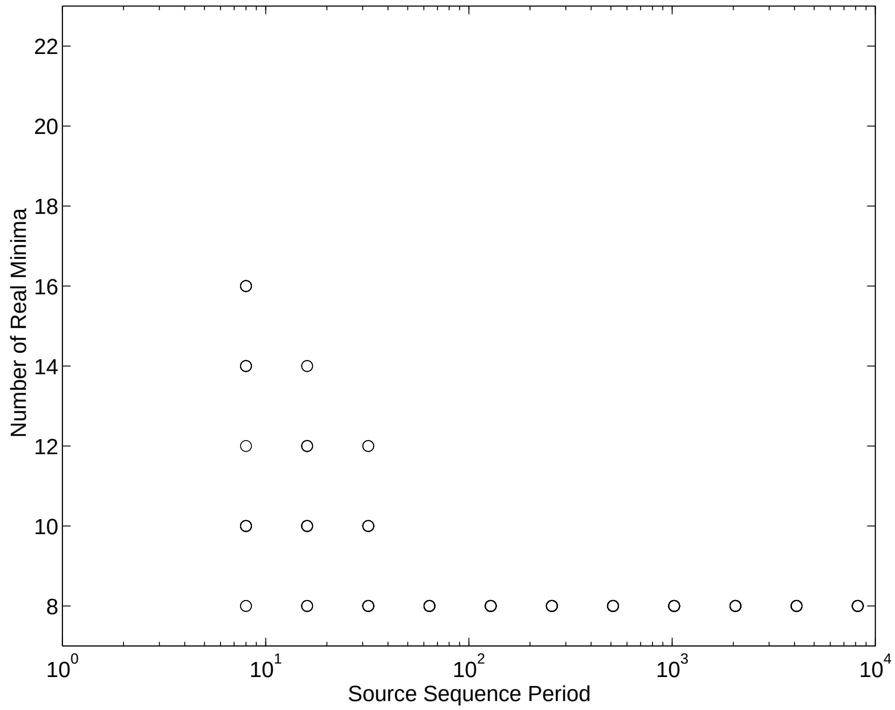

Figure 6.4: Number of Real Minima under source of Period P.

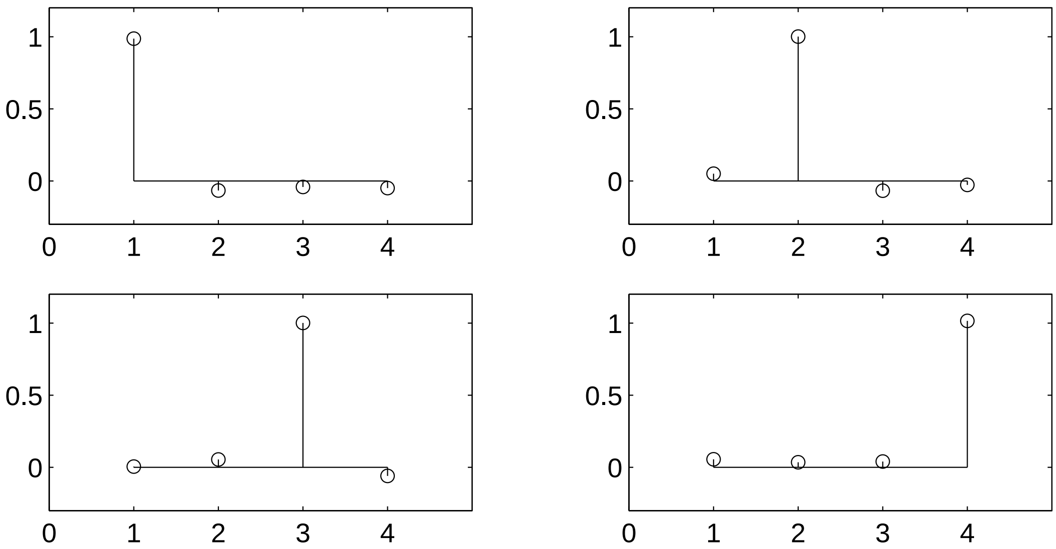

Figure 6.5: Period of 2048, 8 Minima with Low ISI

stationary points. Eight are fairly close to a good equalization setting (may be considered a displacement from perfect equalization by correlation induced deformation), the other two (the one shown and its negative) have high ISI settings (may be considered to be "new" minima created by error surface deformation).

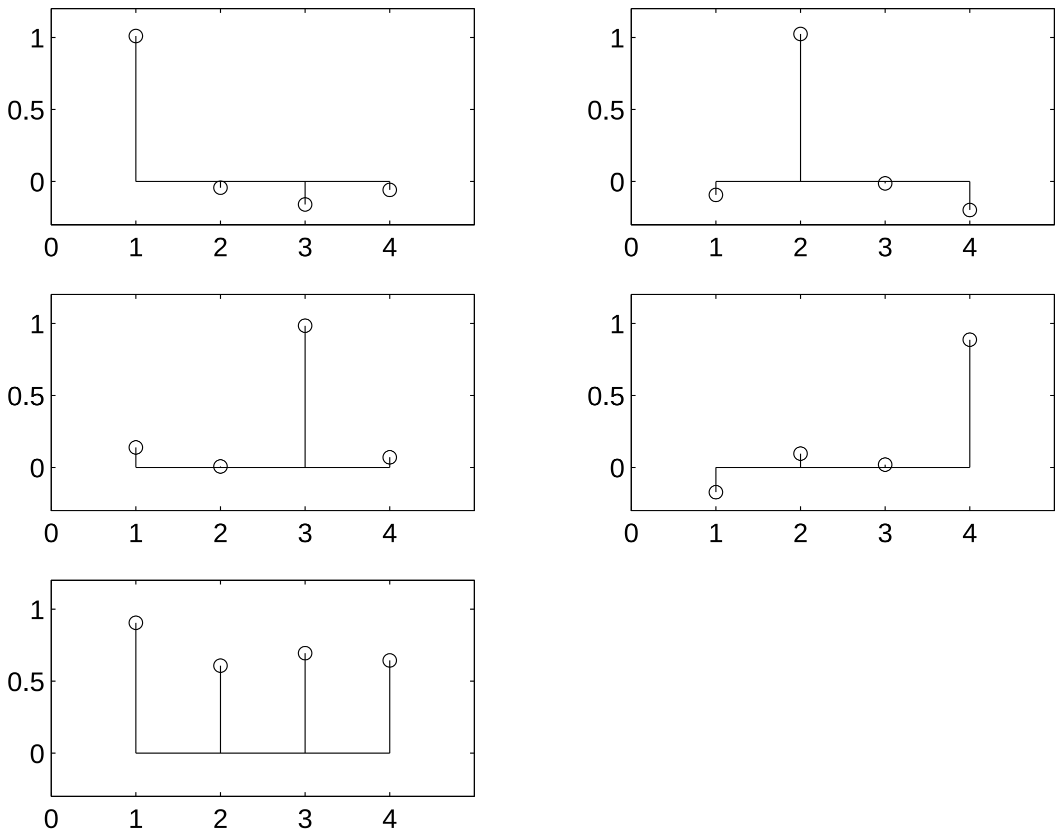

Figure 6.6: Period of 32: 10 Minima, 8 with low ISI, 2 with high ISI

Relation to Morse Theory

In chapter 5, the concept of how the γ manifold restricts the relative number of types of stationary points was discussed. Specifically, by Morse theory the Euler Characteristic of the manifold is related to the stationary points (through the faces of the polytopes by (5.19)). Here, for our 4 tap experiments we have

$$\chi(\mathcal{M}_\gamma) = \chi(\mathcal{S}^3) = 0 \quad = \quad \sum_{i=0}^{3} (-1)^i |\mathcal{F}_i| \tag{6.7}$$

where $|\mathcal{F}_i|$ is the number of stationary points with i negative eigenvalues of its Hessian on $\mathcal{M}_\gamma$. For the source associated with figure 6.6 we have $I_0 = 10$ (minima), $I_1 = 14$, $I_2 = 10$, $I_3 = 6$ (maxima). By (6.7) we have, $I_0 - I_1 + I_2 - I_3 = 10 - 14 + 10 - 6 = 0$. As a check for the correctness of the continuation runs, all 220 runs (incorporating over 17,000 data points) were verified to have the proper Euler character, $\chi(\mathcal{M}_\gamma) = 0$. To yield some insight into the possible homotopy types induced by correlation, the values of I_i were tabulated in Table E in Appendix E. The point here is that the deformation induced by source correlation does more that merely displace the minima existent in the uniformly distributed iid case. This table demonstrates the wide range of classifications possible under a correlated source.

6.3.3 Experiment II: Markov Sources

As another model of temporally correlated sources, we choose a Markov model. This allows the modeling of a white source as well as temporally correlated sources. Furthermore, since convex combinations of Markov transition matrices are themselves valid transition matrices, we can produce a source model which allows smoothly varying $\vec{\mathcal{R}}$. These $\vec{\mathcal{R}}$ may be calculated directly from the transition matrix Ξ as shown in Appendix A.

Consider a Markov state transition matrix, Ξ_w, (in which each state represents an alphabet member) which generates a white, uniformly distributed source. (i.e. each matrix element equals $\frac{1}{M}$ for a M-ary source). We choose a transition matrix, Ξ_c which corresponds to a source correlation of interest and redefine Φ to be

$$\Phi(\lambda) \quad = \quad F(H, \lambda\Xi_c + (1-\lambda)\Xi_w) \tag{6.8}$$

which yields a system wherein performing continuation methods yields a data point of interest at each evaluation of λ.

An example for the case Ξ_c as described in Appendix A demonstrates the stationary point movement from $H = [\,0 \quad 0 \quad 1 \quad 0 \quad 0\,]^{\mathrm{T}}$ for a combined channel-equalizer having a 5 baud span under increasing source correlation. Figure 6.7 plots the stationary point trajectory as λ in (6.8) is varied from 0 to 1. The increasing $\mathcal{ISI}$ is plotted as a function of λ in Figure 6.8. The Hessian of the cost function was checked at each iteration to verify the stationary point remained a stable one.

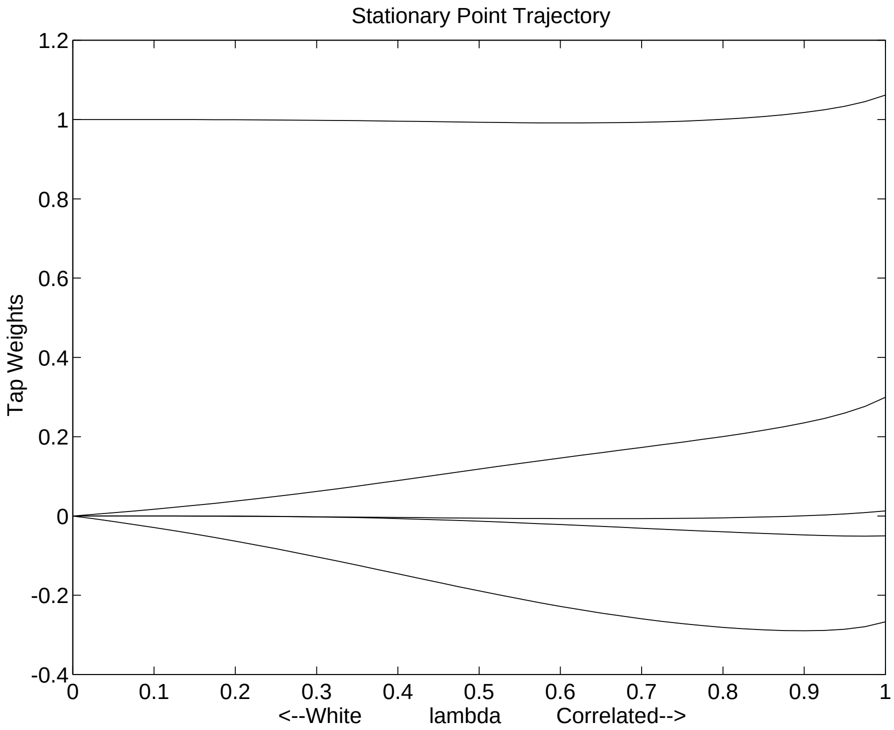

Figure 6.7: Markov Source: Stationary Point Trajectory

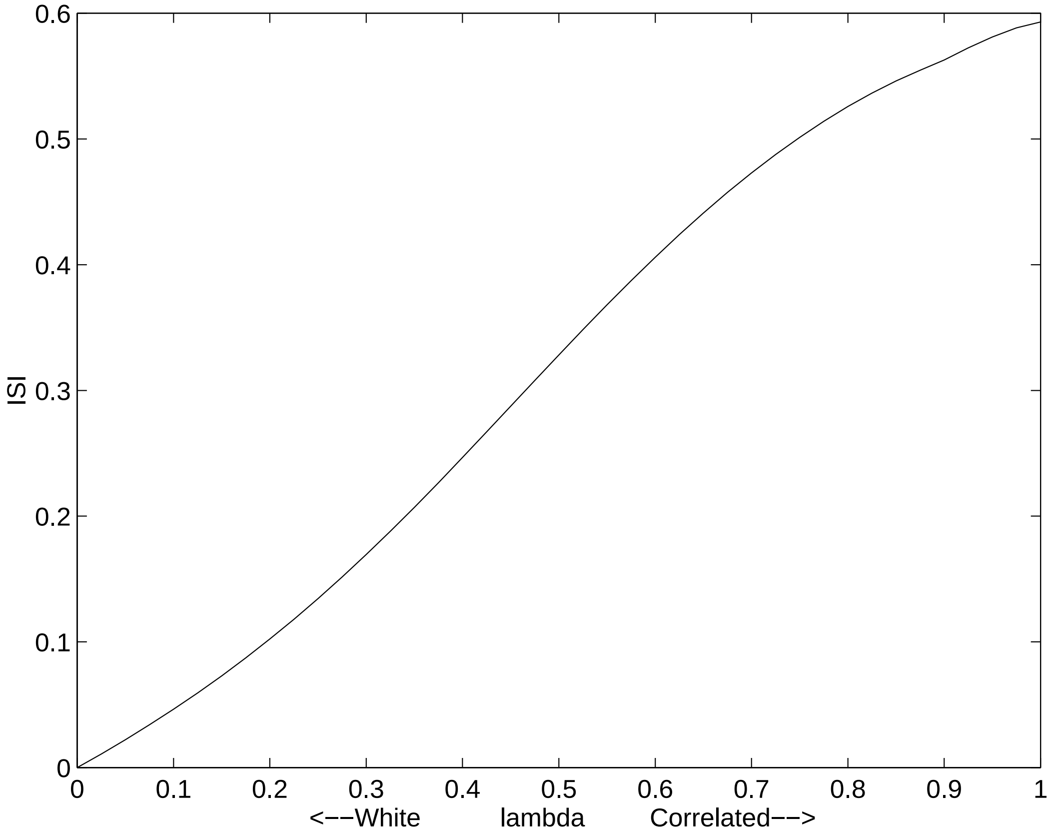

Figure 6.8: Markov Source: ISI versus λ

Chapter 7

Concluding Remarks

This work has investigated the FSE-CMA given the satisfaction of the equalizability condition. This condition allows examination in the combined channel-equalizer space using an equalizer of finite order. Behavior of FSE-CMA is understood through characterization of the CMA error surface. A main point of interest concerning the error surface is the location of stationary points, as the stable stationary points influence the asymptotic behavior, while the saddles influence the transient behavior.

7.1 New Results

Chapter 2 discussed the results of some fundamental papers and ideas in the blind equalization area. Almost all of this addresses baud spaced equalization using *infinitely* long equalizers. Some of such previous work is revisited again here (in Chapter 3), this time presented specifically for the *finite* order fractionally spaced equalizers using CMA. It is shown that earlier results such as global convergence for uniform iid source hold also for the CMA-FSE case.

While this is not a new (nor surprising) result, the phrasing of the problem as a system of multivariate polynomial equations leads to powerful extensions. We are able to quantitatively address the effects of various source distributions on the error surface. The *kurtosis* of the source is identified as the important quantity which influences convergent points (shown analytically) and convergence speed (demonstrated through analysis and numerical examples). Identification of all the stationary point locations, as well as their categorization (e.g. maximum, minimum, or saddle) is stretched to include enumeration of the number of positive and negative eigenvalues of their Hessian. In other words, the relative directional flow of the vector field near the stationary point has been described.

The results of the iid source case are combined with some simple properties of the error function to identify the topological concept of the γ manifold. Further geometric structure is introduced relating the vector field stationary points on the γ manifold to faces of polytopes. The dual polytopes (e.g. cross-polytope and n-cube) describe the vector field for platykurtic and leptokurtic source distributions.

Some topological concepts and observations on the CMA error surface are then noted in Chapter 5. The material was meant to serve as minimal background material necessary before presentation of the Homotopy methods used later in the source correlation efforts found in Chapter 6. The work on iid sources represents a mixture of refining known results and moderate extensions thereof. The true strength perhaps lies in the unified presentation allowed by the novel problem formulation.

The more fundamental contributions to knowledge are found in the later chapters. Herein, the solution to the polynomial system identifying the stationary points is considered for the temporally correlated source. We know of no work that attempts to solve this problem. Two avenues are explored, both using branches of mathematics not typically associated with the adaptive signal processing community. First, a strictly algebraic solution is discussed using Groebner Basis methods. Such methods are of questionable effectiveness for even moderate dimensions of the problem considered. However, the complicatedness of the solutions for a simple example demonstrate that algebraic solution, even when possible, may be difficult to interpret. This outcome motivates the second avenue which incorporates a numerical approach. Homotopy methods are introduced as a method for solving for stationary points for *given* source statistics. Monte Carlo computations are run for a class of correlated sources. The results are presented and discussed in terms of convergent ISI and MSE. An idea of the sensitivity to source correlation is gleaned and connections to the topological effects (e.g. Euler Characteristic) are noted.

7.2 Possible Directions of Future Work

Future work identified at this point may be divided into two different classes. Application of the mathematical tools of Groebner Basis methods and Homotopy methods to other (i.e. non-CMA) problems is an attractive proposition. These methods are powerful and their application in signal processing and related engineering fields is slight. Further use of these tools may yield new results in a variety of investigations.

More closely following the CMA work here, one of the more pressing unanswered question from this work is "How much correlation is too much to insure small stable point displacement?" This question is indeed a difficult one. One of the problems revolves on the issue "How does one quantify correlation?". We have presented a rather ad-hoc definition here and have seen widely varying equalization performance for similar correlations. Secondary issues involve determination of poor performance due to correlated sources and/or corrective measures. Tertiary issues of performance under correlated noise and/or interferers also may be worthy future study.

Appendix A

Markov Sources

A.1 Notation

The notation concerning source models using Markov processes used throughout this thesis is presented. Herein, the states of the Markov process ($\mathcal{S}$) are identified with a particular alphabet member, and the transition from present state to next state is associated with the Markov transition matrix Ξ.

A.1.1 Markov Source for Example C

Specifically, for the sample Markov source model used in Example C presented in Chapter 2, we have the state vector

$$\mathcal{S} \;=\; [\,\mathcal{A}(0) \quad \mathcal{A}(1) \quad \mathcal{A}(2) \quad \mathcal{A}(3) \quad \mathcal{A}(4) \quad \mathcal{A}(5) \quad \mathcal{A}(6) \quad \mathcal{A}(7)\,]^{\mathrm{T}}\,,$$

and,

$$\Xi = \begin{bmatrix} .000 & .600 & .025 & .300 & .025 & .000 & .025 & .025 \\ .025 & .000 & .600 & .025 & .300 & .025 & .000 & .025 \\ .025 & .025 & .000 & .600 & .025 & .300 & .025 & .000 \\ .000 & .025 & .025 & .000 & .600 & .025 & .300 & .025 \\ .025 & .000 & .025 & .025 & .000 & .600 & .025 & .300 \\ .300 & .025 & .000 & .025 & .025 & .000 & .600 & .025 \\ .025 & .300 & .025 & .000 & .025 & .025 & .000 & .600 \\ .600 & .025 & .300 & .025 & .000 & .025 & .025 & .000 \end{bmatrix}$$

wherein the $\Xi(i,j)$ elements give the probabilities of transitioning from state i to state j. Notice by the symmetry of Ξ, we have equiprobability of symbol occurrence. This can be shown formally by recognizing the vector $[\,\frac{1}{8}\ \frac{1}{8}\ \frac{1}{8}\ \frac{1}{8}\ \frac{1}{8}\ \frac{1}{8}\ \frac{1}{8}\ \frac{1}{8}\,]^{\mathrm{T}}$ is a eigenvector of Ξ whose elements are strictly positive and sum to one. Hence, it is the valid steady-state probability vector.

The spectrum of the resulting Markov process is shown in Figure A.1.

A.1.2 Markov Source for Continuation Methods

In chapter 6, experiment 2 a Markov source was used with state transition matrix Ξ_c given by

$$\Xi_c = \begin{bmatrix} 0 & 0.6 & 0.2 & 0.2 \\ 0 & 0 & 0.2 & 0.8 \\ 0.8 & 0.2 & 0 & 0 \\ 0.2 & 0.2 & 0.6 & 0 \end{bmatrix}$$

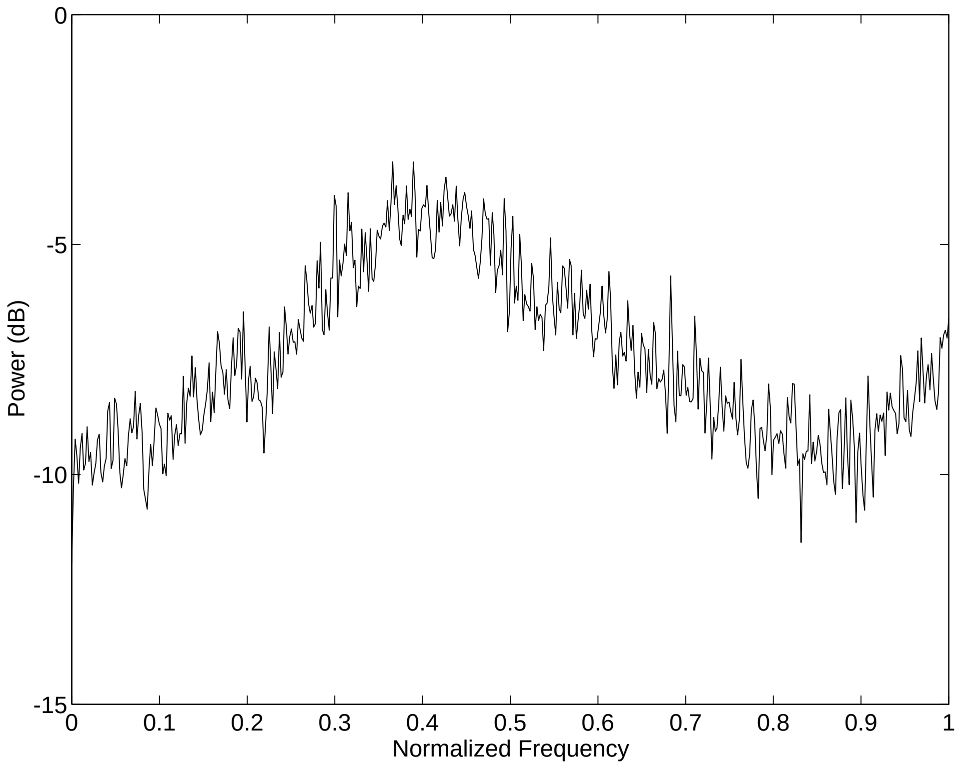

Figure A.1: Spectrum of Example "C" Markov Process

A.2 Moments

With the m-ary source having length m state vector as $\mathcal{S}$, and state transition matrix as Ξ as above, with the steady state probability vector $\Pi = [\,\pi_1 \quad \ldots \quad \pi_m\,]^{\mathrm{T}}$ (where π_i is the steady state probability of state i), then the temporal correlations for our zero mean process with states are then given by (without loss of generality assuming $i \leq j \leq k$),

$$\begin{aligned}
\mathcal{R}^{\substack{0\\i\\j\\k}} &= \sum_{\alpha,\beta,\gamma,\delta=0}^{m-1} a_\alpha a_\beta a_\gamma a_\delta \pi_\alpha (\Xi^{k-j})_{\delta,\gamma} (\Xi^{j-i})_{\gamma,\beta} (\Xi^{i})_{\beta,\alpha} \\
\mathcal{R}^{0}_{i} &= \sum_{\alpha,\beta=0}^{m-1} a_\alpha a_\beta \pi_\alpha (\Xi^{i})_{\beta,\alpha} \qquad \text{(A.1)}
\end{aligned}$$

Appendix B

Oversampling and Sub-Channel Equivalence

The relationship between the fractionally spaced channel and equalizer and the sub-channel model is demonstrated below. The source elements $s(k)$ are baud-

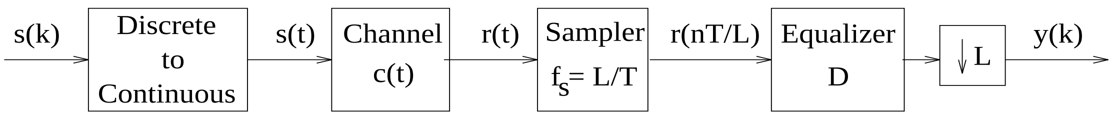

Figure B.1: Fractional Block Diagram

spaced (i.e. they appear each T units of time) are considered to be converted to a continuous time signal

$$s(t) \quad = \quad \sum_{-\infty}^{+\infty} \delta(t - kT)s(k). \tag{B.1}$$

before passing through the physical channel $c(t)$ which has inherently a continuous time transfer function model, The received signal before sampling is then determined by the convolution integral,

$$\begin{aligned}
r(t) &= \int_{-\infty}^{+\infty} c(\tau)s(t-\tau)d\tau \\
&= \int_{-\infty}^{+\infty} c(\tau)\left(\sum_{-\infty}^{+\infty}\delta(t-kT)s(k)\right)d\tau \\
&= \sum_{-\infty}^{+\infty} s(k)c(t-kT). \qquad \text{(B.2)}
\end{aligned}$$

Sampling the received signal faster than baud rate at $\frac{T}{L}$, and grouping into baud spanning vectors we have,

$$\vec{x}(n) = \begin{bmatrix} r(Tn) \\ r(T(n+\frac{1}{L})) \\ r(T(n+\frac{2}{L})) \\ \vdots \\ r(T(n+\frac{(L-1)}{L})) \end{bmatrix} = \begin{bmatrix} \sum s(k)c((n-k)T) \\ \sum s(k)c((n-k)T+\frac{T}{L}) \\ \sum s(k)c((n-k)T+2\frac{T}{L}) \\ \vdots \\ \sum s(k)c((n-k)T+(L-1)\frac{T}{L}) \end{bmatrix}. \qquad \text{(B.3)}$$

Such a grouping spanning a baud allows samples to be considered as vector samples. This formulation is often associated with beamforming and other multidimensional signal processing. In fact, its usefulness here demonstrates a relation between oversampling (temporal sampling) and beamforming (spatial sampling).

Recognize that the terms of the form $c(mT+i\frac{T}{L})$ consist of baud-spaced samples of $c(t)$ with a sub-baud delay of $\frac{iT}{L}$. Letting,

$$c_i(m) = c(mT+\frac{iT}{L}) \qquad \text{(B.4)}$$

to represent the i^{th} sub-channel. We begin to form the concept of a subchannel as depicted Figure B.2 for $L = 3$.

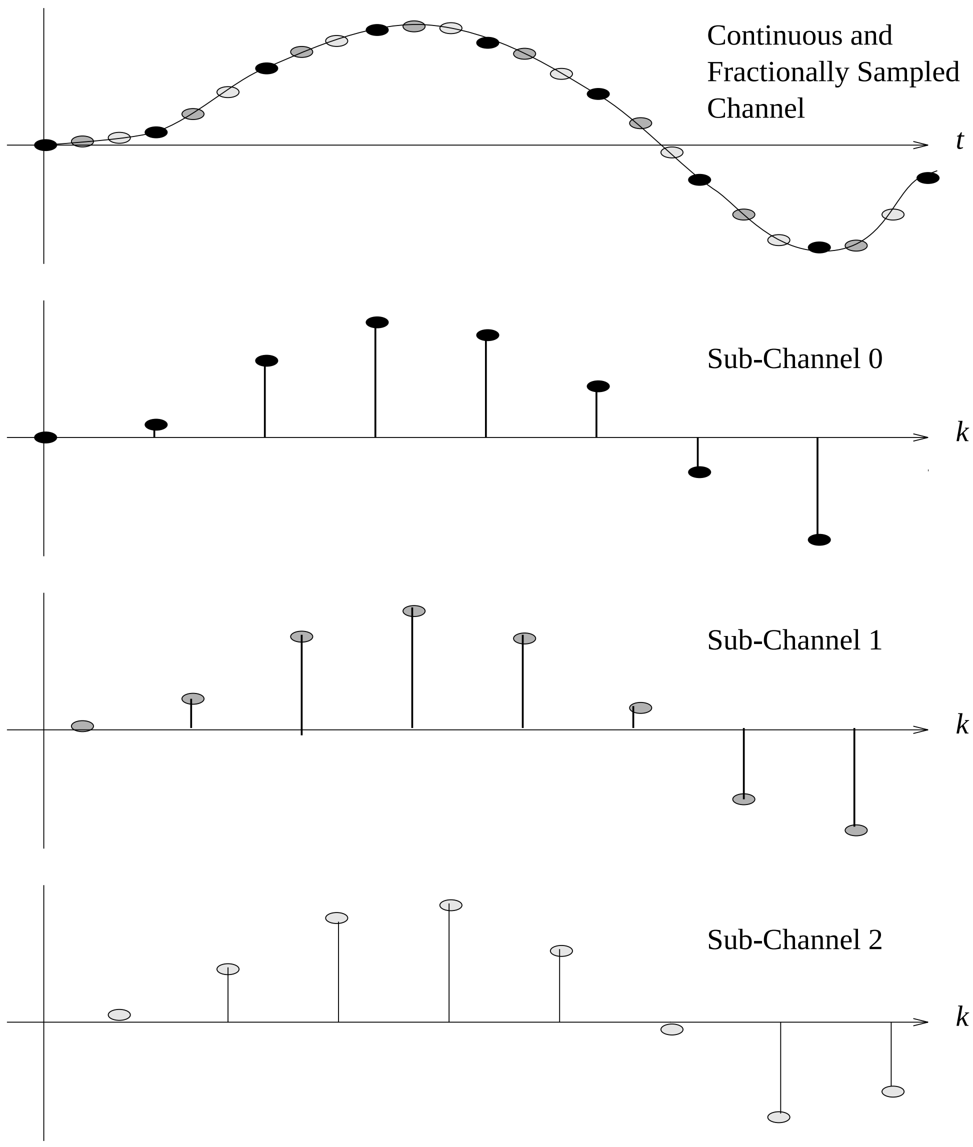

Figure B.2: Subchannel Concept for $L = 3$

Notice now that the i^{th} element of $\vec{x}$ in (B.3) is the result of the convolution sum of the source sequence $s(k)$ and sub-channel c_i,

$$\vec{x}(n) = \begin{bmatrix} s(n) * c_0 \\ s(n) * c_1 \\ s(n) * c_2 \\ \vdots \\ s(n) * c_{L-1} \end{bmatrix} \tag{B.5}$$

where "$*$" represents the convolution operator.

The regressor of the $N+1$ tap equalizer can be written as the vector of the last $N+1$ received samples.

$$X(k) = \begin{bmatrix} \vec{x}(k) \\ \vec{x}(k-1) \\ \vdots \\ \vec{x}(k-(\frac{N+1}{L}-1)) \end{bmatrix} = \begin{bmatrix} s(k) * c_0 \\ \vdots \\ s(k) * c_{L-1} \\ \hline s(k-1) * c_0 \\ \vdots \\ s(k-1) * c_{L-1} \\ \hline \vdots \\ \hline s(k-(\frac{N+1}{L}-1)) * c_0 \\ \cdots \\ s(k-(\frac{N+1}{L}-1)) * c_{L-1} \end{bmatrix} \tag{B.6}$$

We now turn our attention to the desampled equalizer output y which can be written as the inner product of the equalizer regressor $X(k)$ and tap weights D,

$$y(k) \;=\; X^{\mathrm{T}}(k)D \tag{B.7}$$

Noticing that there are $\frac{N+1}{L}$ entries of $X(k)$ corresponding to each subchannel, we denote the regressor entries corresponding to subchannel i as $X_i(k)$. Similarly we form the vector of taps corresponding to each (i.e. multiplied by $X_i(k)$) as D_i. Then, we have the equalizer output written as,

$$y(k) \;=\; X^{\mathrm{T}}(k)D = X_0^{\mathrm{T}}(k)D_0 + X_1^{\mathrm{T}}(k)D_1 + \ldots + X_{L-1}^{\mathrm{T}}(k)D_{L-1} \tag{B.8}$$

which is just a rearrangement of the inner product sum. By this rearrangement we consider the combined continuous channel in cascade with a fractionally spaced equalizer as the parallel sum of L baud-spaced discrete channel, known as the sub-channel model.

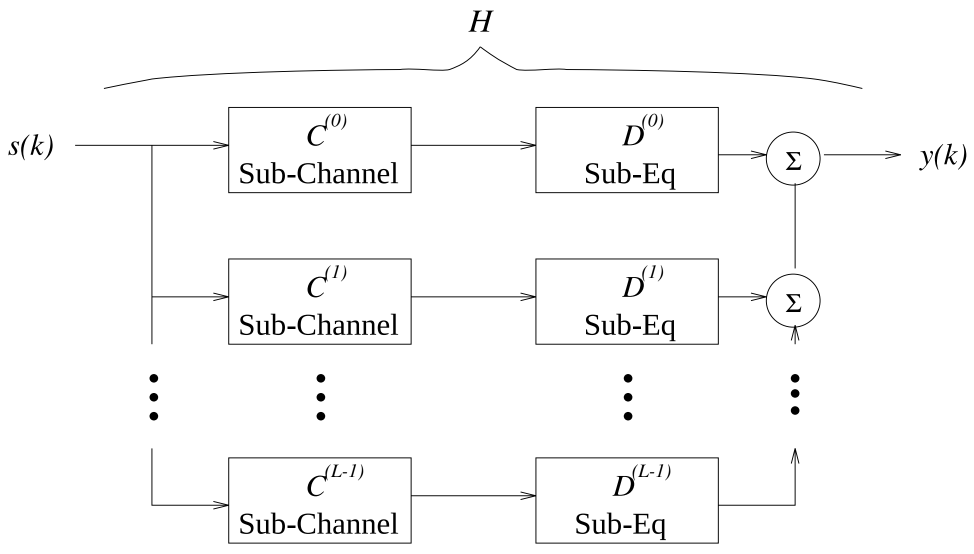

Figure B.3: Sub-Channel Model

Appendix C

Related Reading

[C1] S. A. Alshebeili, A. N. Venetsanopoulos, A. E. Cetin, "Cumulant Based Identification Approaches for Nonminimum Phase FIR Systems," *IEEE Trans. on Signal Processing*, vol. 41, no. 4, Apr. 1993.

[C2] J. Benesty, P. Duhamel, "Fast Constant Modulus Adaptive Algorithm," *IEE Proceedings-F*, vol. 138, no. 4, Aug 1991.

[C3] Z. Ding, "Application Aspects of Blind Adaptive Equalizers in QAM Data Communications," *PhD Thesis, Cornell University*, Aug. 1990.

[C4] M. R. Frater, R. R. Bitmead, C. R. Johnson, Jr., "Local Minima Escape Transients by Stochastic Gradient Descent Algorithms in Blind Adaptive Equalizers," *Automatica*, vol. 31, no. 4, 1995.

[C5] S. B. Gelfand, C. S. Ravishankar, E. J. Delp, "Tree-Structured Piecewise Linear Adaptive Equalization," *IEEE Transaction on Commun.*, vol. 41, no. 1, Jan. 1993.

[C6] F. Gustafsson, B. Wahlberg, "Blind Equalization by Direct Examination of the Input Sequences," *Proc. of IEEE Conf. Acoust., Speech, Signal Processing*, 1992.

[C7] K. Hilal, P. Duhamel, "A General Form for Recursive Adaptive Algorithms Leading to an Exact Recursive CMA," *Proc. of IEEE Conf. Acoust., Speech, Signal Processing*, 1992.

[C8] N. K. Jablon, "Joint Blind Equalization, Carrier Recovery, and Timing Recovery for 64-QAM and 128-QAM Signal Constellations," *IEEE Int'l Conf on Comm.*, 1989.

[C9] N. K. Jablon, "Joint Blind Equalization, Carrier Recovery, and Timing Recovery for High-Order QAM Signal Constellations," *IEEE Trans. on Signal Processing*, vol. 40, no. 6, Jun. 1992.

[C10] B. Jelonnek, K. D. Kammeyer, "Improved Methods for the Blind System Identification Using Higher Order Statistics," *IEEE Trans. on Signal Processing*, vol. 40, no. 12, Dec. 1992.

[C11] C. R. Johnson, Jr., S. Dasgupta, W. A. Sethares, "Averaging Analysis of Local Stability of a Real Constant Modulus Algorithm Adaptive Filter," *IEEE Trans. on Acoust., Speech, and Signal Processing*, vol. 36, no. 6, Jun. 1988.

[C12] R. A. Kennedy, K. Yamazaki, Z. Ding, S. Verdu, S. Vembu, "Approaches to Blind Equalization: Open Problems," *IFAC Int'l. Symp. on Adapt.Sys. in Contr. and Sig. Proc.*, July 1992.

[C13] T. H. Li, "Blind Identification and Deconvolution of Linear Systems Driven by Binary Random Sequences," *IEEE Trans. on Inform. Theory*, vol. 38, no. 1, Jan. 1992.

[C14] R. W. Lucky, "Techniques for Adaptive Equalization of Digital Communication Systems," *Bell System Technical Journal*, Feb. 1966.

[C15] J. E. Mazo, "Analysis of Decision-Directed Equalizer Convergence," *Bell System Techincal Journal*, Dec. 1980.

[C16] R. Mendoza, J. H. Reed, T. C. Reed, T. C. Hsia, B. G. Agee, "Interference Rejection Using the Time-Dependent Constant Modulus Algorithm (CMA) and the Hybrid CMA/Spectral Correlation Discriminator," *IEEE Trans. on Signal Processing*, vol. 39, no. 9, Sept. 1991.

[C17] E. Moulines, P. Duhamel, J.-F. Cardoso, S. Mayrargue, "Subspace Methods for the Blind Identification of Multichannel FIR Filters," *IEEE Trans. on Signal Processing*, Feb. 1995.

[C18] Y. Sato, H. Oda, S. Hashimoto, "Blind Suppression of Time Dependency and Its Extension to Multi-Dimensional Equalization," *IEEE Global Telecommunications Conference*, 1986.

[C19] J. C. Serra, N. L. Esteves, "A Blind Equalization Algorithm without Decision," *Proc. of IEEE Conf. Acoust., Speech, Signal Processing*, vol. 3, 1984.

[C20] W. A. Sethares, G. A. Rey, C. R. Johnson, Jr., "Approaches to Blind Equalization of Signals with Multiple Modulus," *Proc. of IEEE Conf. Acoust., Speech, Signal Processing*, 1989.

[C21] G. Strang, *Linear Algebra and its Applications, Third Edition*, San Diego: Harcourt, Brace, and Jovanovich, 1988.

[C22] L. Tong, R. Liu, V. C. Soon, Y. Huang, "Indeterminacy and Identifiability of Blind Identification," *IEEE Trans. on Circuits and Systems*, vol. 38, no. 5, May 1991.

[C23] L. Tong, G. Xu, T. Kailath, "Fast Blind Equalization via Antenna Arrays," *Proc. of IEEE Conf. Acoust., Speech, Signal Processing*, 1993.

[C24] J. K. Tugnait, "Comments on 'New Criteria for Blind Deconvolution of Nonminimum Phase Systems (Channels)' ," *IEEE Trans. on Inform. Theory*, vol. 38, no. 1, Jan. 1992.

[C25] S. Verdu, B. D. O. Anderson, R. A. Kennedy, "Blind Equalization without Gain Identification," *IEEE Trans. on Inform. Theory*, vol. 39, no. 1, Jan. 1993.

[C26] V. Weerackody, S. A. Kassam, K. R. Laker, "A Convergence Model for the Analysis of Some Blind Equalization Algorithms," *IEEE International Symposium on Circuits and Systems*, vol. 3, 1989.

[C27] D. Yellin, B. Porat, "Blind Identification of FIR Systems Excited by Discrete-Alphabet Inputs," *IEEE Trans. on Signal Processing*, vol. 41, no. 3, Mar. 1993.

[C28] F. C. Zheng, S. McLaughlin, B. Mulgrew, "Blind Equalization of Nonminimum Phase Channels: Higher Order Cumulant Based Algorithm," *IEEE Trans. on Signal Processing*, vol. 41, no. 2, Feb. 1993.

Appendix D

Received Signal Distributions

In this appendix the successful equalization of a received signal which has a very-nearly Gaussian distribution is presented. Consider a Bernoulli source $s(k) \in \{-1, +1\}$, iid with $p(-1) = \frac{1}{2}$, $p(+1) = \frac{1}{2}$, passing through an infinite impulse response (IIR) channel,

$$C(z) = \frac{1}{z - 0.95}$$

The received signal $r(k)$ has the measured distribution from 400000 data points as shown in Figure D.1. Comparison with a true Gaussian distribution (shown as solid line in Figure) shows almost perfect matching. In fact, the measured kurtosis is $\kappa_{\mathrm{R}} = 2.91$ (compared with $K = 3$ for true Gaussian) which also serves to demonstrate its near Gaussian quality.

CMA was used in an baud spaced adaptive equalizer initialized with $D(0) = [1 \quad 0]^{\mathrm{T}}$ and $\mu = 10^{-4}$. Figures D.2, D.3, and D.4 show the resulting output $y(k)$, $\mathcal{ISI}$, and equalizer tap trajectories $D(k)$, respectively. The near Gaussian quality of the received signal has not hampered CMA's convergence. This is in contrast to

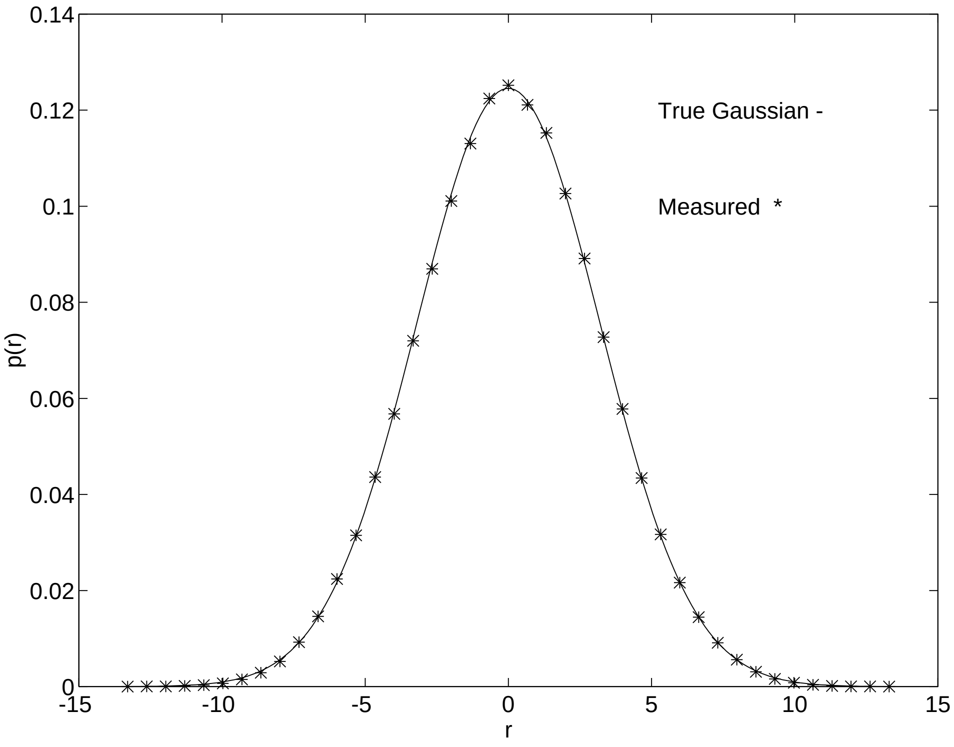

Figure D.1: Histogram of r and Gaussian PDF the example in Chapter 4 wherein CMA's convergence is seriously effected as the *source* kurtosis approaches 3 (e.g. $\kappa_S \to 3$).

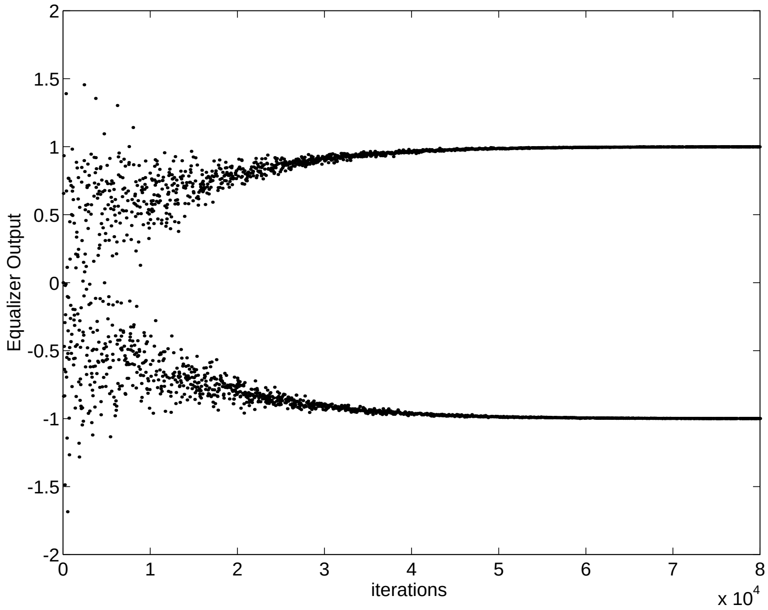

Figure D.2: Equalizer Output

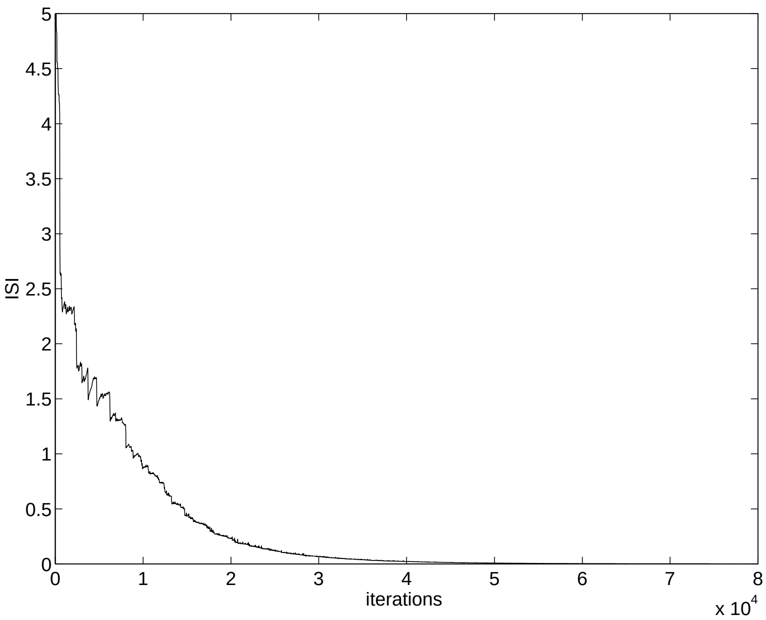

Figure D.3: ISI Trajectory

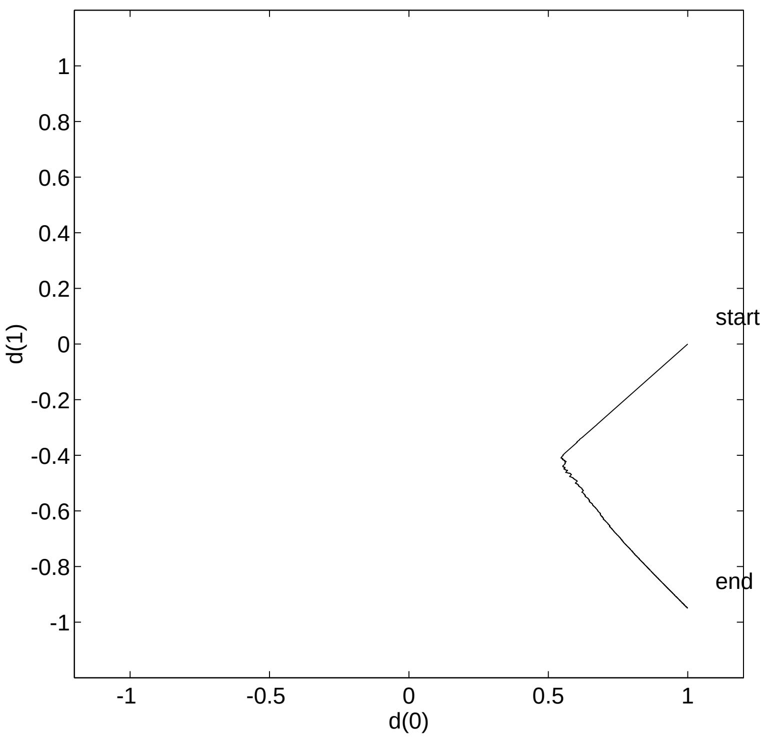

Figure D.4: Equalizer Tap Trajectory

Appendix E

Tabulations of Homotopy Types

For the four tap channel-equalizer system investigated using the continuation methods, a maximum of 80 stationary points was possible on $\mathcal{M}_\gamma$ (the remaining one is at the origin). Only strictly real stationary point parametrizations are achievable for a real equalizer. Hence, only strictly real stationary points were considered further. For each of the 220 source sequences, all stationary points were computed. For each strictly real stationary point, the *morse index* was determined (i.e. the number of negative eigenvalues of the Hessian evaluated at that point tangent to $\mathcal{M}_\gamma$).

The results are tabulated below in Table E. Here N is the total number of strictly real stationary points on the γ manifold. The columns I_0 are the number of stable stationary points (have no negative eigenvalues on $\mathcal{M}_\gamma$), I_1 are saddles with one negative eigenvalue on $\mathcal{M}_\gamma$, I_2 are saddles with two negative eigenvalues on $\mathcal{M}_\gamma$, and I_3 are maxima of $\mathcal{M}_\gamma$ with 3 negative eigenvalue on $\mathcal{M}_\gamma$. The point of this table is to show that many homotopy types are possible due to source correlation even for this low dimensional example. It has been verified that the alternating sum of I_i is zero, meeting the Euler Characteristic (i.e. $\chi(\mathcal{S}) = 0$).

Table E.1: Homotopy Types Occuring under Correlation

$N = 28$			
I_0	I_1	I_2	I_3
8	10	6	4

$N = 36$			
I_0	I_1	I_2	I_3
8	14	10	4

$N = 40$			
I_0	I_1	I_2	I_3
8	12	12	8
8	14	12	6
8	16	12	4
10	14	10	6

$N = 44$			
I_0	I_1	I_2	I_3
8	14	14	8
8	16	14	6
10	16	12	6
12	18	10	4

$N = 48$			
I_0	I_1	I_2	I_3
8	16	16	8
8	18	16	6
10	18	14	6
10	20	14	4
12	20	12	4

$N = 52$			
I_0	I_1	I_2	I_3
8	16	18	10
8	18	18	8
8	20	18	6
10	18	16	8
10	20	16	6
10	22	16	4

$N = 56$			
I_0	I_1	I_2	I_3
8	18	20	10
8	20	20	8
8	22	20	6
10	20	18	8
10	22	18	6

$N = 60$			
I_0	I_1	I_2	I_3
8	20	22	10
8	22	22	8
10	22	20	8
12	22	18	8
12	24	18	6
14	22	16	8

$N = 64$			
I_0	I_1	I_2	I_3
8	20	24	12
8	22	24	10
8	24	24	8
10	24	22	8
12	24	20	8
14	24	18	8

$N = 68$			
I_0	I_1	I_2	I_3
8	24	26	10
12	26	22	8
14	26	20	8

$N = 72$			
I_0	I_1	I_2	I_3
8	24	28	12
14	28	22	8

$N = 76$			
I_0	I_1	I_2	I_3
8	24	30	14
14	30	24	8
16	30	22	8

$N = 80$			
I_0	I_1	I_2	I_3
8	24	32	16
16	32	24	8

Appendix F

Definitions of Topological Terms

This appendix contains definitions of the topological terms used in this thesis, particularly in Chapter 5. These definitions, taken from [36], are meant to provide more precise definitions than those used in the presentation of Chapter 5, which was a bit conversational in tone. Not all of the terms below are used in Chapter 5, but serve as intermediate definitions.

F.1 Functions

Inclusion: For $X \subset Y$, the function $i : X \rightarrow Y$ defined by $i(x) = x \in Y$ for every $x \in X$ is called the *inclusion function* of X into Y.

Restriction: Let $f : X \rightarrow Y$ be a given function and A be a subset of X. Define $g : A \rightarrow Y$ by taking $g(x) = f(x)$ for every $x \in A$. This function g will be called the *restriction* of the given function f to the subset A; in symbols

$$g = f|A.$$

Extension: If $g = f|A$, then the function $f : X \to Y$ is said to be an *extension* of the function $g : A \to Y$ over the set X.

F.2 Topological Spaces

Topology: Let X be a given set of objects called the points of X. A *topology* in X is a nonempty collection of subsets

$$\tau \subset 2^X$$

of X called *open sets* satisfying the following four axioms.

1. The empty set is open.
2. The set X itself is open.
3. The union of any family of open sets is open.
4. The intersection of any two (and hence any finite number of) open sets is open.

A set X is said to be topologized if a topology τ has been given in X. A topologized set X will be called a *topological space* or simply a *space* and the topology tau in X is called the *topology of the space* X.

Basis: A *basis* of a topology τ in X is a subcollection β of τ such that every open set U in τ is a union of some open sets in β. In other words, for every $U \in \tau$ and each point $x \in U$, there is a $V \in \beta$ such that

$$x \in V \subset U$$

The open sets of a given basis β will be called the *basic open sets* of the space X.

Sub-basis: A *sub-basis* of a topology τ in X is a subcollection σ of τ such that finite intersections of open sets in σ form a basis of τ. In other words, for every $U \in \tau$ and each point $x \in U$, there is a $V \in \beta$ such that

$$x \in V \subset U.$$

Neighborhood Let X be a given space and p a given point in X. A set $N \subset X$ is said to be a *neighborhood* of the point p in the space X iff there exists an open set U of X such that

$$p \in U \subset N.$$

Hence a neighborhood of a point p in a space X is a set in X containing not only the point p itself but also some open set of X which contains p.

F.3 Sets in a Space

Interior Point: The point p is said to be an *interior point* of the set E provided that there exists a neighborhood N of p in X contained in E.

Exterior Point: The point p is said to be an *exterior point* of the set E provided that there exists a neighborhood N of p in X which contains no point of E.

Boundary Point: A point is said to be a *boundary point* of E in case every neighborhood N of p in X contains at least one point in E and at least one point not in E.

Related concepts are:

- The set $\mathrm{Int}(E)$ of all interior points of E is called the *interior* of E.

- The set $\mathrm{Ext}(E)$ of all exterior points of E is called the *exterior* of E.
- The set $\partial(E)$ of all boundary points of E is called the *boundary* of E in space X.
- The *closure* of a set E in a space X, $\mathrm{Cl}(E)$ is the smallest closed set of X which contains E.

Accumulation Point: A point p of a space X is said to be an *accumulation point* or *cluster point* or *limit point* of a set E in X iff every neighborhood N of p in X contains at least one point of E other than p.

Derived Set: The set E' of all accumulation points of E in X is called the *derived set* of E in X.

Dense: A set E in space X is said to be *dense* in X iff $\mathrm{Cl}(E)=X$.

Separable: A space X is said to be *separable* iff it contains a countable subset which is dense in X.

F.4 Maps

Continuous Functions (Maps): Consider a function

$$f : X \to Y$$

of which both the domain X and the range Y are spaces. The function f is said to be *continuous at a point* p of X iff, for every neighborhood N of the point $f(p)$ in Y, there exists a neighborhood M of the point p in X such that $f(M) \subset N$. The function f is said to be *continuous* iff it is continuous at every point in X. Continuous functions will be called *maps*.

Theorem. If $f : X \to Y$ is a function from a space X into a space Y with a given basis and a given sub-basis of its topology, then the following statements are equivalent.

1. The function $f : X \to Y$ is a map.
2. The inverse image $f^{-1}(U)$ of each open set U in Y is open in X.
3. The inverse image $f^{-1}(V)$ of each basic open set V in Y is open in X.
4. The inverse image $f^{-1}(W)$ of each sub-basic open set W in Y is open in X.
5. The inverse image $f^{-1}(F)$ of each closed set F in Y is closed in X.
6. $f[\mathrm{Cl}(A)] \subset \mathrm{Cl}[f(A)]$ for each $A \subset X$.
7. $f^{-1}[\mathrm{Cl}(B)] \supset \mathrm{Cl}[f^{-1}(B)]$ for each $B \subset Y$.

Open Map: A map $f : X \to Y$ from a space X into a space Y is said to be *open* iff the image $f(U)$ of every open set U in X is open in Y.

Closed Map: A map $f : X \to Y$ from a space X into a space Y is said to be *closed* iff the image $f(F)$ of every closed set U in X is open in Y.

Bijective Map: For any bijective map (one-to-one and onto) $f : X \to Y$, the following statements are equivalent

1. The inverse function $f^{-1} : Y \to X$ is continuous.
2. $f : X \to Y$ is open.
3. $f : X \to Y$ is closed.

Homeomorphism: By a *homeomorphism* or *topological map*, we mean a bijective map $f : X \to Y$ which satisfies the equivalent conditions above.

Topological Equivalence: If a homeomorphism $h : X \to Y$ exists, then the two spaces X and Y are said to be *homeomorphic* or *topologically equivalent.* Each space X and Y are said to be a *homeomorph* of the other.

Topological Property: A property which when possessed by a space is also possessed by each of its homeomorphs is called a *topological property.*

Topology: Formally, *topology* is the study of topological properties of spaces.

Induced Topology: Consider the function $f : X \to Y$ from a set X to a set Y. Let τ be an arbitrary topology in X. Define a collection θ of subsets of Y as follows: a subset V of Y is in θ iff the inverse image $f^{-1}(V)$ is in τ. θ is the largest topology in Y which makes f a map. This topology θ is said to be the *induced topology* in Y by the function f and the topology τ in X, and will be denoted by $f_*(\tau)$

On the other hand, let η be an arbitrary topology in Y. Then it is obvious that the collection

$$\psi = \{f^{-1}(V) | V \in \eta\}$$

of subsets of X is a topology in X. ψ is the smallest topology in X which makes f a map. This topology η is said to be the *induced topology* in X by the function f and the topology η in Y and will be denoted by $f^{-1}(\eta)$.

F.5 Subspaces

Relative Topology: Let E be a given subset of a space X with a topology τ. Then, the inclusion function $i : E \subset X$ induces a topology $i^{-1}(\tau)$ in E. This topology $i^{-1}(\tau)$ in E will be called the *relative topology* in E with respect to τ.

Subspace: When topologized by the relative topology $i^{-1}(\tau)$, E will be called a *subspace* of the space X.

Retraction: Consider the case where $Y = E$ and $g : E \to Y$ is the identity map on E. Then an extension of g over the space X will be a map $r : X \to E$ such that $r|E$ is the identity map on E. Such a map $r : X \to E$ will be called a *retraction* of X onto E. If a retraction of X onto E exists, this subspace E of X is said to be a *retract* of the space X.

Covering: By a *covering* or *cover* of a space X, we mean a collection γ of subspaces of the space X such that the union of all members of γ is the whole space X. If every member of γ is open, γ is said to be an *open cover* of X. If every member of γ is closed, γ is said to be an *closed cover*of X.

Imbedding: By an *imbedding* of a space X into a space Y, we mean an injective (one-to-one) map $f : X \to Y$ which defines a homeomorphism from X onto $f(X)$.

F.6 Sum and Product of Spaces

Indexed Family of Spaces: Consider a given indexed family

$$\mathcal{F} = \{X_\mu | \mu \in M\}$$

of sets. If each of the sets X_μ is a space, $\mathcal{F}$ is called an *indexed family of spaces*. Furthermore, if $\mu \neq \nu$ implies that $X_\mu \cap X_\nu$ is empty, then $\mathcal{F}$ is said to be disjoint.

Topological Sum: Consider an arbitrarily given indexed family

$$\mathcal{F} = \{X_\mu | \mu \in M\}$$

of spaces and denote by X the union of all sets X_μ, that is,

$$X = \bigcup_{\mu \in M} X_\mu.$$

Define a collection τ of subsets of X as follows: A subset U of X is in τ iff $U \cap X_\mu$ is an open set of the space X_μ for every $\mu \in M$. Note this is a topology in X. When topologized by τ, the space X will be referred to as the *topological sum*, or *sum*, of the family $\mathcal{F}$ of spaces and denoted by

$$X = \sum_{\mu \in M} X_\mu.$$

Topological Product: Let,

$$\mathcal{F} = \{X_\mu | \mu \in M\}$$

be an arbitrarily given indexed family of spaces and consider the Cartesian product

$$\Phi = \prod_{\mu \in M} X_\mu.$$

The Φ consists of all function $f : M \to X$ of M into the union X of all sets X_μ in $\mathcal{F}$ such that $f(u) \in X_\mu$ for every $\mu \in M$.

Define a topology τ in Φ as follows. For an arbitrary $\mu \in M$, and any open set U_μ of X_μ, the set

$$U_\mu^* = \{f \in \Phi | f(\mu) \in U_\mu\}$$

will be called a *sub-basic open set of* Φ defined by $U_\mu \subset X_\mu$. Let σ denote a collection of all sub-basic open sets of Φ. Define the topology τ to be the smallest topology in Φ containing the collection σ. This topology will be called the *product topology* in Φ. When topologized with τ, Φ is said to be the *topological product*, or *product*, of the family $\mathcal{F}$ of spaces, denoted

$$\Phi = \prod_{\mu \in M} X_\mu.$$

F.7 Homotopy and Isotopy

Homotopy: Let X and Y be given spaces and consider a family

$$\{h_t : X \to Y | t \in I\}$$

of maps indexed by the real numbers of the unit interval $I = [0, 1]$. The family $\{h_t\}$ is said to be *continuous* iff the function

$$H : X \times I \to Y,$$

defined by $H(x, t) = h_t(x)$ for each $x \in X$ and each $t \in I$, is continuous. A continuous family $\{h_t\}$ of maps, or equivalently the map H, is usually called a *homotopy*.

Isotopy: If h_t above is an imbedding for every $t \in I$, the continuous family $\{H_t\}$ is called an *isotopy*.

Homotopic: Let $f, g : X \to Y$ be two given maps. If there exists a homotopy $\{h_t : X \to Y | t \in I\}$ such that $h_0 = f$ and $h_1 = g$, then f and g are said to be *homotopic*. Intuitively, $f, g : X \to Y$ are homotopic iff f can be continuously changed into g.

Deformation/Contraction: Let X be a subspace of a space Y. A homotopy $\{h_t : X \to Y | t \in I\}$ is called a *deformation* iff h_0 is the inclusion map. Furthermore, if h_1 is a constant map, then the deformation h_t is called a *contraction*.

Deformation Retract: Let A be a subspace of a space X. If a deformation $\{h_t : X \to X | t \in I\}$ exists such that h_1 is a retraction of X onto A, then the subspace A is called a *deformation retract* of X.

Homotopy Equivalence: A map $f : X \to Y$ is said to be a *homotopy equivalence* iff there exists a map $g : Y \to X$ such that the composed maps $g \circ f : X \to X, f \circ g : Y \to Y$ are homotopic on the identity maps on X and Y respectively. In this case, the map $g : Y \to X$ is also a homotopy equivalence.

F.8 Polytopes

Simplexes: Let n be a given non-negative integer and consider a given set V of $n+1$ distinct objects. By the *n-dimensional simplex spanned by V*, we mean the closed subspace σ_V of the topological power R^V of the real line R which consists of all functions

$$f : V \to R$$

satisfying the following conditions:

1. $f(v) \geq 0$ for every $v \in V$.
2. $\sum_{v \in V} f(v) = 1$.

The $n+1$ objects in V are called the *vertices* of the simplex σ_V. Frequently V is called an *abstract simplex* and σ_V, the *topological realization* of V.

Unit Simplex Let $\triangle^n$ denote the *unit simplex* in the Euclidean space R^{n+1} which consists of all points $(x_0, x_1, \ldots, x_n)$ in R^{n+1} such that $x_i \geq 0$ for each $i = 0, 1, \ldots, n$ and that $x_0 + x_1 + \ldots + x_n = 1$.

q-face Let W be an arbitrary subset of V. If W consists of $q+1$ objects, then it determines a q-dimensional simplex σ_W. For each point $g \in \sigma_W$, there is a unique point $f_g \in \sigma_V$ such that

$$f_g(v) = \begin{cases} g(v), & (\text{ if } v \in V), \\ 0, & (\text{ if } v \in V \backslash W). \end{cases}$$

The assignment $g \rightarrow f_g$ defines an imbedding

$$i : \sigma_W \rightarrow \sigma_V$$

of σ_W into σ_V. Identify g with f_g for every $g \in \sigma_W$ and obtain σ_W as the closed subspace of σ_V defined by

$$\sigma_W = \{f \in \sigma_V | f(v) = 0 \text{ for each } v \in V \backslash W\}.$$

Such a simplex σ_W is called a *q-dimensional face* of σ_V or a *q-face* of σ_V. If the dimension q of σ_W is not emphasized, σ_W is called a *face* of σ_V; in symbols,

$$\sigma_W \leq \sigma_V.$$

Improper Face: σ_V has only one n-face, namely σ_V itself; this is called the *improper* face of σ_V. Other faces are called *proper faces*.

Abstract Simplicial Complex: By an *abstract simplicial complex* with vertices in a set V, we mean a family of finite subsets of V satisfying the condition that K is *hereditary*, i. e. every subset of any set in K is also in K.

Subcomplex Let K and L be any two abstract simplicial complexes with vertices V and W respectively. If $L \subset K$, then L is said to be a *subcomplex* of K.

Topological Realization Let K be an arbitrarily given abstract simplicial complex. We will construct a space

$$P = |K|$$

called the *topological realization* as follows.

For each finite set $F \in K$, consider the simplex σ_F defined in the previous section. These simplexes $\{\sigma_F | F \in K\}$ (without the identification introduced in studying their faces) are by definition disjoint topological spaces. Form their topological sum

$$S = S(K) = \sum_{F \in K} \sigma_F.$$

Then S is clearly a metrizable space containing every simplex σ_F as an open and closed subspace.

Introduce a relation $\sim$ in S as follows. Let $f \in \sigma_F$ and $g \in \sigma_G$ be any two points in S. Then they are real functions $f : F \to R$ and $g : G \to R$. We define $f \sim g$ iff the following conditions are satisfied.

1. $f(v) = 0$ for every $v \in F \backslash G$;

2. $g(v) = 0$ for every $v \in G \backslash F$;

3. $f(v) = g(v)$ for every $v \in F \cap G$.

The quotient space

$$P = |K| = S/\sim$$

of the space $S = S(K)$ of this equivalence relation $\sim$ is called the *topological realization* of the abstract simplicial complex K. We will also call P a *simplicial polytope*. In mathematical literature, P is usually called a *simplicial complex* and is denoted by K instead of $|K|$.

Adjunction Space: An *adjunction space* for an arbitrarily given map

$$f : A \to Y$$

defined on a closed subspace A of a space X into another space Y as follows.

Without loss of generality, assume X and Y are disjoint. Consider the topological sum

$$W = X + Y$$

of the spaces X and Y.

Introduce a relation $\sim$ in the space W as follows. Let u and v be any two points in the space W. Then we define $u \sim v$ iff at least one of the following four equation makes sense and is satisfied

$$u = v, \quad f(u) = v, \quad u = f(v), \quad f(u) = f(v).$$

The quotient space

$$Z = W/\sim$$

of the space W over this equivalence relation $\sim$ is called the *adjunction space* obtained by adjoining X to Y by means of the given map $f : A \to Y$.

F.9 Cellular Polytopes

Abstract n-cells: Consider a given sequence

$$S = \{S_n | n = 0, 1, \ldots\}$$

of disjoint sets, where the leading set S_0 is nonempty. The members of the set S_n will be called the *abstract n-cells.*

Characteristic Map: Give each S_n the discrete topology. We will construct a sequence

$$\{P_n | n = 0, 1, \ldots\}$$

of spaces as follows. First, we take $P_0 = S_0$ a discrete space. Next, assume that $n > 0$ and P_{n-1} has already been constructed. If S_n is the empty set, we define $P_n = P_{n-1}$. Otherwise, assume that there is a given family

$$\{\phi_\psi : \partial\triangle^n \to P_{n-1} | \psi \in S_n\}$$

of maps indexed by the abstract n-cells. Here, $\partial\triangle^n$ denotes the boundary sphere of the unit n-simplex $\triangle^n$. The map ϕ_ψ will be called the *characteristic map* of the abstract n-cell ψ. Consider the topological products

$$X_n = S_n \times \triangle^n, \qquad A_n = S_n \times \triangle^n.$$

Then, A_n is a closed subspace of X_n. Define a function

$$f_n : A_n \to P_{n-1}$$

by taking $f_n(\psi, t) = \phi_\psi(t)$ for every $\psi \in S_n$ and every $t \in \partial\triangle^n$. Since S_n is discrete, each $\psi \times \partial\triangle^n$ is open in A_n and hence f_n is continuous. Then we define P_n to be the adjunction space obtained by adjoining X_n to P_{n-1} by means of the map f_n. This completes the inductive construction of the sequence of spaces $\{P_n | n = 0, 1, \ldots\}$.

Imbed each P_{n-1} as a closed subspace of P_n, obtaining an expanding sequence

$$P_0 \subset P_1 \subset \ldots P_{n-1} \subset P_n \subset \ldots$$

of spaces. The topological sum

$$P = \sum_{n=0}^{\infty} P_n$$

will be called the *cellular polytope* determined by the given abstract cells and the given characteristic maps.

CW-Complex Cellular polytopes are usually called *CW-complexes*, where C stands for closure-finiteness and W stands for Whitehead (or weak) topology.

Appendix G

Definitions of Ideals, Varieties, and Related Terms

This appendix contains definitions of the terms used in Chapter 6 of this thesis, particularly with respect to the concepts concerning Groebner Bases. These definitions, taken from [20], provide more precise definitions than those used in the presentation of Chapter 6.

Field: A *field* consists of a set k and two binary operations "$\cdot$" and "$+$" defined on k for which the following conditions are satisfied:

1. $(a + b) + c = a + (b + c)$ and $(a \cdot b) \cdot c = a \cdot (b \cdot c)$ for all $a, b, c \in k$ (associative).
2. $a + b = b + c$ and $a \cdot b = b \cdot c$ for all $a, b \in k$ (commutative).
3. $a \cdot (b + c) = a \cdot b + a \cdot c$ for all $a, b, c \in k$ (distributive).
4. There are $0, 1 \in k$ such that $a + 0 = a \cdot 1 = a$ for all $a \in k$ (identities)
5. Given $a \in k$, there is $b \in k$ such that $a + b = 0$ (additive inverses).

6. Given $a \in k$, $a \neq 0$, there is $c \in k$ such that $a \cdot c = 1$ (multiplicative inverses).

Commutative Ring: A *commutative ring* consists of a set R and two binary operations "$\cdot$" and "$+$" defined on R for which the following conditions are satisfied:

1. $(a + b) + c = a + (b + c)$ and $(a \cdot b) \cdot c = a \cdot (b \cdot c)$ for all $a, b, c \in R$ (associative).
2. $a + b = b + c$ and $a \cdot b = b \cdot c$ for all $a, b \in R$ (commutative).
3. $a \cdot (b + c) = a \cdot b + a \cdot c$ for all $a, b, c \in R$ (distributive).
4. There are $0, 1 \in R$ such that $a + 0 = a \cdot 1 = a$ for all $a \in R$ (identities)
5. Given $a \in R$, there is $b \in R$ such that $a + b = 0$ (additive inverses).

Monomial: A *monomial* in $x_1, \ldots, x_n$ is a product of the form

$$x_1^{\alpha_1} \cdot x_2^{\alpha_2} \cdot \ldots \cdot x_n^{\alpha_n}$$

where all of the exponents $\alpha_1, \ldots, \alpha_n$ are non-negative integers. The *total degree* of this monomial is the sum $\alpha_1 + \ldots + \alpha_n$.

Polynomial: A *polynomial* f in $x_1, \ldots, x_n$ with coefficients in k is a finite linear combination (with coefficients in k) of monomials. We will write a polynomial f in the form

$$f = \sum_{\alpha} a_\alpha x^\alpha, \quad a_\alpha \in k$$

where the sum is over a finite number of n-tuples $\alpha = (\alpha_1, \ldots, \alpha_n)$. The set of all polynomials in $x_1, \ldots, x_n$ with coefficients in k is denoted $k[x_1, \ldots, x_n]$.

Coefficient, Term, Total Degree: Let $f = \sum_\alpha a_\alpha x^\alpha$ be a polynomial in $k[x_1, \ldots, x_n]$.

1. We call a_α the *coefficient* of the monomial x^α.
2. If $a_\alpha \neq 0$, then we call $a_\alpha x^\alpha$ a *term* of f.
3. The *total degree* of f, denoted $\deg(f)$, is the maximum $|\alpha|$ such that the coefficient a_α is nonzero.

Affine Space: Given a field k and a positive integer n, we define the n-dimensional *affine space* over k to be the set

$$k^n = \{(a_1, \ldots, n) | a_1, \ldots, a_n \in k\}.$$

Affine Variety: Let k be a field, and let $f_1, \ldots, f_s$ be polynomials in $k[x_1, \ldots, x_n]$. Then we set

$$\mathcal{V}(f_1, \ldots, f_s) = \{(a_1, \ldots, a_n) \in k^n | f_i(a_1, \ldots, a_n) = 0 \text{ for all } 1 \leq i \leq s\}.$$

We call $\mathcal{V}(f_1, \ldots, f_s)$ the *affine variety* defined by $f_1, \ldots, f_s$.

Ideal (Definition 1): A subset $I \subset k[x_1, \ldots, x_n]$ is an *ideal* if it satisfies:

1. $0 \in I$
2. If $f, g \in I$, then $f + g \in I$.
3. If $f \in I$ and $h \in k[x_1, \ldots, x_n]$, then $hf \in I$.

Ideal (Definition 2): Let $f_1, \ldots, f_s$ be polynomials in $k[x_1, \ldots, x_n]$. Then we set

$$\langle f_1, \ldots, f_s \rangle = \left\{ \sum_{i=1}^{s} h_i f_i | h_1, \ldots, h_s \in k[x_1, \ldots, x_n] \right\}.$$

Notice $\langle f_1, \ldots, f_s \rangle$ is an ideal, in agreement with definition 1.

Ideal (Definition 3): Let $\mathcal{V} \subset k[x_1, \ldots, x_n]$ be an affine variety. Then we set

$$I(\mathcal{V}) = \{f \in k[x_1, \ldots, x_n] | f(a_1, \ldots, a_n) = 0 \text{ for all } (a_1, \ldots, a_n) \in \mathcal{V}\}.$$

Note that $I(\mathcal{V})$ is an ideal.

Monomial Ordering: A *monomial ordering* on $k[x_1, \ldots, x_n]$ is any relation $>$ on $Z^n_{\geq 0}$ (the n-tuples of positive integers), or equivalently, any relation on the set of monomials x^α with $\alpha \in Z^n_{\geq 0}$ satisfying:

1. $>$ is a total (or linear) ordering $Z^n_{\geq 0}$.
2. If $\alpha > \beta$ and $\gamma \in Z^n_{\geq 0}$, then $\alpha + \gamma > \beta + \gamma$.
3. $>$ is a well-ordering on $Z^n_{\geq 0}$. This means that every nonempty subset of $Z^n_{\geq 0}$ has a smallest element under $>$.

Polynomial Terms: Let $f = \sum_\alpha a_\alpha x^\alpha$ be a nonzero polynomial in $k[x_1, \ldots, x_n]$ and let $>$ be a monomial order.

1. The *multidegree* of f is

$$\text{multideg}(f) = \max(\alpha \in Z^n_{\geq 0} | a_\alpha \neq 0)$$

2. The *leading coefficient* of f is

$$\text{LC}(f) = a_{\text{multideg}(f)} \in k.$$

3. The *leading monomial* of f is

$$\text{LM}(f) = x^{\text{multideg}(f)} \in k.$$

4. The *leading term* of f is

$$\text{LT}(f) = LC(f) \cdot LM(f)$$

Leading Term of Ideal: Let $I \subset k[x_1, \ldots, x_n]$ be an ideal other than $\{0\}$.

1. We denote by $\mathrm{LT}(I)$ the set of leading terms of elements of I. Thus,

$$\mathrm{LT}(I) \quad = \quad \{cx^\alpha |\text{ there exists } f \in I \text{ with } \mathrm{LT}(f) = cx^\alpha\}.$$

2. We denote by $\langle \mathrm{LT}(I) \rangle$ the ideal generated by the elements of $\mathrm{LT}(I)$.

Groebner Basis: Fix a monomial order. A finite subset $G = \{g_1, \ldots, g_t\}$ of an ideal I is said to be a *Groebner basis* (or a *standard basis*) if

$$\langle \mathrm{LT}(g_1), \ldots, \mathrm{LT}(g_t) \rangle \quad = \quad \langle \mathrm{LT}(I) \rangle.$$

Variety of Ideal: Let $I \subset k[x_1, \ldots, x_n]$ be an ideal. We will denote by $\mathcal{V}(I)$ the set

$$\mathcal{V}(I) \quad = \quad \{(a_1, \ldots, a_n) \in k^n | f(a_1, \ldots, a_n) = 0 \text{ for all } f \in I\}.$$

Elimination Ideal: Given $I = \langle f_1, \ldots, f_s \rangle \subset k[x_1, \ldots, x_n]$, the k^{th} *elimination ideal* I_k is the ideal of $k[x_{k+1}, \ldots, x_n]$ defined by

$$I_k \quad = \quad I \cap k[x_{k+1}, \ldots, x_n].$$

Appendix H

Bernstein's Theorem and Application to CMA

In this appendix is a presentation of Bernstein's Theorem. The first section herein contains a distilled form of the original statement found in [11]. The second section gives an example of Bernstein's Theorem specific to the system of equations describing the CMA stationary points.

H.1 Bernstein's Theorem (General Case)

Laurent polynomials: By a *Laurent polynomial* we mean a function $f(x_1, x_2, \ldots, x_n) \in [x_1, x_1^{-1}, \ldots, x_n, x_n^{-1}]$. These are regarded as functions on the manifold $T = (C^\star)^n$, that is, the n-dimensional complex torus. Each Laurent polynomial is a linear combination of of monomials $x^q = x_1^{q_1} x_2^{q_2} \ldots x_n^{q_n}$. The set of all monomials constitutes a lattice $M = Z^n$.

Support By the *support* $\mathrm{supp}(f)$ of a polynomial $f(x) = \sum c_q x^q$ we mean the set of all q for which $c_q \neq 0$.

Given a system of equations $F : f_1(x) = 0$ $(i = 1, 2, \ldots, n)$, we seek an estimate of the number of roots of the system in term of the supports $\mathrm{supp}(f_i)$.

Let $\mathcal{S} = (S_1, S_2, \ldots, S_n)$ be a collection of n finite subsets of the lattice M. We consider all systems F such at $\mathrm{supp}(f_i) \subset S_i$. Then for systems in general position (that is, all systems excepts for some algebraic submanifold in the space of coefficients) the roots of the system F are isolated, and $L(F)$, the number of roots counted according to their multiplicities, does not change, that is, it depends only on $\mathcal{S}$. We denote this number $L(\mathcal{S})$

Let $V_n(S)$ denote the volume of the convex hull of a set S in R^n, setting the volume of the unit parallelepiped of the lattice equal to one. Then the (Minkowski's) mixed volume of $\mathcal{S}$ is the number

$$V(\mathcal{S}) \;=\; (-1)^{n-1} \sum V_n(S_i) + (-1)^{n-2} \sum V_n(S_i + S_j) + \ldots V_n(S_1 + \ldots + S_n)$$

The arrived at result is

Bernstein's Theorem: $L(S_1, S_2, \ldots, S_n) = V(S_1, S_2, \ldots, S_n)$. That is, the number of solutions on the complex torus to a system of equations is equal to the mixed volume of the support sets.

H.2 Two-tap CMA Example

Consider a channel-equalizer system of two taps (i.e. $H = [\, h_0 \quad h_1 \,]$). In system F describing the CMA stationary points all monomial of order 3 and order 1 appear in all equations. That is, with each equation having the identical support, we are said to have an *unmixed* system of equations. In such a case the mixed volume V is simply the volume of the convex hull of the support lattice (also know as the Newton polytope). Hence, the lattice is as shown in Figure H.1.

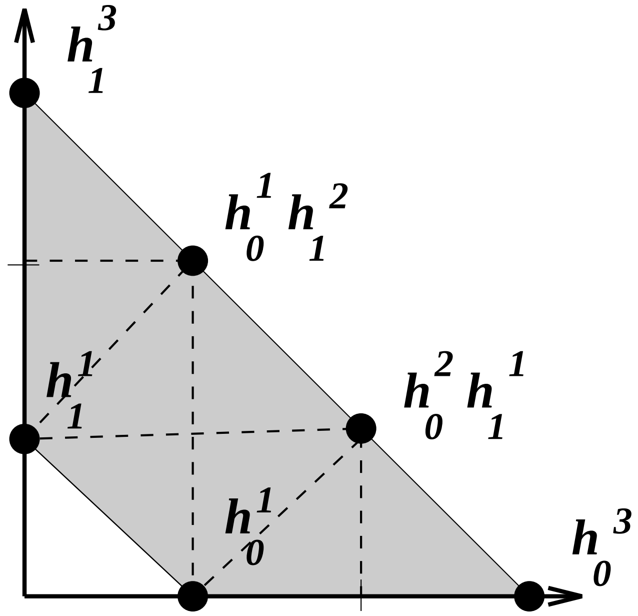

Figure H.1: Support Lattice for Two Tap CMA Example

The shaded region denotes the convex hull of the support lattice M and can be seen to have a volume of 8 (realizing the unit simplex is defined to have a volume of 1). This corresponds to the existence of 8 stationary points of CMA on the complex torus. Adding the single known maximum (at the origin) yields the 9 stationary points in agreement with the 3^{n+1} figure pointed out in Chapter 6.

Bibliography

[1] K. H. Alkhamie, Z. Q. Luo, "Blind Equalization using Second-Order Statistics," *Proc. of IEEE Conf. Acoust., Speech, Signal Processing*, May 1995.

[2] E. L. Allgower, *Numerical Continuation Methods*, Berlin: Springer Verlag, 1990.

[3] S. T. Alexander, "Transient Weight Misadjustment Properties for the Finite Precision LMS Algorithm," *IEEE Trans. Acoust. Speech Signal Process.*, vol. ASSP-35, 1987.

[4] M. E. Austin, "Decision-feedback Equalization for Digital Communications over Dispersive Channels," Tech. Rep. 437, MIT Lincoln Lab., Lexington, MA, Aug. 1967.

[5] C. A. Belfiore, J. H. Park, Jr., "Decision Feedback Equalization," *Proc. IEEE*, vol. 67, Aug. 1979.

[6] S. Bellini, "Blind Equalization," *Alta Frequenza*, vol. LVII, no. 7 Sept. 1988.

[7] S. Bellini, "Bussgang Techniques for Blind Equalization," *IEEE Global Telecom. Conf.*, Houston, 1986.

[8] S. Bellini, "Blind equalization and deconvolution," *SPIE*, vol. 1565, 1991.

[9] S. Bellini, F. Rocca, "Near Optimal Blind Deconvolution," *Proc. of IEEE Conf. Acoust., Speech, Signal Processing*, May, 1988.

[10] A. Benveniste, M. Goursat, G. Ruget, "Robust Identification of a Nonminimum Phase System: Blind Adjustment of a Linear Equalizer in Data Communications," *IEEE Trans. on Automat. Contr.*, vol. AC-25, no. 3, Jun. 1980.

[11] D. N. Bernstein, "The Number of Roots of a System of Equations," *Functional Analysis and Appl. 9*, (1975), 1-4XS.

[12] R. R. Bitmead, S. Y. Kung, B. D. O. Anderson, T. Kailath, "Greatest Common Divisors via Generalized Sylvester and Bezout Matrices," *IEEE Trans. on Automat. Contr.*, vol. 23, no. 6, Dec., 1978.

[13] B. S. Bourgeois, A. B. Martinez, "Nonlinear Behavior of the Adaptive LMS Algorithm," *IEEE trans. Circuits and Systems II: Analog and Digital Signal Process*, vol. 42, Feb. 1995.

[14] M. G. Bulmer, *Principles of Statistics*, New York: Dover Publications, 1967.

[15] C. Cariscos, B. Liu, "A Roundoff Error Analysis of the LMS Adaptive Algorithm," *IEEE Trans. Acoust. Speech Signal Procss.*, vol. 32, 1984.

[16] A. B. Carlson, *Communication Systems*, New York: McGraw-Hill, 1975.

[17] Y. Chen, C.L. Nikias, J.G. Proakis, "CRIMNO: Criterion with Memory Nonlinearity for Blind Equalization," *Int. Sig. Proc. Workshop on HOS*, Chamrousse, France, July 1991.

[18] C. K. Chan, J. J. Shynk, "Stationary Points of the Constant Modulus Algorithm for Real Gaussian Signals ," *IEEE Trans. Acoust. Speech Signal Procss.*, vol. 38, Dec. 1990.

[19] F. M. Coetzee, V. L. Stonick, "Sequential Homotopy-Based Computation of Multiple Solutions to Nonlinear Equations," *Proc. of IEEE Conf. Acoust., Speech, Signal Processing*, 1995.

[20] D. Cox, J. Little, D. O'Shea, *Ideals, Varieties, and Algorithms*, Berlin: Springer Verlag, 1992.

[21] Z. Ding, C.R. Johnson, Jr., R.A. Kennedy, "On the (Non)Existence of Undesirable Equilibria of Godard Blind Equalizers," *IEEE Trans. of Signal Processing*, vol. 40, no. 10, Oct. 1992..

[22] Z. Ding, C.R. Johnson, Jr., R.A. Kennedy, "Non-Global Convergence of Blind Recursive Indentifiers Based on Gradient Descent of Continuous Cost Functions," *Proc. of the 29th Conference on Decision and Control*, Dec. 1990.

[23] Z. Ding, R.A. Kennedy, "On the Whereabouts of Local Minima for Blind Adaptive Equalizers," *IEEE Trans. on Circuits and Systems-II: Analog and Digital Signal Processing*, vol. 39, no. 2, Feb. 1992.

[24] Z. Ding, R. A. Kennedy, B. D. O. Anderson, C. R. Johnson, Jr., "Local Convergence of the Sato Blind Equalizer and Generalizations Under Practical Constraints," *IEEE Trans. on Info. Theory*, vol. 39, no. 1, Jan. 1993.

[25] Z. Ding, C.R. Johnson, Jr., "On the Non-Vanishing Stability of Undesirable Equilibria for FIR Godard Blind Equalizers," *IEEE Trans. on Signal Processing*, vol. 41, no. 5, May 1993.

[26] Z. Ding, R.A. Kennedy, B. D. O. Anderson, C. R. Johnson, Jr., "Ill-Convergence of Godard Blind Equalizers in Data Communications Systems," *IEEE Trans. on Comm.*, vol. 39, no. 9, Sept. 1991.

[27] D.L. Donoho, "On Minimum Entropy Deconvolution," *Applied Time Series Analysis*, D.F. Findley, Ed., New York: Academic Press, 1981.

[28] E. Eweda, "Comparsion of RLS, LMS and Sign Algorithms for Tracking Randomly Time-Varying Channels," *IEEE Trans. on Signal Process.*, vol. 42, Nov. 1994.

[29] I. Fijalkow, C. E. Manlove, C. R. Johnson, Jr., "Adaptive Fractionally Spaced Blind CMA Equalization," *Submitted to IEEE trans. on Signal Processing*, 1994.

[30] G. J. Foschini, "Equalizing Without Altering or Detecting Data," *AT&T Technical Journal*, vol. 64, no. 8, Oct. 1985.

[31] V. Guillemin, A. Pollack, *Differential Topology*, Englewood Cliff, NJ: Prentice-Hall, 1974.

[32] R. D. Gitlin, S. B. Weinstein, "Fractionally-spaced Equalization: An Improved Digital Transversal Equalizer," *Bell Sys. Tech. Journal*, vol. 60, Feb. 1981.

[33] R. D. Gitlin, J. F. Hayes, S. B. Weinstein, *Data Communications Principles*, New York: Plenum Press, 1992.

[34] D.N. Godard, "Self-Recovering Equalization and Carrier Tracking in Two-Dimensional Data Communication Systems," *IEEE Trans. on Commun.*, vol. COM-28, No. 11, Nov. 1980.

[35] S. Haykin, *Blind Deconvolution*, Englewood Cliff, NJ: Prentice-Hall, 1994.

[36] S. T. Hu, *Elements of General Topology*, San Franciso: Holden-Day, 1964.

[37] Y. Hua, H. Yang, W. Qiu, "Source Correlation Compensation for Blind Channel Identification Based on Second-Order Statistics," *IEEE Signal Processing Letters*, vol. 1, No. 8, Aug. 1994.

[38] C. R. Johnson, Jr., B. D. O. Anderson, "Godard Blind Equalizer Error Surface Characteristics," *Int'l Journal of Adaptive Control and Signal Processing*, in press.

[39] C.R. Johnson, Jr., J. P. LeBlanc, V. Krishnamurthy, "Godard Blind Equalizer Misbehavior with Correlated Sources: Two Examples," *Moroccan Journal of Control Computer Science and Signal Processing*, Vol. II, Number 3, June 1993.

[40] C.R. Johnson, Jr., "Admissibility in Blind Adaptive Channel Equalization," *IEEE Control Systems*, Jan. 1991.

[41] D. L. Jones, "Learning Characteristics of Transpose-Form LMS Adaptive Filters," *IEEE trans. Circuits and Systems II: Analog and Digital Signal Process.*, vol. 39, Oct. 1992.

[42] T. Kalker, H. Park, M. Vetterli, "Groeber Basis Techniques in Multidimensional Multirate Systems," *Proc. of IEEE Conf. Acoust., Speech, Signal Processing*, May 1995.

[43] R. A. Kennedy, B. D. O. Anderson, R. R. Bitmead, "Blind Adaptation of Decision Feedback Equalizers: Gross Convergence Properties," *Int'l Journal of Adaptive Control and Signal Processing*, vol. 7, 1993.

[44] L. C. Kinsey, *Topology of Surfaces*, New York: Springer-Verlag, 1993.

[45] V. Krishnamurthy, S. Dey, J. P. LeBlanc, "Blind Equalization of IIR Channels using Hidden Markov Models and Extended Least Squares," *accepted for publication in IEEE Sig. Proc. Trans.*, in press.

[46] R. Laroia, N. Farvardin, S. A. Tretter, "On Optimal Shaping of Multidimensional Constellations," *IEEE Trans. on Info. Theory*, vol. 40, No. 4, July 1994.

[47] J. P. LeBlanc, I. Fijalkow, B. Huber, C. R. Johnson, Jr., "Fractionally Spaced CMA Equalizers Under Periodic and Correlated Inputs," *Proc. of IEEE Conf. Acoust., Speech, Signal Processing*, May 1995.

[48] J. P. LeBlanc, K. Doğançay, R. A. Kennedy, C. R. Johnson, Jr., "Effects of input data correlation on the convergence of blind adaptive equalizers," *Proc. of IEEE Conf. Acoust., Speech, Signal Processing*, May 1994.

[49] Y. Li, Z. Ding, "Blind Channel Identification based on Second Order Cyclostationary Statistics," *Proc. of IEEE Conf. Acoust., Speech, Signal Processing*, 1993.

[50] Y. Li, Z. Ding, "Global Convergence of Fractionally Spaced Godard Adaptive Equalizers," *submitted to IEEE Trans. on Sig. Process.*, Feb. 1994.

[51] R. W. Lucky, H. R. Rudin, "An Automatic Equalizer for General-Purpose Communications Channels," *Bell System Technical Journal*, Nov. 1967.

[52] O. Macchi, E. Eweda, "Convergence Analysis of Self-Adaptive Equalizers," *IEEE Trans. on Inform. Theory*, vol. IT-30, no. 2, 1984.

[53] J.E. Mazo, "Design of a finite impulse response for the Viterbi algorithm and decision feedback equalizer," *Proc. IEEE Int. Conf. Communications, ICC-74*, June 1974.

[54] J. Milnor, *Morse Theory*, Princeton, NJ: Princeton University Press, 1963.

[55] A. P. Morgan, *Solving Polynomial Systems using Continuation for Engineering and Scientific Problems*, Englewood Cliff, NJ: Prentice-Hall, 1987.

[56] M. Morse, *Peaks, Pits, and Passes* (film), Martin Learning Aids: Mathematical Association of America, 1966.

[57] G. Picchi, G. Prati, "Blind Equalization and Carrier Recovery Using a "Stop-and-Go" Decision-Directed Algorithm," *IEEE Trans. on Commun.*, vol. COM-35, no. 9, Sept. 1987.

[58] S.U.H. Qureshi, "Adaptive Equalization," *Proc. of the IEEE*, vol. 73, no. 9, Sept 1985.

[59] G. A. Rey, "Local Stability Analysis of the Constant Modulus Algorithm for Adaptive Equalization," *Master's Thesis, Cornell University*, 1989.

[60] Y. Sato, "A Method of Self-Recovering Equalization for Multilevel Amplitude-Modulation Systems," *IEEE Trans. on Commun.*, Jun. 1975.

[61] N. Seshadri, "Joint Data Recovery and Channel Estimation Using Blind Trellis Search Techniques," *IEEE Global Telecomm. Conf.*, 1990.

[62] O. Shalvi, E. Weinstein, "New Criteria for Blind Deconvolution of Nonminimum Phase Systems (Channels)," *IEEE Trans. on Inform. Theory*, vol. 36, no. 2, Mar. 1990.

[63] O. Shalvi, E. Weinstein, "Reply to 'Comments on 'New Criteria for Blind Deconvolution of Nonminimum Phase Systems (Channels)' ," *IEEE Trans. on Inform. Theory*, vol. 38, no. 1, Jan. 1992.

[64] O. Shalvi, E. Weinstein, "Super-Exponential Methods for Blind Deconvolution," *IEEE Trans. on Inform. Theory*, vol. 39, no. 2, Mar. 1993.

[65] V. Solo, "The Limiting Behavior of LMS," *IEEE Trans. Acoust. Speech Signal Process.*, vol. 37, 1989.

[66] L. Tong, G. Xu, T. Kailath, "Blind Identification and Equalization Based on Second-Order Statistics: A Time Domain Approach," *IEEE Trans. on Info. Theory*, Mar. 1994.

[67] L. Tong, G. Xu, T. Kailath, "Blind Identification and Equalization Based on Second-Order Statistics: A Frequency-Domain Approach," *IEEE Trans. on Info. Theory*, Jan. 1995.

[68] J. K. Tugnait, "Comments on 'New Criteria for Blind Deconvolution of Nonminimum Phase Systems (Channels)' ," *IEEE Trans. on Inform. Theory*, vol. 38, no. 1, Jan. 1992.

[69] J.R. Treichler, M. G. Agee, "A New Approach to Multipath Correction of Constant Modulus Signals," *IEEE Trans. on Acoustics, Speech, and Signal Processing*, April 1983.

[70] J. R. Treichler, V. Wolff, C. R. Johnson, Jr., "Observed Misconvergence in the Constant Modulus Adaptive Algorithm," *Proc. 25th Asilomar Conference on Signals, Systems and Computers*, Nov. 1991.

[71] G. Ungerboeck, "Fractional Tap-Spacing Equalizer and Consequences for Clock Recovery in Data Modems," *IEEE Trans. on Communications*, vol. com-24, no. 8, Aug. 1976..

[72] V. Weerackody, S. A. Kassam, "Blind Equalization using Lattice Filters," *Int'l Conf. on Comm.*, 1988.

[73] V. Weerackody, S. A. Kassam, K. R. Laker, "A Convergence Model for the Analysis of Some Blind Equalization Algorithms," *Proc. IEEE Int. Symp. Circuits Syst*, May 1989.

[74] A. S. Willsky, *Digital Signal Processing and Control and Estimation Theory: Points of Tangency, Areas of Intersection, and Parallel Directions*, Cambridge, Massachusetts: MIT Press, 1979.

[75] E. Zervas, J. G. Proakis, V. Eyuboglu, "Effects of Constellation Shaping on Blind Equalization," *SPIE*, 1991.

[76] F. Zheng, S. McLaughlin, B. Mulgrew, "Blind Equalization of multilevel PAM series via Higher-Order Cumumlant Fitting," *Int'l Conf. Comm.*, 1991.